

FEDERAL UNIVERSITY OF MINAS GERAIS  
School of Engineering  
Graduate Program in Electrical Engineering

Hugo R. Torquato

**Enhancement of rooftop-PV  
hosting-capacity based on decentralized  
battery energy storage systems**

Belo Horizonte

2023



Hugo R. Torquato

# **Enhancement of rooftop-PV hosting-capacity based on decentralized battery energy storage systems**

Final thesis presented to the Graduate  
Program in Electrical Engineering of the  
Federal University of Minas Gerais in partial  
fulfillment of the requirements for the degree  
of Master in Electrical Engineering.

Advisor: Danilo I. Brandao  
Co-advisor: Hélio M. A. Antunes

Belo Horizonte  
2023

Hugo R. Torquato    Enhancement of rooftop-PV hosting-capacity based on decentralized battery energy storage systems/ Hugo R. Torquato. – Belo Horizonte, 2023-    122 p. : il. (algumas color.) ; 30 cm.

Supervisor: Advisor: Danilo I. Brandao

Thesis (Doctorate) – FEDERAL UNIVERSITY OF MINAS GERAIS

School of Engineering

Graduate Program in Electrical Engineering

, 2023.

1. Palavra-chave1. 2. Palavra-chave2. 2. Palavra-chave3. I. Orientador. II. Universidade Federal de Minas Gerais. III. Escola de Engenharia. IV. Título.

*Dedication here...*



# Acknowledgements

Acknowledgments...










# Resumo

Redes de distribuição de energia estão cada vez mais se aproximando da respectiva capacidade de suportar novas unidades de geração descentralizadas (GD). Na literatura, vários estudos e aplicações empregam estratégias de controle de tensão com o objetivo de incrementar a capacidade de hospedagem (HC) da rede. Entretanto, é fundamental destacar que estratégias relacionadas à redução da potência ativa podem restringir o montante efetivamente entregue à rede, impactando negativamente o retorno financeiro do investidor do empreendimento. Já as estratégias relacionadas ao controle de potência reativa podem resultar em uma elevação da mesma e causar elevação do nível de corrente nos elementos, o que pode provocar problemas de qualidade de energia. Com o intuito de proporcionar a elevação no HC e amenizar os cenários descritos, nesta dissertação propõe o dimensionamento de armazenadores, de pequeno porte, a serem instalados juntos das unidades fotovoltaicas. Para a elaboração deste estudo, a aplicação OpenDSS foi associada com uma estrutura em banco de dados por meio de uma lógica desenvolvida em *Python*, capaz de identificar a rede, calcular o fluxo de potência, identificar a operação em HC e salvar os resultados para processamento posterior. A metodologia proposta é aplicada a uma rede de baixa tensão de forma a avaliar o caso de estudo em vários cenários em diferentes perspectivas. Dentre eles o cenário operando sem GD, operando com GD, operando com GD e controle *Volt-Var*, operando com GD e controle *Volt-Watt* operando com GD e ambos os controles. A capacidade máxima de redução na potência ativa é avaliada em três configurações: reduções de 15%, 30% e 50%. Ao final do estudo, é possível notar uma melhor resposta no incremento do HC da rede quando ambas estratégias de controle operam de forma conjunta, resultando em um incremento médio de aproximadamente 40%. Especificamente relacionado ao controle de potência ativa, é notável que pequenos bancos de baterias promovem significativa redução na perda de energia, principalmente em níveis de redução mais elevados, como 50%. A energia perdida foi mensurada e indicadores de desempenho estabelecidos para quantificar o dimensionamento da bateria. Entre os indicadores, destacam-se a comparação da potência perdida com a potência na unidade geradora, a relação *E-Rate* que associa a potência máxima do armazenados com sua respectiva energia, a relação entre a energia da GD e a demanda das cargas e, por fim, o coeficiente  quantifica a eficiência da redução da energia em elevar o HC da rede.

Palavras-chave: Capacidade de hospedagem. Geradores distribuídos. Armazenadores de energia. Redes de Distribuição. *Volt-Var*. *Volt-Watt*.



# Abstract

Many electrical grids are reaching their maximum penetration capacity of distributed generation. In literature, several studies and applications consider voltage control strategies to increase the grid hosting capacity. However, it is important to note that implementing active power curtailment control can limit the amount of active power that distributed generator (DG) owners can supply to the grid, which can negatively affect their revenue. Additionally, reactive power control can increase the reactive power in the system, leading to higher current measurements and potential quality issues. To address these issues, this thesis aims at sizing appropriately the battery storage units to be installed with photovoltaic generators to increase the hosting capacity (HC). The proposed approach involves a methodology that associates the OpenDSS software with a database structure using a logic developed in Python to recognize the grid, trigger the power flow calculation, identify the violation of standard operation requirements for distribution systems, and save the results for further data processing. The final outcome considers various scenarios to analyze the low-voltage grid, defined as a case study for this study, from different perspectives. These include scenarios without distributed generation, with only photovoltaic generation, only operating with volt-var control, only operating with volt-watt control, and with both voltage control strategies combined. The allowable curtailment limits cover three configurations, such as 15%, 30%, and 50% maximum power reduction, and affect specifically the active power control cases. In conclusion, by implementing voltage control techniques that utilize both active and reactive controls simultaneously, the HC results of the case study improved by around 40%. Regarding active power control, it was noticed that utilizing small battery energy storage systems (BESS) can greatly reduce revenue loss and allow greater HC of distribution grids. The amount of curtailed energy was measured, and various performance indicators were used to quantify the appropriate size of the BESS. These indicators include comparing curtailed power with the PV unit, the E-Rate coefficient, which associates the BESS maximum power and energy metrics, the generation ratio between DG and load demand, and the HC coefficient, which measures the effectiveness of curtailed energy in enhancing HC results.

Keywords: Hosting Capacity. Distributed Generator. Volt-Var. Volt-Watt. Battery Energy Storage System. Distribution Systems



# List of Figures

Figure 1 – Distributed generation availability map - Minas Gerais, Brazil. . . . .	25
Figure 2 – Performance index as an indicator of operation quality based on the number of generators installed in the grid. . . . .	33
Figure 3 – Illustrative Volt-Var curve. . . . .	38
Figure 4 – Illustrative <i>Volt-Var</i> and <i>Volt-Watt</i> curve. . . . .	39
Figure 5 – Storage technologies association to their applicability. . . . .	40
Figure 6 – Boxplot example and concepts. . . . .	45
Figure 7 – Box plot skewness: (a) Skewed left; (b) Symmetric data set; (c) Skewed right. . . . .	46
Figure 8 – Flowchart of the developed tool using multiple software to estimate the HC value and size of the distributed small BESS units. . . . .	50
Figure 9 – BESS Sizing store procedure illustration. . . . .	52
Figure 10 – LV grid street view. . . . .	62
Figure 11 – LV grid single-line diagram. . . . .	63
Figure 12 – Load Power Profile: (a) Active Power; (b) Reactive Power. . . . .	67
Figure 13 – Block diagram of the PVSystem element model. . . . .	68
Figure 14 – Simplified block diagram of the PVSystem operation with InvControl element. . . . .	70
Figure 15 – HC box plots divided by case studies: 15% active power curtailment. .	77
Figure 16 – HC box plots divided by case studies: 30% active power curtailment. .	78
Figure 17 – HC box plots divided by case studies: 50% active power curtailment. .	79
Figure 18 – Voltage control strategies response: (a) Control response; (b) Power response. . . . .	83
Figure 19 – Active power curtailment reduction at 15%: (a) Single VW control operation; (b) Combined control operation, VV and VW. . . . .	84
Figure 20 – Active power curtailment reduction at 30%: (a) Single VW control operation; (b) Combined control operation, VV and VW. . . . .	85
Figure 21 – Active power curtailment reduction at 50%: (a) Single VW control operation; (b) Combined control operation, VV and VW. . . . .	85

Figure 22 – Average power measurement in the transformer: (a) Case 1 - Operation without PV elements; (b) Case 5 - Operation with PV elements and both VV and VW controls. . . . .	89
Figure 23 – Activation locations frequency for a 15% curtailment limit: (a) Number of occurrences by bus; (b) Occurrence representation into the grid. . . .	90
Figure 24 – Activation locations frequency for a 30% curtailment limit: (a) Number of occurrences by bus; (b) Occurrence representation into the grid. . . .	91
Figure 25 – Activation locations frequency for a 50% curtailment limit: (a) Number of occurrences by bus; (b) Occurrence representation into the grid. . . .	92
Figure 26 – BESS sizing results box plots considering 15% active curtailment: (a) Maximum Battery Power; (b) Battery Adjusted Energy. . . . .	95
Figure 27 – BESS sizing results box plots considering 30% active curtailment: (a) Maximum Battery Power; (b) Battery Adjusted Energy. . . . .	95
Figure 28 – BESS sizing results box plots considering 50% active curtailment: (a) Maximum Battery Power; (b) Battery Adjusted Energy. . . . .	96
Figure 29 – Average power comparison when PV operating at 15% curtailment with and without BESS: (a) PV with VW control; (b) PV with VV and VW control. . . . .	101
Figure 30 – Average power comparison when PV operating at 30% curtailment with and without BESS: (a) PV with VW control; (b) PV with VV and VW control. . . . .	102
Figure 31 – Average power comparison when PV operating at 50% curtailment with and without BESS: (a) PV with VW control; (b) PV with VV and VW control. . . . .	102
Figure 32 – Hosting capacity boxplots divided by case studies . . . . .	115



# List of Tables

Table 1 – Description of the voltage operation ranges. . . . .	36
Table 2 – Total number of loads connected per phase. . . . .	67
Table 3 – Grid metrics comparison between reference results and the proposed case study. . . . .	75
Table 4 – A HC comparison between reference results and the proposed case study.	76
Table 5 – Average HC values for the proposed case scenarios with 15% curtailment.	77
Table 6 – Average HC values for the proposed case scenarios with 30% curtailment.	78
Table 7 – Average HC values for the proposed case scenarios with 50% curtailment.	79
Table 8 – Comparison of HC enhancements based on curtailment scenarios and voltage control techniques. . . . .	80
Table 9 – Number of elements operating in a HC condition with a voltage control strategy and 15% curtailment. . . . .	86
Table 10 – Number of elements operating in a HC condition with a voltage control strategy and 30% curtailment. . . . .	86
Table 11 – Number of elements operating in a HC condition with a voltage control strategy and 50% curtailment. . . . .	87
Table 12 – List of buses frequently operating with voltage control activated. . . . .	89
Table 13 – BEES average results by curtailment configuration operating with VW control. . . . .	93
Table 14 – BEES average results by curtailment configuration operating with VV and VW controls. . . . .	94
Table 15 – Average E-ratio and PV power ratio results by curtailment with VW control. . . . .	97
Table 16 – Average E-ratio and PV power ratio results by curtailment with VV and VW control. . . . .	98
Table 17 – Average PV by Load ratio energy results by curtailment configuration. .	98
Table 18 – Average HCC results by curtailment configuration. . . . .	99
Table 19 – HCC examples for each curtailment scenario. . . . .	99
Table 20 – Average HC values comparison when considering PV with VW control and BESS units for different curtailment scenarios. . . . .	100

Table 21 – Average HC values comparison when considering PV with VV and VW control and BESS units for different curtailment scenarios.. . . . .	101
Table 22 – Data structure of the monitor table in the database. . . . .	114
Table 23 – Service Transformer Data Overview. . . . .	117
Table 24 – Wire Data Overview. . . . .	117
Table 25 – Geometry Data Overview. . . . .	118
Table 28 – Load Shape Data Overview . . . . .	118
Table 26 – Lines Data Overview. . . . .	121
Table 27 – Load Data Overview. . . . .	122

# List of Algorithms

1	Implementation of OpenDSS object. . . . .	53
2	Implementation of the logic responsible for identifying the PV locations. .	54
3	Implementation of OpenDSS PV System elements. . . . .	55
4	Implementation of OpenDSS Inverter elements with VV Control. . . . .	55
5	Implementation of OpenDSS Inverter elements with VW Control. . . . .	55
6	Implementation of OpenDSS Inverter elements with VV and VW Control.	55
7	Implementation of OpenDSS Monitor elements. . . . .	56
8	Implementation of the daily power flow calculation logic. . . . .	57
9	Implementation of the figure of merits validation logic. . . . .	58
10	Implementation of the HC identification calculation process. . . . .	59
11	Implementation of the logic responsible for executing multiple simulations with different PV allocations. . . . .	59
12	OpenDSS specification of Wire element. . . . .	64
13	OpenDSS specification of Line Geometry element. . . . .	64
14	OpenDSS specification of Line element. . . . .	65
15	OpenDSS specification of Transformer element. . . . .	65
16	OpenDSS specification of LoadShape element. . . . .	66
17	OpenDSS specification of Load element. . . . .	66
18	OpenDSS specification of PV System Curves elements. . . . .	68
19	OpenDSS specification of PV System element. . . . .	69
20	OpenDSS specification of VV and VW XYCurves elements . . . . .	70
21	OpenDSS specification of InvControl element. . . . .	71
22	SQL query implementation responsible for retrieving voltage data from a monitor element. . . . .	115
23	SQL query implementation responsible for defining a store procedure that retrieves inverter controls measurements. . . . .	116



# List of abbreviations and acronyms

BESS	Battery energy storage system
COM	Component Object Model
DER	Distributer energy resources
DG	Depth of Discharge
DLL	Dynamic-link library
DoD	Deth od Discharge
DSO	Distribution System Operator
EES	Electric Energy Storage
EPRI	Electric Power Research Institute
HC	Hosting Capacity
HCC	Hosting Capacity Coefficient
IDE	Integrated development environment
IQR	Interquartile Range
KPI	key performance indicators
LAV	Lower Adjacent Value
Li-Ion	Lithium-Ion
LV	Low voltage
MV	Middle voltage
Ni-Cd	Nickel-Cadmium
NSP	Network Service Providers
OpenDSS	Open Distribution System Simulator



PbA	Lead-Acid
PCC	Point of Common Coupling
PPC	Point of plant control
PU	Per Unit
PV	Photovoltaic
Q1	First Quartile
Q2	Second quartile
Q3	Third Quartile
RDBMS	Relational Database Management System
SQL	Standard Query Language
UAV	Upper Adjacent Value
VV	Volt-Var
VW	Volt-Watt

# Contents

<b>1</b>	<b>Introduction</b>	<b>23</b>
1.1	State-of-the-Art	26
1.2	Objectives	29
1.2.1	General Objectives	29
1.2.2	Specific Objectives	29
1.3	Thesis Structure	29
<b>2</b>	<b>Figure of merits, control strategies, and battery energy storage</b>	<b>31</b>
2.1	HC Definition	32
2.2	Evaluated figures of merit	35
2.3	Voltage Control Strategies	37
2.4	Battery energy storage sizing	40
2.5	BOX PLOT Overview	44
2.6	Final considerations of the chapter	46
<b>3</b>	<b>Developed tool for HC estimation and BESS sizing</b>	<b>47</b>
3.1	Logic and architecture of developed tool	48
3.2	BESS Sizing Process	51
3.3	Implementation Definitions	53
3.3.1	DSS Objective Implementation	53
3.3.2	Implementation of OpenDSS PV and Smart Inverter elements	54
3.3.3	Monitors Implementation	56
3.3.4	Daily Power flow Implementation	57
3.3.5	Evaluation of the figure of merits	57
3.3.6	HC Identification Implementation	58
3.3.7	Simulation Control Implementation	59
3.4	Chapter Conclusion	60
<b>4</b>	<b>Low-Voltage Grid Case Study</b>	<b>61</b>
4.1	Low-Voltage Grid	62
4.1.1	Line Geometry and Wire Elements	64
4.1.2	Line Element	64
4.1.3	PCC Transformer	65
4.1.4	Load Element	65
4.1.5	PVSystem Element	67
4.1.6	InvControl Element	69
4.2	Chapter Conclusion	72
<b>5</b>	<b>Simulation Results</b>	<b>73</b>
5.1	Hosting capacity analysis	74

5.1.1	Baseline Comparison . . . . .	75
5.1.2	Curtailment condition at 15% . . . . .	77
5.1.3	Curtailment condition at 30% . . . . .	78
5.1.4	Curtailment condition at 50% . . . . .	79
5.1.5	Curtailment Condition Comparison . . . . .	80
5.2	Control strategies . . . . .	81
5.2.1	Detailed Control Activation . . . . .	82
5.2.2	Power Loss . . . . .	84
5.2.3	Activation counts . . . . .	86
5.2.4	Activation locations frequency . . . . .	88
5.3	BESS Sizing analysis . . . . .	93
5.3.1	Average BESS Sizing results . . . . .	93
5.3.2	Average BESS KPI results . . . . .	97
5.3.3	HC Results Considering BESS Units . . . . .	100
<b>6</b>	<b>Final considerations and feature works . . . . .</b>	<b>103</b>
6.1	Conclusion . . . . .	103
6.2	Future works . . . . .	105
6.3	Published Articles . . . . .	105
	<b>References . . . . .</b>	<b>107</b>
	<b>Appendix A Database Structure . . . . .</b>	<b>113</b>
	<b>Appendix B Case Study Overview Data . . . . .</b>	<b>117</b>



# Chapter 1

## Introduction

The large number of distributed generators (DG) introduced in electrical grids are overwhelming the systems that, in most cases, are not equipped to handle the amount of energy and power these units produce. The hosting capacity (HC) concept emerged in this context, and it is a metric developed to determine the maximum amount of energy a system can receive without compromising power quality operation. A study conducted by (Torquato et al. [2018]) identified the HC condition for 50,000 LV grids to determine the maximum amount of power each system can receive without compromising power quality standards. The research assessed that saturation occurs in approximately 20-50% of the MV/LV transformer nominal power, leading to voltage and current increases or voltage imbalances if the system operates above this rate. Although other concerns may arise, as described by (Bank [2018]), the aforementioned ones are the most common power quality issues identified in the literature regarding LV systems that operate with high PV penetration.

The authors of (Ustun and Aoto [2019a]) also highlight the adverse impacts of high DER penetration and classify it as a supply security issue caused by the intermittent nature of this primary energy source. The authors evaluate the consequences of using a LV grid with smart inverters aiming to quantify their advantages and disadvantages in long-term incomes. Another study conducted by (Mulenga et al. [2022]) uses two areas in Sweden to quantify the HC value in LV systems with PV penetration. The case study uses a deterministic and stochastic approach to consider the probability of a customer installing a PV unit and the impact it would cause. This analysis assists the author in planning investments and decisions. In another perspective but also associated with a high DER penetration ratio, (Karimi et al. [2016]) quantifies the consequences and identifies the voltage and current rises as grid operation concerns, but considering an island grid case study. Additionally, (Mohammadi and Mehraeen [2017]) measures the adverse effects of high PV penetration on distribution systems, focusing on grid protection and the impact of power quality issues on their operation.

Furthermore, this topic becomes more relevant in the literature as the number of installed DERs increases. Power quality issues often arise due to the mismatch between peak generation, usually during the day, and the low load demand during this period, a characteristic of residential consumers that also results in a reverse power flow. To ensure a consistent power supply to the ~~end-user~~, measurements like voltage, frequency, and waveform are used to identify and address maintenance needs. As an overall analysis and grouping of the advances in this research area, (Ismael et al. [2019]) discusses the HC concept and the consequences of high DG penetration levels in LV systems. The author also argues about possible improvements that could increase the number of generators connected to the grid without causing any problems and focus explicitly on the PV penetration impacts. (Gandhi et al. [2020]) presents the first two-part review covering the consequences on LV grids, detailing the most frequent impacts on power systems and how they limit new PV connections in the grids under these conditions.

Most radial distribution grids were not designed to handle distributed generation configurations. This issue becomes more severe as DER penetration increases in electrical power systems (EPS) across the globe. Standards have been created to centralize the main operation requirements and recommendations for DER interconnection with EPSs to address the lack of uniformity in regulation. These documents focus on operational performance, testing procedures, providing safety considerations, and defining abnormal condition responses for those units. The (IEEE-1547 [2018]) is a standard example widely used around the world, and it divides the DER operation into categories and argues about their operations and characteristics.

The first category group is related to reactive power capability and voltage regulation performance and has two items. Category A is the first and includes the overall inverter used in the power grid, which operates under a unitary power factor and has functionalities like island mode. Category B is the second and covers supplemental capabilities required to integrate the DER unit effectively and the requirements mentioned earlier. Category A is mainly used at low penetration levels with minimum voltage regulation capability, such as constant power factor, constant reactive power, and voltage-reactive power (VV) modes. Category B is associated with higher penetration levels and meets all operation modes from category A, plus active power-reactive and voltage-active power (VW).

Additionally, the second group is related to abnormal conditions and divides the units based on their ability to respond to events. The first of three classifications is category I, which covers the basic needs of the power system's operation and is widely used among the installed DER units. Category II includes standard requirements to prevent tripping and covers more disturbances than the first, but the third category, III, is the most robust and requires coordination with existing interconnections for operation. The

usage pattern remains the same, where simple applications can operate effectively with category I, but as the DER penetration increases, more sophisticated control is necessary, requiring category II or III, depending on the operation levels.

Figure 1 displays the current state of substations in Minas Gerais, shifting the focus from theoretical to practical implications. This figure shows that exceeding HC limits is not a mere concern but a reality within MV/LV grids. All the red squares indicate substations that have already reached their maximum capacity and cannot accommodate additional PV connections without infrastructure reinforcements, representing 79.1% of the total number of substations. Otherwise, the grid in this area may exceed the HC values leading to power quality issues. The orange locations represent the substations that have reached their limits but have planned structural improvements to increase their boundaries, representing 12.2%. The green locations can still receive more PV units, representing 7.5% but with the majority concentrated in the southeastern region of the state, and the gray ones are scheduled to be installed but are not yet operational, only 1.17% of the total number of substations. This information is available publicly on (CEMIG [2023]) ~~and is one of the steps for requesting a new installation.~~

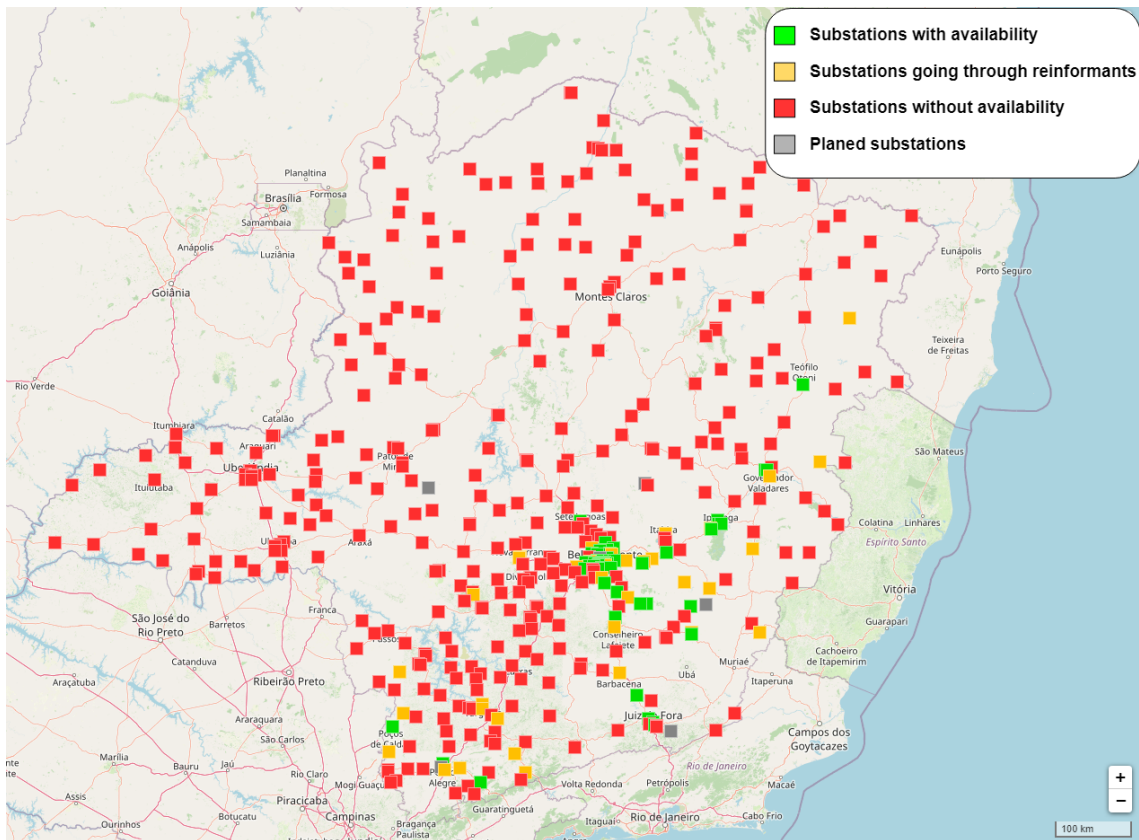


Figure 1 – Distributed generation availability map - Minas Gerais, Brazil.

Source: Adapted from (CEMIG [2023])

## 1.1 State-of-the-Art

While the use of distributed energy resources (DERs) complies with environmental policies by promoting cleaner energy generation, it also assembles new challenges that must be addressed to maximize its potential fully. The most significant issues are the power quality and system reliability, as discussed in the previous section. As a result, various strategies are developed in the literature to address these concerns and enhance grid supportability, thereby enabling more DER units. These new techniques benefit DER owners and network service providers (NSPs).

To improve HC rates, the initial set of resources centers on feeder demand and incorporates strategies such as grid reinforcement. These methods involve increasing the cross-section of the conductor or replacing the transformer with more robust and expensive ones. On-load tap changer transformers are an alternative, although they can produce excessive physical tap changes that increase maintenance costs and failure rates when facing fast voltage fluctuations caused by high PV penetration. Such techniques require high investment, human resources allocated in long-term implementation projects, and also promoting outages to replace the elements, as discussed in a report by (Rajabi and Elphick [2022]).

The authors in (Rajabi and Elphick [2022]) also discuss emerging techniques that have the potential to improve HC rates, including the Thyristor Controlled Reactor (TCR), which provides fast reactive power compensation to manage voltage fluctuation scenarios, static var compensator (SVC), which enhances system operation by controlling reactive power, and the static synchronous compensator (STATCOM), which is a synchronous voltage generator that is connected in parallel to the distribution system and can exchange reactive power. However, these methods only focus on reactive control and generate satisfactory results under a high X/R ratio grid. The LV grids are predominantly but not exclusively low X/R ratio, which requires a solution that can provide a reasonable response for both scenarios.

Another option to consider is utilizing ancillary services to implement voltage control strategies in PV and BESS inverters. This can enhance grid reliability and allow other operation configurations, such as peak-shaving for BESS units. Although it is a promising approach, further standard reexaminations must align it with existing regulations, as discussed in (Gandhi et al. [2020]). Thus, DER inverter control strategies offer a resourceful solution to minimize the power quality concerns in LV grids. It is highly adaptable and can operate with high X/R ratios through volt-var (VV) controlling reactive power and low X/R ratios through active power curtailments from volt-watt (VW) control. However, the former over-stress the feeders, and the latter strategy causes a financial penalty for the end-user.

Furthermore, voltage control strategies have gained significant attention in the literature. Focusing on VV control first, a study by (Luo and Shi [2020a]) examines a scenario where voltage rise is the primary limiting factor in integrating PV elements into a LV grid. The author has analyzed various VV, PF(P), and Q(U) techniques using a generic LV grid model and concludes that implementing the controls can improve the PV average penetration by 38% compared to not using any control, from 36% HC to approximately 50%. The author concludes that this can lead to enhancements in HC and reduce voltage rise occurrences. Moreover, (Ustun and Aoto [2019b]) investigates the potential benefits of smart inverters in distribution networks. It uses a self-developed platform to investigate the operation of those units, concluding by graphic comparisons that the inverters located farther away from the PCC tend to activate control techniques before the ones closer to it. This allows the closer inverters to continue operating at full capacity while the farther ones regulate voltage violations at the end of the grid. Nevertheless, VW control is also often discussed in the literature. The investigation by (Amuna et al. [2021]) evaluates VV and VW controls, comparing the precedence priority between vars and watt, always respecting the generator and inverter limits. The author estimated the effectiveness of the controls using a modified IEEE 13-bus grid and concluded that VV control returned the best results on increasing HC. The study ranked operation outcomes based on the voltage regulation index, which quantifies the results by summing up the absolute values of voltage deviation from the per unit value. Lower index values are better, and reactive power control is approximately twice as effective as active power control and fixed power factors at the same rate. Despite its limitations, the IEEE 1547-2003 standard has made PV units the most commonly used among DG units, but this scenario is changing with the 2018 version.

Additionally, a study by (Bletterie et al. [2016a]) focused on watt power control and compared fixed curtailment with VW control. The findings showed that using a 70% fixed approach resulted in a 6% power reduction, whereas the VW technique only resulted in a 1% reduction. This implies that 5% of the annual energy yield was curtailed unnecessarily in the proposed case study. A consequence of several factors, such as the unbalanced curtailment of single-phase generators and not considering grid conditions like voltage measurements, which curtail power for specific locations that require voltage control. Furthermore, (Liu et al. [2020]) confirmed that power curtailment effectively mitigates technical issues within LV grids with high PV penetration. To compare the VW effectiveness, the authors evaluated different optimal power flow schemes on a real 22 kV feeder in Australia. The optimal approaches removed penalties across PV elements, unlike VW control which favors units closer to the PCC with fewer curtailment occurrences. However, this optimization must be carefully quantified and evaluated to justify its fairness.

Expanding the DER options, there have been numerous studies linking BESS units in the power system operation to enhancing HC value. Like the one developed by (Lee

et al. [2020]), which compares three energy storage configurations while the distribution circuits operate with a central control as a microgrid. The first configuration utilizes a large battery at the substation, a medium-sized community storage along the grid, and a scenario where all customers have a smaller unit. The authors performed financial analysis and observed that community storage was the more economical to enhance HC, even though the increase is slightly lower for the first scenario at 35.4% compared to the individual case at 37.5%, the smaller BESS units required for the first scenario can help reduce installation costs. It was also concluded that substation automation and power control actions could increase penetration levels and achieve higher PV penetration without upgrading the grid infrastructure. However, for achieving a 100% PV penetration, noteworthy grid reinforcements are required. In another study by (Zeraati et al. [2019]), high PV penetration with storage operations was evaluated using plug-in electrical vehicle batteries. The authors proposed combined control techniques to regulate voltage in LV grids, utilizing battery energy to store the active power curtailed by power control strategies. The author mentioned that small storage units could assist grid operation by storing curtailed energy in vehicles. The optimal usage during the assessment occurred at 11:30 a.m., which aligns with peak PV generation, and, according to (Wu et al. [2011]), there is an approximately 50% chance of a vehicle being parked during this period.

Numerous studies have been conducted on reducing power loss caused by VW control curtailment, with some suggesting methods to minimize it. However, few have measured the actual reduction and utilized this information to size a BESS that can help DG owners deal with adverse financial impacts. A theoretical calculation quantifies the amount of energy that would be lost and highlights the potential benefits of incorporating this approach in residential DER applications. Even a slight increase in storage size can significantly impact absorbing the curtailed power. To achieve this goal, this master's thesis evaluates the hosting capacity of a low-voltage distribution grid and assesses the enhancements promoted by the voltage control strategy, such as VV, VW, and VV combined with VW. The VW strategy's active power reduction is quantified and used to size BESS units responsible for absorbing this energy. Key performance indicators of this storage unit are evaluated to contextualize the unit in grid operation, such as likely installation location, size indicators, and battery rate metrics.



## 1.2 Objectives



### 1.2.1 General Objectives

The objective of this master's thesis is to assess the distribution grid HC using a self-developed software architecture that can increase the permissible penetration of PV units while maintaining power quality standards. Voltage control methods are employed to achieve this objective, making it possible to use the results to calculate the theoretical size of BESS units to absorb the energy that would be lost due to active power curtailment.

### 1.2.2 Specific Objectives

To achieve the general goals, the following specific objectives are defined:

- Develop a framework architecture combining software widely used in the industry, such as OpenDSS, Python, and SQL Database.
- Validate the proposed methodology with a case study with a known and validated HC value.
- Evaluate the effectiveness of voltage control strategies, including VV, VW, and a combination of both.
- Determine the suitable size for a BESS unit to capture active power that would be lost during VW control.

## 1.3 Thesis Structure

The current Chapter 1 discusses the motivations behind this study and the state-of-the-art techniques used to enhance HC. It focuses explicitly on voltage control strategies and BESS operations in LV grids. Additionally, this chapter outlines the study's objectives and how this document is organized.

Chapter 2 provides detailed information regarding the essential concepts used in this study. The discussion includes the figures of merit evaluated to define HC conditions for different simulation cases using voltage control strategies. The chapter also covers the equations used in the BESS sizing calculation and explains the box plot analysis, a concept used to display the results.

Chapter 3 presents the methodology defined to identify and analyze the HC conditions based on the definitions presented in Chapter 2. It includes information on the used software, execution logic architecture, and the BESS sizing process.

Chapter 4 outlines the proposed case study grid and the OpenDSS implementation. It presents the grid location and a single-line diagram illustrating the distribution system. The explanations of the variables and elements definitions are also detailed. This chapter aims to provide enough information for the grid to be used in future works.

Chapter 5 discusses the results obtained from the study. It begins with a case study validation, moves forward to the HC analysis for all case simulations, and ends with BESS size results. Average results are presented to establish reliability due to the high sensibility on several aspects like PV location disposition.

Chapter 6 presents comments and final observations related to the findings. It also presents the suggested feature work and considerations regarding the study's next steps. The published papers related to this study are also presented in this chapter.

Lastly, Appendix A explains the database structure used. It details the advantages of using SQL Server to store, process, and retrieve the measured information. Appendix B shows the grid configuration describing the lines, loads, and transformer parameters.



## Chapter 2

# Figure of merits, control strategies, and battery energy storage

This chapter discusses the main concepts used in this master's thesis. It begins by explaining how the HC concept was introduced in the power system studies, followed by describing how it is used to visualize the DG penetration levels in a grid. This chapter also presents the figures of merit used to calculate the HC and explains their impact on the grid. Furthermore, it details methods to improve the HC value, focusing on voltage control strategies and operating with PV elements to enhance performance. The discussion covers the operation of the control method, its effectiveness, and all possible activation conditions.

Although the HC value improves using those techniques, the active power control can lead to disadvantages for the DG owner by reducing the amount of energy delivered to the grid, affecting their incomes. And the increase in current measurements may cause violations in the operation of the feeder elements in the grid. Therefore, a local BESS unit is proposed and sized to absorb the energy that would be lost, injecting it into the grid later. Finally, the box plot concept is introduced, explained, and discussed according to the usage in the results of this thesis. This method is a resourceful method to display data distribution and compare similar groups of information, the related concepts are also detailed further in this chapter.

## 2.1 HC Definition

To fully understand the HC concept, it is important to clarify the operational requirements of a power grid. According to a discussion by (Bollen and Hassan [2011]), these objectives can be divided into two main groups: primary and secondary. Both are critical, but the first focuses on the customer's needs, while the second is related to the Network Service Providers (NSP). Primary objectives include power quality and supply reliability, while secondary objectives focus on the grid's condition, including proper equipment load, protection activation, and energy security operation. Typically, achieving the second aim leads to good metrics for the first, but inserting DG units on the end user side can disturb this balance. They are often intermittent power sources that don't send generation data to the central control system. This lack of information can cause prediction errors that may affect the system's operation, although it is not likely to collapse the system entirely.

The power grid is responsible for transporting electricity from generators to consumers while meeting acceptable performance indicators. These indicators are evaluated based on the primary and secondary aims that assess the overall operation of the grid. However, integrating new energy sources into the system can be challenging because it depends on various factors, such as the grid's characteristics and the properties of the new energy source. A comprehensive review of this subject by (Ismael et al. [2019]) identifies the common difficulties in LV systems, which include feeder and transformer overloads, voltage magnitude variations, and power quality disturbances. Section 2.2 presents more details regarding the figures of merit used, the most frequent difficulties mentioned in the literature.

Considering an overall performance index that tends to decrease as the power quality indicator deteriorates, the reduction is not an issue as long as the operation stays in an acceptable range. The Hosting Capacity concept comes into play in such situations and refers to the amount of distributed generation that can be accommodated before the performance becomes unacceptable. In other words, it measures the power the grid can receive without compromising the operation quality requirement. Figure 2 illustrates this idea by comparing the generation growth with the performance index. As the DG insertion increases, the system operates closer to the unacceptable area until it finally crosses the line. This is known as the HC condition, initially introduced by André Even, nonetheless gained recognition with the publication of (Bollen and Hassan [2011]). A book that provides detailed explanations, demonstrations, and conditions related to the Hosting Capacity concept.

Moreover, in Figure 2, the performance index only represents one electric metric that reaches a forbidden operation area when the DG penetration increases. However, this index can assume several other metrics with different operational limits, such as

voltage, current and imbalance measurements. In this case, the HC condition is the lowest result that reached its limit. This fact highlights the importance of selecting the proper performance indexes to identify a reliable HC condition, as it is not a single calculation based on a fixed amount of variables. For example, suppose three PV units have exceeded the uncontrolled voltage limit, and two have exceeded the uncontrolled current limit. In that case, the grid's HC condition will be determined by the two units that exceeded the current limit, even if the voltage limit was not reached.

To calculate the HC approach, four steps must be taken. Firstly, the performance indicators are the most sensitive metrics when the grid operates at a high DG penetration level, followed by determining the operational limits associated with these indicators. The power flow calculation is the third item and ends with the HC condition. For this study, the performance indicators and their limits are presented in Section 2.2. The HC is determined using Equation 2.1, which involves dividing the sum of all PV active power by the nominal capacity of the PCC transformer that connects the LV with the MV. Detailed information on the HC identification process is shown in Section 3.1 and elements definition in Section 4.1.

Additionally, (Palmitier et al. [2016]) highlights the uncertainty associated with

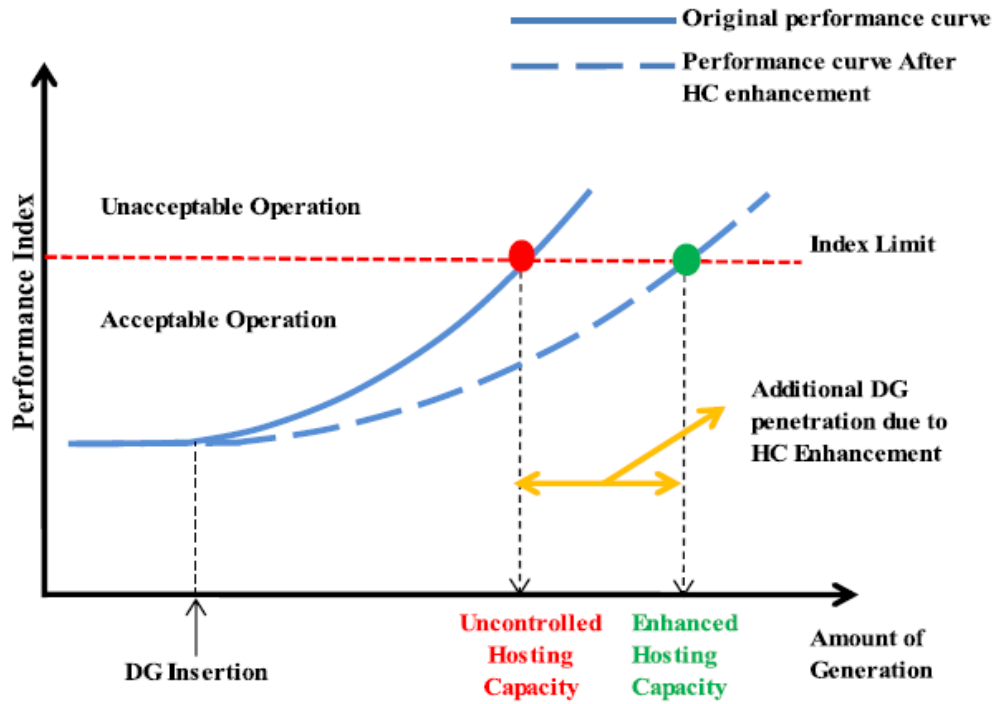


Figure 2 – Performance index as an indicator of operation quality based on the number of generators installed in the grid.

Fonte: (Ismael et al. [2019])

the HC identification process and suggests analyzing the results as a group of data instead of a single value. This approach is adopted in the current study, as explained in the methodology section 3. According to the authors, the HC value is sensitive to the generation installation location, different unit ratings, and the intermittent power source profile.

$$HC(\%) = 100 * \frac{\sum_1^n P_n}{T_{nom}} \quad (2.1)$$

Where (HC%) is the hosting capacity in percentage values, ( $n$ ) represents one PV element, ( $P_n$ ) represents the active power delivered to the grid by a specific element, and ( $T_{nom}$ ) is the nominal power from the MV-LV transformer.

For a more detailed analysis of possible outcomes in the HC, higher values indicate increased DG penetration while still maintaining grid operation. This benefits both generator owners by allowing more DG installations and the NSP by reducing power quality problems. Figure 2 also illustrates this outcome, comparing the original performance curve, solid line, with the performance after HC enhancement, dashed one. This difference represents the added penetration that benefits both groups. This enhancement can be achieved by several options, such as network configuration, voltage control strategies, voltage compensation, energy storage techniques, and restricting new DG installations. However, this study focuses on voltage control strategies to enhance HC values, and a storage system is also sized to absorb curtailed power that would be lost by active power control. Section 2.3 has more information regarding these control techniques.



## 2.2 Evaluated figures of merit

Several factors can affect the HC metric, including the specifications of the LV system, the configuration, and the location of the DG unit. These factors must be considered during investigations to assess HC accurately. Remember that high levels of DG penetration can result in several impacts, such as voltage fluctuations, current rises, and voltage imbalance, which are more probable in an LV grid, as explained in Chapter 1.

The HC value can also vary depending on the regulations in the country where the study is conducted by defining the acceptable operating ranges, like voltage levels, permissive current magnitude, and frequency deviations. (Papathanassiou et al. [2014]) is a valuable resource for comparing these differences as it provides general guidelines for interconnecting DGs into power grids in various countries. Most of those regulations are based on standards that set boundaries that prioritize safety and optimized operation metrics while ensuring that power elements are not sacrificed.

This study considers various factors that affect LV grids and utilizes figures of merit that address common issues to calculate the HC value. These concerns follow the operational limits outlined in PRODIST's module 8 document (Brazilian Elec. Reg. Agency [Set.2020]), which focuses on quality meters in electrical distribution systems. The document establishes several methodologies for obtaining power indicators and establishes reference values to be followed during operation, covering both product and service quality perspectives to ensure smooth operations in LV grids. The study focuses on three main issues identified and consolidated as major issues in LV grids. Detailed descriptions are presented below:

- **Voltage fluctuation:** There are three types of supply conditions: normal, precarious, and critical. To classify the grid operation, Table 1 provides information on the voltage measurement range for each condition. This study considers a voltage violation when the grid operates in precarious conditions for more than 5% of the simulation period.
- **Current violations:** The operational limits of each element are assessed and compared with the current measurement of the corresponding unit. This study considers a voltage violation when the current flowing through the element operates above its current/thermal limit for more than 5% of the simulation period.
- **Voltage imbalance:** The allowable voltage imbalance for LV grids is 3%, considering LV grids. The calculation method used is based on positive and negative sequence voltages, as defined in equation 2.2. This study considers a voltage imbalance violation when equation 2.2 returns values higher than 3% for more than 5% of the simulation period.

Table 1 – Description of the voltage operation ranges.

Operation Condition	Voltage Range Description
Normal Supply	Values between 0.92 pu and 1.05 pu
Precarious Supply	Undervoltage: Values Between 0.86 pu and 0.92 pu Overvoltage: Values between 1.05 pu and 1.06 pu
Critical Supply	Undervoltage: Values smaller than 0.86 pu Overvoltage: Values grater than 1.06 pu

$$UF\% = \frac{V_2}{V_1} * 100 \quad (2.2)$$

Where (UF%) is the voltage unbalance factor, ( $V_1$ ) is the positive sequence voltage, and ( $V_2$ ) is the negative sequence voltage.



## 2.3 Voltage Control Strategies

Exploring the voltage control strategies utilized in the present study, a comprehensive report published by (EPRI [2013]) provides a detailed overview of the functionality of the smart inverters. It aims to help the industry understand inverter features and promote protocol uniformity. While the current study focuses on the VV and VW voltage control strategies, the report covers a wide range of smart inverter controls, such as energy storage operations, PV, and wind power systems, and their use in connection/disconnection functions. Additionally, (IEEE-1547 [2018]) is another standard for distribution resources interconnection and interoperability with the grid. It regulates DERs' operations and specifies requirements to enhance grid operation.

The voltage control technique monitors a specific location where the DG is installed and adjusts the power output in order to maintain performance standards within the limits outlined in Section 2.2. The method used for ensuring voltage and power quality can be effective, but it has potential drawbacks. It may increase the current level due to increased reactive power, impacting grid operation. Additionally, the generator's owner could experience a decrease in revenue, primarily with VW control, as it reduces the amount of energy produced by the unit.

The primary goal of the VV control system is to maintain acceptable voltage profiles by controlling the reactive output power of a PV unit. If the voltage exceeds the upper limit, the control system absorbs power and operates in the inductive zone to reduce the voltage magnitude. On the other hand, if it drops below the lower limit, it injects reactive power into the grid to increase the voltage value and remain within the normal operation limits. Additionally, (Luo and Shi [2020b]) describes configurations like the watt priority, which ensures maximum active power generation when the inverter is operating at its power limit, but VV control requests more reactive power to maintain the voltage grid. Equation 2.3 shows the reactive power limits allowed, which is also adopted in this thesis.

$$Q_{pv} = \pm \sqrt{S_{pv}^2 - P_{pv}^2} \quad (2.3)$$

The behavior of VV control is illustrated in Figure 3. In this control system, the power response is determined by a predefined array of voltage and power references, represented as  $V_n$  and  $Q_n$ , respectively. As the voltage  $V$  changes in terms of pu units, the reactive power follows the solid red line reference. It injects power if the voltage is below  $V_2$  or absorbs power if greater than  $V_4$ . The values between  $V_1$ ,  $V_2$ , and  $V_3$ ,  $V_4$  are calculated using the linearization method based on the reference points, and the semicircle on the left shows the resultant power combination. For instance, considering a voltage value between  $V_1$ ,  $V_2$ , the resultant reactive power is the reflection on the Y-axis, along with the existing active output but respecting the watt priority configuration.

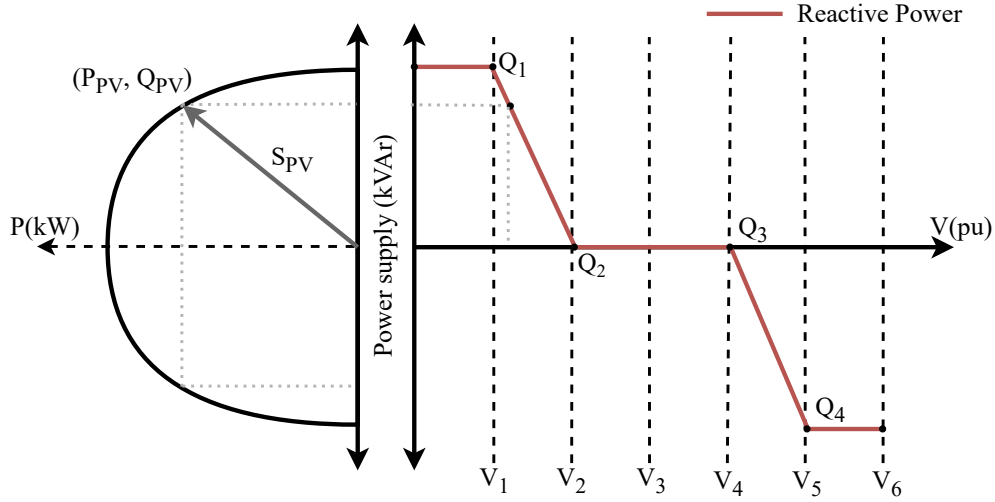


Figure 3 – Illustrative Volt-Var curve.

Source: Author

The primary goal of the VW control system is to maintain acceptable voltage profiles by controlling the active output power of a PV unit. The operation is similar to VV, but it only assesses the upper voltage limit. This function considers a maximum reduction limit which is defined in an input array when creating the inverter element. Consequently, the active power output begins to decrease as the voltage exceeds the threshold value until it reaches the specified curtailment limit or ceases active power generation entirely if allowed. This voltage control technique is efficient when a low X/R grid operates with low demand and high DG generation, which often causes overvoltage violations. In this thesis, the soft curtailment configuration is used, which reduces active power production only in the location where the violation occurs. This concept appeared in (Etherden and Bollen [2014]) and has been noticed by (Bletterie et al. [2016b]) that the soft curtailment reduces the amount of energy loss due to precise control activation compared to the hard curtailment case, which reduces all PV simultaneously.

Figure 4 depicts the control behaviors for both VW and VV. Only two power values are actually necessary for the predefined array that defines the inverter power response,  $P_1$  representing the beginning of the curtailment and  $P_2$  defining the maximum allowed curtailment. Considering both controls, Figure 4 presents an illustrative operation while the following list outlines all possible scenarios and the corresponding power response based on voltage measurement. It should be noted that all voltage limits are established in accordance with Module 8 (Brazilian Elec. Reg. Agency [Set.2020]) to ensure compliance with voltage operation limits. Nonetheless, the VW reduction ratio is not a static value in this study, and this definition will be discussed further in Section 3.1, which also presents the threshold for each control and the different active power curtailment levels analyzed.



- $V_{reg} < V1$ : Supply maximum active and reactive power.
- $V1 < V_{reg} < V2$ : Supply maximum active power and absorb a fraction of reactive.
- $V2 < V_{reg} < V3$ : Supply maximum active power only.
- $V3 < V_{reg} < V4$ : Supply maximum active power only.
- $V4 < V_{reg} < V5$ : Supply maximum active power and absorb a fraction of reactive.
- $V5 < V_{reg} < V6$ : Supply a fraction of active power and absorb maximum reactive.
- $V_{reg} > V6$ : Supply a fraction of active power and absorb maximum reactive.

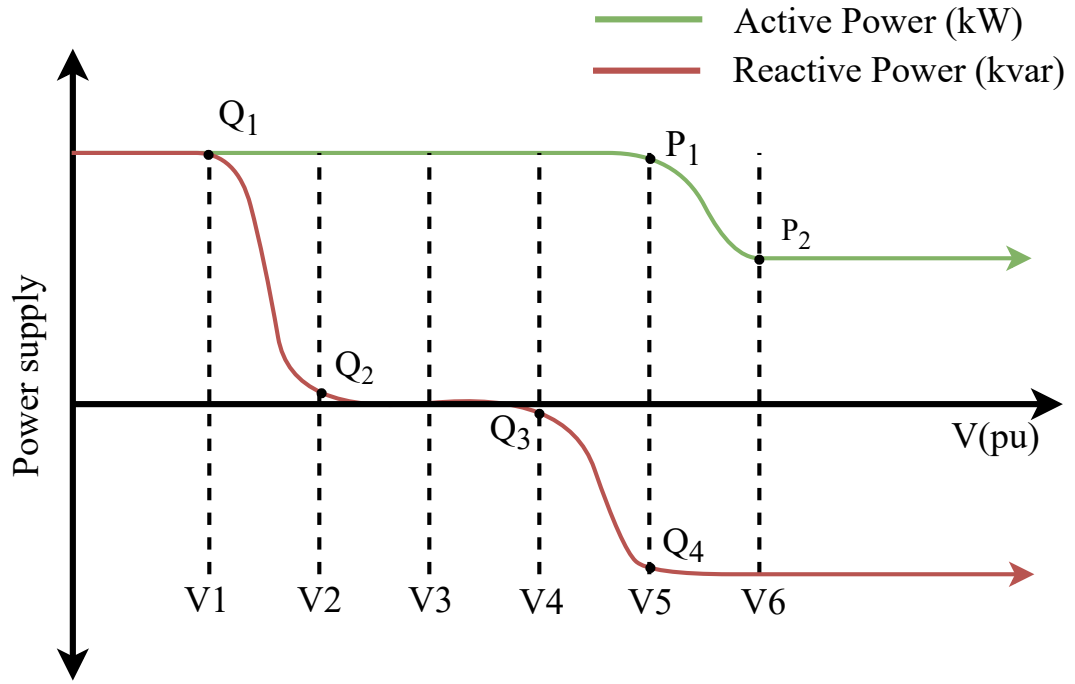


Figure 4 – Illustrative *Volt-Var* and *Volt-Watt* curve.

Source: Author

Both control strategies aim to improve PV efficiency by maintaining voltage stability within specific limits. However, the metric that evaluates the activation frequency is based on the number of times control is activated per PV element. For example, if a bus is selected ten times to receive a PV element but only six require voltage regulation, the final count would be six. This concept is designed to identify which buses in the grid are more vulnerable to electrical violations and how often require control to support the operation, the proposed analysis in this study is presented in Section 5.2,

## 2.4 Battery energy storage sizing

Electric energy storage (EES) refers to a system that can convert electrical power into a secondary form of energy, store it, and then convert it back into electricity when needed. This includes applications such as Pumped Hydro (PHS), flywheels, supercapacitors, and batteries, but they have distinct power ranges and are suitable for different specific applications. Figure 5 shows the type associated with the respective power requirement range and their proposes. It's important to note that there is no one-size-fits-all solution for energy storage that covers all scenarios. Narrowing down the scope of the analysis, this thesis focuses on end-user applications operating around 10kW of power requirement level *considering a duration varying from minutes to days*, making the Battery element the most suitable option as marked in Figure 5 with the red squares.

Before diving into the BESS types, some considerations must be pondered before choosing the battery for a specific application. First, the voltage operation, load profile, temperature requirements, service life duration, physical limitations related to the installation location, safety, and cost must all be considered, according to (David Linden [2002]).

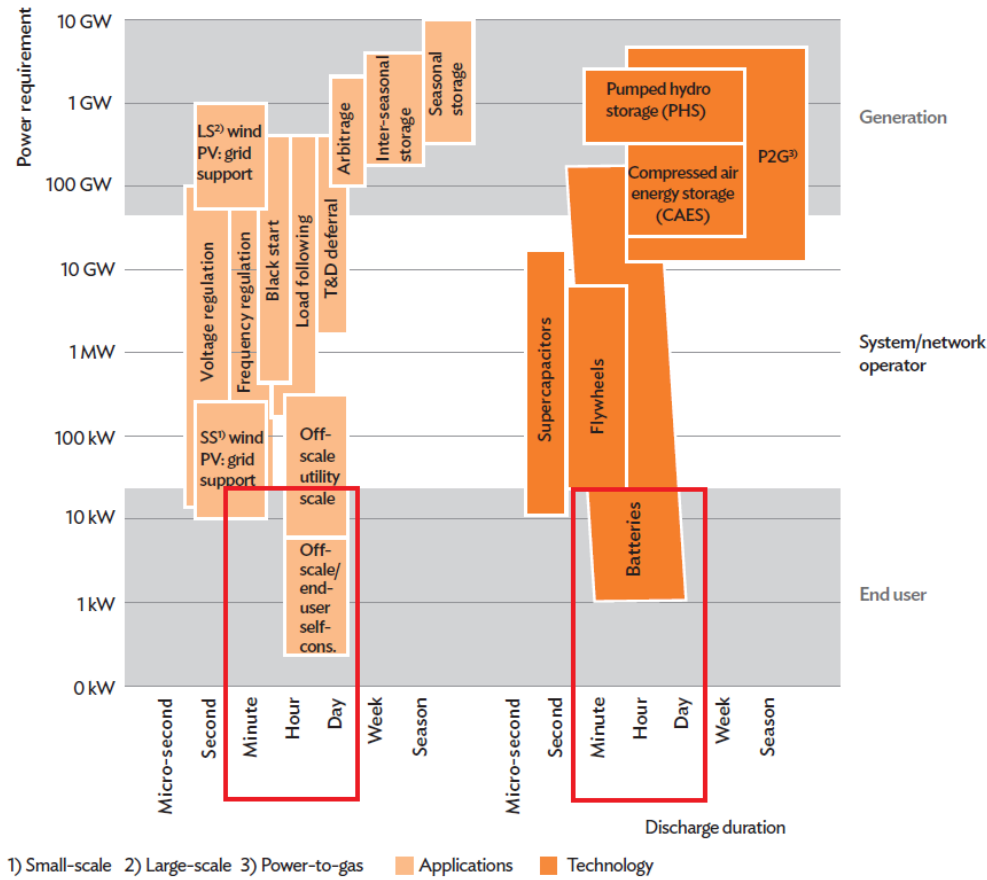


Figure 5 – Storage technologies association to their applicability.

Source: Adapted from (Bank [2018])

Once these factors are estimated, the battery requirements should meet the application's energy density, specific energy, and specific power needs. By definition, energy density is the amount of energy stored per unit of volume or mass measured in Watthour/Liter ( $Wh/L$ ), while specific energy refers to the amount of energy stored per unit of mass measured in Watthour/kilogram ( $Wh/kg$ ), and maximum power is the peak power that must be delivered to the grid measured in Watts ( $W$ ). Finally, specific power is the maximum power the battery can deliver per unit of mass measured in Watts/kilogram ( $W/kg$ ).

For a detailed description of BESS definitions, please refer to (Bank [2018]) and (David Linden [2002]), which cover various aspects of batteries, including chemistry reactions, applications, and usages within the power grid. Here's a quick overview list of the available battery types:

- Lead-Acid (PbA) is commonly used in vehicles due to its ability to handle high load current with low capital investment. Although it is a mature technology, it has low specific power.
- Nickel-Cadmium (Ni-Cd) has the lowest cost per cycle and is frequently used in portable computers. However, it has low specific energy and memory effects, so it must be fully discharged periodically.
- Nickel-Metal Hydride (Ni-MH) is an improved version of Ni-Cd that replaces the toxic cadmium with metal, resulting in higher energy density and less voltage depression. However, it has a limited discharge current, which reduces its life when discharging with high load currents.
- Lithium-Ion (Li-Ion) is widely used in electronics and has the highest energy density with no memory effects, like Ni-Cd. However, it requires special protection to prevent thermal degradation at high temperatures.

Several battery types are available and, according to (Zubi et al. [2018]), Li-Ion is the most promising option for operating in the electrical grid. The author argues that this technology may gain market share as the cost barrier is reduced. The benefits associated with Li-Ion technology include high energy density improved efficiency in the charging/discharging process, and a longer lifespan. However, safety is a concern with this technology due to the presence of lithium, oxygen, and flammable electrolytes, but this issue is being extensively investigated in the literature.

The following equations determine the size requirements for each BESS unit. The first, Equation 2.4, identifies the maximum power capacity that the unit has utilized during the day, and this value is referred to as  $BESS_{MaxPower}$  in ( $kW$ ). The second, Equation 2.5, determines the unadjusted capacity, which results in the theoretical energy requirement

based exclusively on power consumption over time. The battery factors and adjustments are incorporated in Equation 2.6, where the Depth of Discharge (DoD) and battery efficiency factors are applied to calculate the adjusted capacity. The voltage operation value is included in the denominator to calculate the adjusted capacity based on current values. However, in this thesis, we are using the metric of  $kWh$  instead of  $Ah$ , and the reference values of Li-ion battery type are considered to determine the size of the BESS unit since it is one of the most promising options for power systems.

$$BESS_{MaxPower} = \max\{PV_{power}[i]\} \quad (2.4)$$

$$BESS_{Power}[kWh] = \sum_0^N Power(N)[kW] * Duration(H) \quad (2.5)$$

$$BESS_{Capacity}[kWh] = \frac{BESS_{Power}[kW]}{DoD[\%] * Eff[\%]} \quad (2.6)$$

Where  $BESS_{MaxPower}$  refers to the energy that would be lost by VW control limiting the PV active power output.  $PV_{power}[i]$  refers to the highest amount of power PV can be generated at a particular time of day (i).  $BESS_{Power}$  represents the unadjusted capacity without including the DoD and efficiency coefficients.  $BESS_{Capacity}$  represents the adjusted capacity, considering the coefficients.  $Duration$  is the interval between samples.  $DoD$  is the allowable depth of charge. And  $Eff$  is the battery efficiency.

The size metrics for a BESS unit operating with a PV generator are determined by  $BESS_{Power}$  and  $BESS_{Capacity}$ . Moreover, the sizing process is presented based on several works in the literature, including the handbooks (Bank [2018]) and (David Linden [2002]), a Lead-Aid IEEE standard (IEEE-1547 [2018]), and papers that also appeared in Chapter 1 like (Ma et al. [2014a]), (Bhoye and Sharma [2014]), and (Ma et al. [2014b]). These sources use a similar formulation to size the BESS in their studies, and they also cover the number of cells in series and parallel. However, this thesis doesn't calculate the number of cells in series and parallel because the focus is on evaluating the battery requirements to reduce power loss with active power control strategies and regulate voltage levels within acceptable operation.

Additionally, the metrics are compared to the PV unit's output power, resulting in four essential performance indicators. The first one is the E-rate, determined by Equation 2.7, and evaluates how fast the battery is charged or discharged. It can affect the BESS lifetime when operating with higher paces, as discussed in (David Linden [2002]).

The second indicator looks at the PV component. It calculates the ratio between the maximum battery power and the maximum power produced by the PV unit. This generates a percentage outcome, and the calculation method is described in Equation 2.8.

The end results create a correlation between the energy storage system and the actual energy generation, comparing the size of the element designed to absorb the extra energy that would be lost by VW curtailment.

The third indicator assesses the hosting capacity coefficient (HCC). It measures the energy that needs to be curtailed through VW control divided by the capacity above the initial HC result operating without any control. As discussed in (Etherden et al. [2015]), Equation 2.9 is responsible for calculating this metric, a valuable tool to evaluate the improvement brought by the curtailment. Higher values indicate excessive curtailment without much increase in the overall grid HC, which is unfavorable for investors since much power is lost without significant gains. Conversely, small values can mean a slight power reduction, demonstrating that the VW was inefficient. However, it could also indicate a significant improvement in HC due to a slight curtailment. In conclusion, it is a resourceful metric but must not be analyzed alone, requiring context and extra parameters to extract the correct coefficient analysis.

The fourth indicator is closely tied to the size of the PV system. However, it is included with the other KPIs since it affects the associated BESS. This metric compares the PV system's energy output with the consumer's demand. Equation 2.10 outlines the calculation for this metric, which provides insight into the power supply ratio, highlighting the demand covered by DG operations in a daily operation. However, it is essential to note that there is a discrepancy between the peak times of PV generation, which occur in the middle of the day, and the distribution grid load profile, which typically sees peak demand from residential customers at the start of the night.

$$E - rate = \frac{BESS_{MaxPower}[kW]}{BESS_{Capacity}[kWh]} \quad (2.7)$$

$$BessPVRatio = \frac{BESS_{MaxPower}[kW]}{PV_{Power}[kW]} \quad (2.8)$$

$$HCC(\%) = \frac{Energy\ to\ be\ curtailed}{Energy\ Above\ Initial\ HC} \quad (2.9)$$

$$PVLoadRatio(\%) = \frac{\sum S_{PV}}{\sum S_L} \quad (2.10)$$

Where the E-rate represents the BESS discharge rate.  $PV_{Power}$  represents the active PV power reference.  $BessPVratio$  represents the ratio between BESS and PV maximum power.  $S_{PV}$  represents the energy from PV elements. And  $S_L$  represents the energy from Load elements.



## 2.5 BOX PLOT Overview

The box plot is a resourceful method to visualize and compare different data groups, highlighting the distribution shape, the average result, the median sample, and the dispersion of the data set. (Cleveland [1993]) is a book about data visualization techniques, including boxplots. It explores the theoretical definition of the concept with different usages and examples applied in data analysis. However, (McKinney [2017]) gives a more practical approach for this technique using the Pandas library and Python program language, the same tools used to develop this study.

For a better understanding of this concept, Figure 6 illustrates the technique, and a list of specific concepts is presented below:

- **Quartiles:** A fraction value is used as a reference to help visualize distributions is divides the dataset into equal fractions. In this case, three quartiles are used to divide the samples into four equal sections with 25% of the samples on each one of them.
- **Median:** Represented by a dashed line, it is the center of the distribution. Also considered as second quartile (Q2).
- **Average:** Represented by a solid line, it is the average distribution value.
- **First Quartile (Q1) :** Represents the median from the dataset starting in the first sample until Q2.
- **Third Quartile (Q3):** Represents the median from the dataset starting in Q2 until the last sample within the quartiles.
- **Interquartile Range (IQR):** Represents the range between Q1 and Q3, half of the samples are inside this rectangular box.
- **Upper Adjacent Value (UAV):** Represents the largest value that could be smaller than or equal to  $(Q3 + 1.5 \times IQR)$ .
- **Lower Adjacent Value (LAV):** Represents the smallest value that could be greater than or equal to  $(Q1 - 1.5 \times IQR)$ .
- **Whiskers:** Represents the IQR outside range until UAV or LAV value.
- **Outliers:** Represented by a circular point, these are values beyond the whiskers range, more than 1.5 times IQR range. However, it provides information regarding the distribution shape and highlights that it does not follow most of the group.

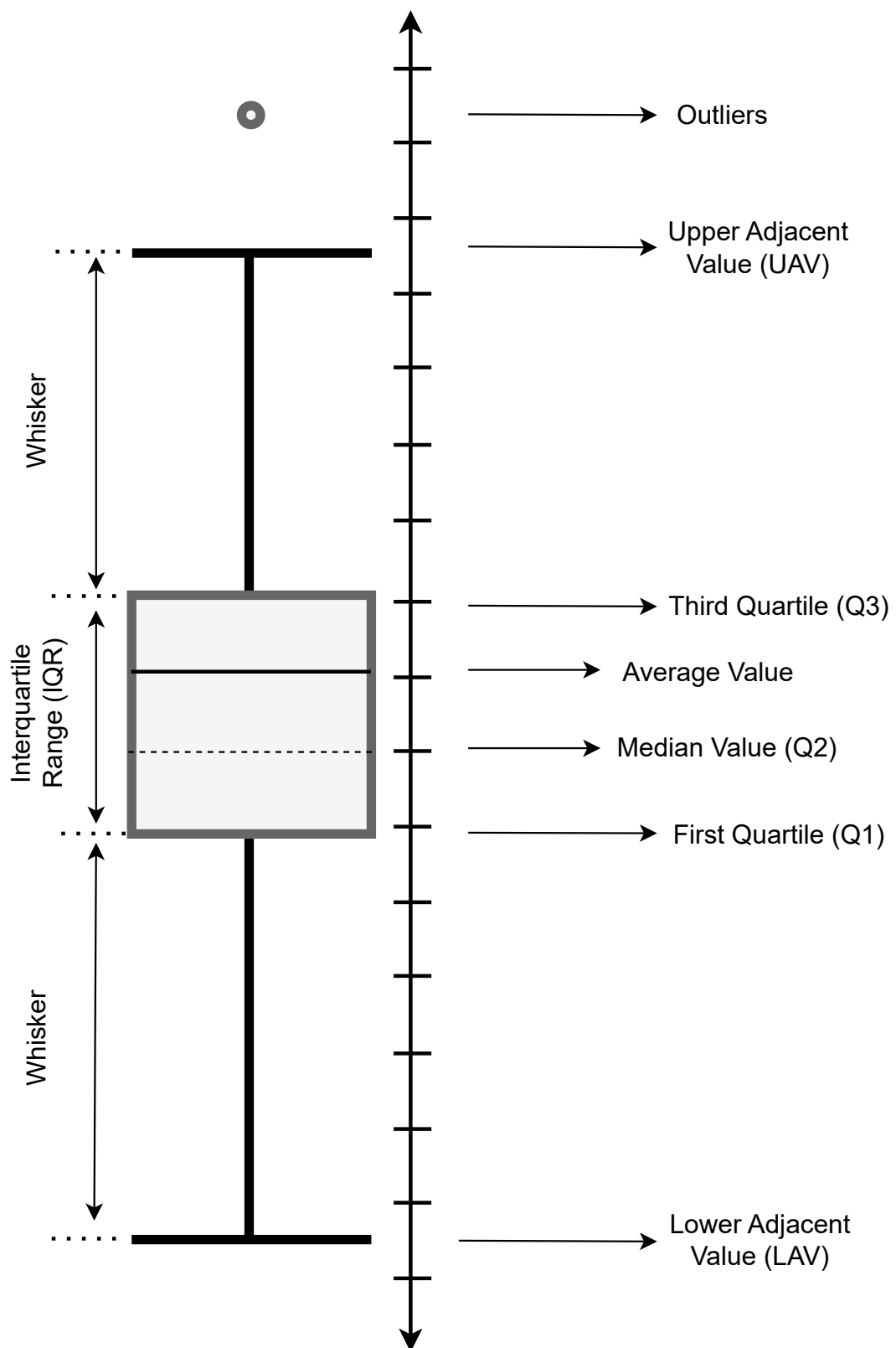


Figure 6 – Boxplot example and concepts.

Source: Author

Furthermore, the box plot interpretation can offer valuable insights related to the dataset, and the book (Bruce and Bruce [2020]) explores these concepts, among other topics. As an example, the symmetry of the dataset, also known as skewness, provides resourceful information about how the results are distributed along the result range, Figure 7 illustrates this concept. The normal distribution scenario happens when the median value is almost in the middle, and the whiskers are about the same length on both sides, Figure 7b. However, it can also display skewness when the median is closer to one of the quartiles, Q1 or Q3. Skewed right or positive skew when the median is closer to the bottom, Figure 7c, and skewed left or negative skew when closer to the top, Figure 7a.

In addition, the dispersion can also be evaluated by analyzing the IQR, which captures the range where 50% of the samples are concentrated. It is calculated as the difference between the third and first quartile  $Q3 - Q1$ . A smaller IQR implies uniformity within the data set. The opposite interpretation for larger IQR indicates variability.

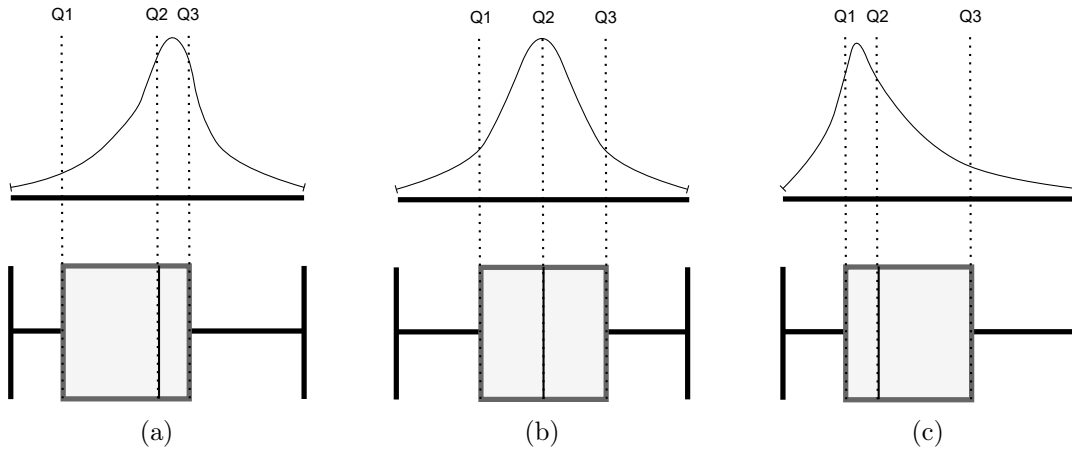


Figure 7 – Box plot skewness: (a) Skewed left; (b) Symmetric data set; (c) Skewed right.

Source: Author

## 2.6 Final considerations of the chapter

This chapter explores the key concepts in developing the HC identification approach outlined in this study. To start, it defines the HC concept based on quality issues, identifying potential violations that may occur due to high PV penetration in the LV grid. It also establishes the limits of the figure of merits and presents all necessary considerations for calculating the maximum power the distribution grid can handle. It also discusses the pros and cons of these techniques and suggests a feasible solution, which involves storing curtailed energy in a BESS unit to reduce loss for the DG owner. In this analysis, present BESS element concepts and describe available technologies. Finally, it defines a term used in the results, enhancing the comprehensibility of Chapter 5 by describing how each data group is presented.



## Chapter 3

# Developed tool for HC estimation and BESS sizing

This chapter provides a detailed explanation of the methodology used in this study. The first topic covered is the Python logic that takes the OpenDSS grid definition as input and uses it as a starting point for simulations in all possible case scenarios. A flowchart is presented, which outlines the OpenDSS definition, the proposed logic, and the database interaction used to store and process data. The database iteration is extensively used in the final step of the execution, utilizing SQL Server functionalities to generate the analysis presented in [Chapter 5](#).

Additionally, the BESS sizing logic is discussed in this chapter, focusing on logical execution and overall implementation. Further details on how data is extracted from the database are provided in [Appendix A](#). The chapter ends with a detailed discussion of the Python implementation, which aims to present the core concepts of the proposed logic, increase the comprehensibility of this work, and facilitate the implementation of future studies that may use this document as a reference.

### 3.1 Logic and architecture of developed tool

The logic developed to evaluate the grid under HC conditions and the proposed software architecture is presented in Figure 8, a workflow diagram illustrating all the important details regarding this process. The proposed solution uses three different platforms, which are OpenDSS, SQL Server, and Python, represented in pink, blue, and yellow, respectively. The OpenDSS is a resourceful open-source software tool for simulating and analyzing power distribution systems developed by the Electric Power Research Institute (EPRI). SQL Server is a relational database management system (RDBMS) widely used for managing and storing structured data in a robust, efficient, and scalable way developed by Microsoft. Python is a high-level programming language with extensive libraries and frameworks that make the development process robust.

As software versions, the results were generated using OpenDSS version 9.6.1.2, SQL Server 2017, and Python 3.10. As specific libraries, the py-dss-interface is a Python-OpenDSS interface that explores the official OpenDSS version functionalities without installing it. (Radatz [2023]) has detailed information regarding this package. Moreover, for data manipulation, this project uses the Pandas library (McKinney et al. [2023]), another powerful and flexible open-source tool. The intercommunication between Python and the database uses the *open-source SQLAlchemy library developed by* (Bayer et al. [2023]), an object-relational mapper that gives application developers access to SQL functionalities using Python.

Before detailing the workflows, the simulation and case concepts are frequently used in this study and are worth highlighting for better understanding and easy checkpoint. They are defined in the list below, along with each case scenario definition:

- **Simulation:** represents a unique randomly selected group of PV locations, which is evaluated for all proposed cases.
- **Case:** represents a unique voltage control scenario associated with a simulation configuration under test.
  - **Case 1:** Simulates without PV units, it generates the base grid operation result.
  - **Case 2:** Simulates with PV units but without any control, it generates the baseline HC condition.
  - **Case 3:** Simulates with PV units and VV control, it generates the HC condition controlling only the reactive power.
  - **Case 4:** Simulates with PV units and VW control, it generates the HC condition controlling only the active power.
  - **Case 5:** Simulates with PV units, VV and VW control, it generates the HC condition controlling both the reactive and active powers.

The execution flow starts with the grid definition, described in section 4, as input variables to the logic in Python. The first pink square from Figure 8 represents the first communication between Python and OpenDSS to define all grid elements and associated curves. Moreover, it compares the simulation number with the predefined amounts to be performed and moves forward if smaller. Otherwise, the execution triggers the data processing, which will be explained later in this section. In summary, the execution process evaluates three different curtailment levels for the VW control, 15%, 30%, and 50% active reduction, under 150 simulations of distinct arrangements for all proposed case scenarios.

Furthermore, the first step inside the Simulation loop covers the PV installation location definition. This study assumes a 20% PV penetration ratio, based on the number of consumers, rounded up if it returns decimal values. The PVSystem definition command is automatically adjusted to follow the phase of the chosen bus and also associates a unique InvControl element to make the voltage strategy controls independent from each other. All configurations set, the analysis begins with Case 1, which executes only once because there is no power increase, it just collects grid operation data. The other Case scenarios also start with no PV generation, but it increases after each power flow if no violation occurs, the increase ratio is equal to 1.5% of the nominal MV-LV transformer power in the PCC connection. If the violation check returns true, the logic will reduce the PV reference power by the same ratio and save these results in the database as HC condition. This procedure repeats for all Cases and all Simulations until everything is processed.

The last execution step is called data processing. The data comes from monitors from OpenDSS, which collects electrical metrics every 15 minutes for all elements in the grid. Only the HC condition is saved in the database, and the power flows in between are deleted due to the small informational value associated with it. The amount of storage data may change depending on the application but in terms of numbers, each simulation collects around 1.5 million records considering all case scenarios.

Moreover, the beginning of the data processing step changes the database operation from transnational to analytical. In other words, it will not receive new measurements, but calculations and arrangements with the existing data will start. The PVSystem active and reactive data are the first to be extracted and used to calculate the HC values for each simulation case, following the procedure described in Section 2.1. Based on HC results, the statistical analysis is performed and saved in the database to be presented in section 5.1. Detailing the PV system operation, a group of store procedures creates two tables that associate electrical metrics to their respective element for each case in each simulation, focusing on voltage control activation and power measurements. It generates the results presented in Section 5.2. Another group of procedures processes all power data samples to identify the power that would be lost by VW control and, with that, performs the BESS sizing procedure described in Section 2.4.

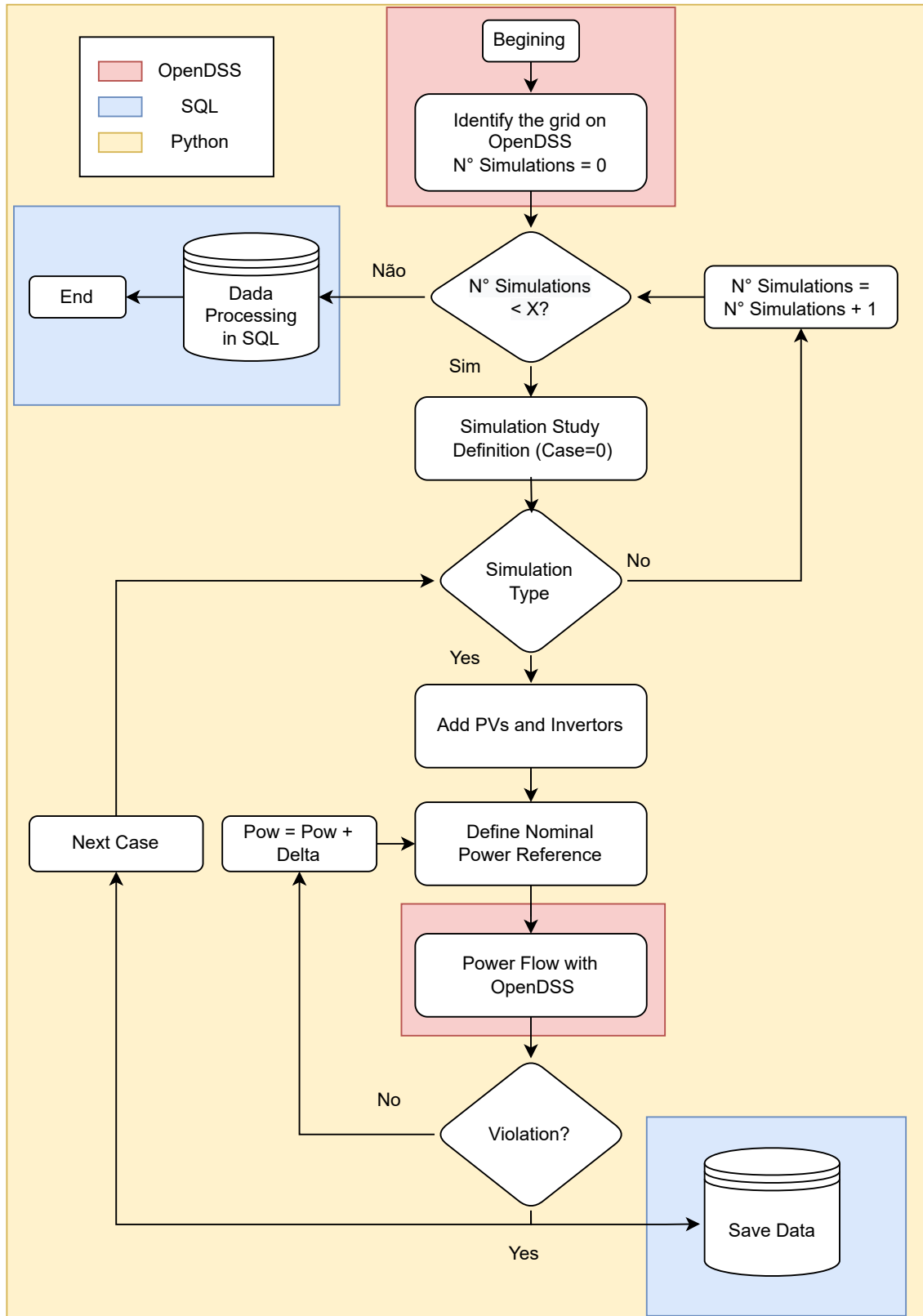


Figure 8 – Flowchart of the developed tool using multiple software to estimate the HC value and size of the distributed small BESS units.

Source: Author

## 3.2 BESS Sizing Process

The BESS sizing process starts by measuring specific electrical metrics for each PV element, such as active and reactive power values. As described in Section 3.1, each unit has a monitor associated with it and collects data every 15 minutes during a daily simulation. These metrics are transferred to the database, as explained in Appendix A, and prepared to be processed by four different store procedures. Together, they are responsible for the BESS sizing calculation, based on the process described in Section 2.4, and evaluate the energy that would be lost with active power control, for the VW case and also for the combined control operation.

Examining the stored procedures in detail, the first one creates an entity relating all power data for each element based on the monitor data table. This table holds the measurements for all active elements operating in the proposed case study. It is presented at the beginning of the diagram, on the left side, and the logic filters this table, searching for active power measurements associated with PV system elements. At this stage, each record is related to its own phase because it is the method employed by the monitor element to store data. A single table with all active power measurements is created as an outcome of this first store procedure, it evaluates the values for both cases that use VW control.

The second store procedure uses the resulting table as a starting point to calculate the 3-phase power for each PV unit, considering each simulation case scenario. A second table is created to store this information and be used as the data source for the third procedure, responsible for the energy calculation. It follows the procedure defined in Section 2.4 to calculate the unadjusted battery capacity based on 3-phase power measurements and the time between each sample. This procedure also creates a new table in the database, relating the energy results to the respective PV unit.

The fourth procedure is the one responsible for the sizing process. It utilizes the previous resulting tables as input and provides the BESS size power and adjusted capacity as a result. This store procedure defines a temporary table summarizing the timestamps operation values employed in the previous procedures into daily-based results. Moreover, the DoD and the efficiency factor are applied to the unadjusted capacity, as described in Section 2.4 and with the magnitude of 0.80 and 0.98 respectively. Resulting in the adjusted values used as the final energy requirement for the BESS unit, along with the maximum active power measurement registered.

As a result, the procedure creates a fourth table to exhibit the calculated BESS requirements based on all elements for all simulation cases that include the VW control strategy. To illustrate this process and enhance comprehension, Figure 9 presents each store procedure and its resulting table with a small description of its findings. As explained

in Appendix A, table tblMonitorData holds all the measurement data from the monitors, and it is the data source used to start the sizing process. Thus, the first procedure retrieves power data from the specified table and operates as a data source for the next procedure, it also saves the processed data into a new table. This process repeats until reaching the fourth procedure, saving the BEES size findings in a new table. The table content description is also shown in Figure 9, providing an illustration regarding the process described in this section.

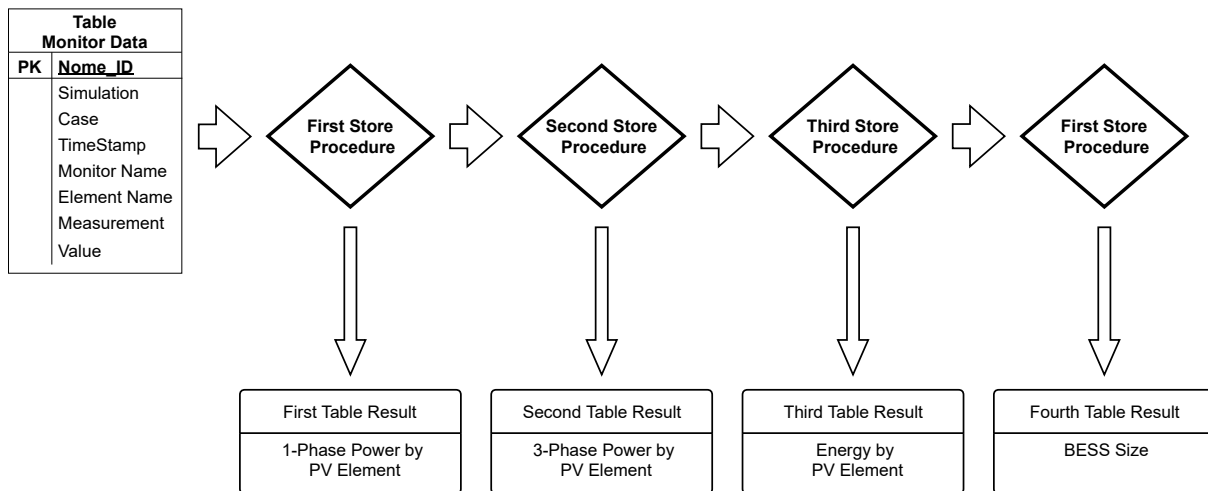


Figure 9 – BESS Sizing store procedure illustration.

Source: Author



### 3.3 Implementation Definitions

This section presents the implementation process responsible for the HC identification logic. The discussion focuses on Python logic and provides an overview of the process without getting into the specifics of the code, aiming to enhance the overall understanding of the process. However, the code is available in the following GIT repository: <https://github.com/HugorTorquato/Projeto-Mestrado>. Additionally, the discussion starts with the specific implementations and gradually expands until it reaches the full identification process.

The individual implementation begins with the OpenDSS object, used throughout the code to access OpenDSS functionalities. It proceeds to the PV and smart inverter implementation, covering all potential control definitions, as well as the monitor elements responsible for collecting electrical measurements. These measurements are used in the figure of merit validation step and are also transferred to the database when an HC condition is identified.

Moreover, the general perspective of the HC identification process is detailed, showing how the code covers all proposed cases, associating all elements into the case study, and solving the daily power flow. Finally, the loop responsible for defining the number of simulations required to identify the PV unit distribution and current limits is presented. This loop connects all the previous implementations, following the workflow backward. The purpose of this section is to improve comprehension of the study and facilitate the implementation of studies that may use this document as a reference.

#### 3.3.1 DSS Objective Implementation

The OpenDSS object is commonly referenced in this implementation and uses the `py_dss_interface` library. It enables developers to conduct studies by creating a local OpenDSS instance, bypassing the need for communication between OpenDSS and Python. It improves performance and makes work easier. The code in Algorithm 1 demonstrates how it is utilized in this study. The first step is to import the library, followed by defining and compiling the Rede2 as an OpenDSS objective associated with the case study grid. This objective definition is crucial because other logic requires a case study to be executed.

---

**Algorithm 1** Implementation of OpenDSS object.

---

```
...
import py_dss_interface

Rede2 = py_dss_interface.DSSDLL() # Opendss object
Rede2.text("compile " + Rede_Path + "\Master.dss")
...
```

---

### 3.3.2 Implementation of OpenDSS PV and Smart Inverter elements

The Algorithm 2 presents the process of defining the PV location. This involves identifying the bus names where load elements are present and creating a list of potential choices that include all of them. **This method determines voltage operation, conversion for reference power adjustment, and phase definition for PV installation based on the selected bus.** The selection decision is based on the HC identification of a residential neighborhood in which consumers are responsible for generating PV energy. Furthermore, to introduce variability in the analysis, a random "choice" method is used. This is crucial as the study evaluates 150 simulations with five cases each, resulting in 150 different PV distributions. It's important to note that the configuration remains constant for case evaluation but changes for each simulation execution.

---

**Algorithm 2** Implementation of the logic responsible for identifying the PV locations.

---

```

...
def FindBusGD(Rede2, Num_GDs):
    vet_choice = GetAllLoadsBusNames(Rede2)
    for i in range(Num_GDs):
        choice = random2.choice(vet_choice)
        vet_choice.remove(choice) if choice in vet_choice else 0
        Barras_GDs.append(choice)
    ...

```

---

After determining the PV locations, Algorithm 3 details how to implement the PV unit. This process involves configuring each element individually, as explained in Subsection 4.1.5, which covers all the relevant parameters and considerations. The same method also defines the associated inverter and its configuration, although this may differ depending on the control strategy employed. Algorithm 4 outlines VV control, Algorithm 5 outlines VW control, and Algorithm 6 outlines the combined operation of both controls. The primary difference lies in the specific reference curve that defines the voltage response and calibration metrics associated with the control conversion accuracy, please refer to (Paulo Radatz and Peppanen [2020]) for detailed information regarding these metrics.

Section 3.3.4 contains the power flows calculation implementation, which includes the "Add\_PVs" method. This particular logic is responsible for assigning the necessary load shape to each PV unit, defining the voltage control curves used by the inverters, and invoking the "Create\_PV" method, which is comprehensively described in the current subsection.



**Algorithm 3** Implementation of OpenDSS PV System elements.

---

```

...
def Create_PV(Rede2, Name, Pmp, FP, Irrad, Temp, Case):
    Command = "New PVSystem." + Name + " phases=" + \
        str(Identify_Phases1) + \
        " bus1=" + str(DF_PV.loc[index, 'Bus']) + \
        str(Identify_Phases0) + " Pmpp=" + str(Pmp) + \
        " kv=" + str(kvbase) + " kVA=" + str(Pmp) + \
        " con=wye EffCurve=Eff" + \
        "%Cutin=0.1 %cutout=0.1 P-TCurve=FactorPVsT" + \
        " pf=1 VarFollowInverter=true" + \
        " irradiance=" + str(Const_Irrad) + \
        " temperature=" + str(Const_Temp) + \
        " daily=irrad Tdaily=Temp wattpriority=yes"
    Rede2.text(Command)
...

```

---

**Algorithm 4** Implementation of OpenDSS Inverter elements with VV Control.

---

```

...
Command ="New InvControl.InvPVCtrl_" + Nome + " DERList=PVSystem." + \
    Name + " mode=VOLTVAR voltage_curvex_ref=rated" + \
    " vvc_curve1=vv_curve " \
    " varchangetolerance=0.5 voltagechangetolerance=0.01" + \
    " deltaQ_factor=-1 RefReactivePower=VARAVAL" + \
    " monVoltageCalc=AVG"# EventLog=yes"
Rede2.text(Command)
...

```

---

**Algorithm 5** Implementation of OpenDSS Inverter elements with VW Control.

---

```

...
Command ="New InvControl.InvPVCtrl_" + Nome + " DERList=PVSystem." + \
    Name + " mode=VOLTWATT voltage_curvex_ref=rated" + \
    " voltwatt_curve=vw_curve DeltaP_factor=-1" + \
    " VoltwattYAxis=PAVAILABLEPU " + \
    " varchangetolerance=0.5 voltagechangetolerance=0.01" + \
    " monVoltageCalc=AVG"# EventLog=yes"
Rede2.text(Command)
...

```

---

**Algorithm 6** Implementation of OpenDSS Inverter elements with VV and VW Control.

---

```

...
Command ="New InvControl.InvPVCtrl_" + Nome + " DERList=PVSystem." + \
    Name + " Combimode=VV_VW voltage_curvex_ref=rated" \
    " vvc_curve1=vv_curve" + \
    " deltaQ_factor=-1 RefReactivePower=VARAVAL" \
    " voltwatt_curve=vw_curve DeltaP_factor=-1" \
    " VoltwattYAxis=PAVAILABLEPU " + \
    " varchangetolerance=0.5 voltagechangetolerance=0.01" + \
    " monVoltageCalc=AVG"# EventLog=yes"
Rede2.text(Command)
...

```

---

### 3.3.3 Monitors Implementation

Algorithm 7 outlines the implementation of each component of the monitor element in two parts. The first is the "Add\_Monitors" method, which serves as the entry point for this logic. It groups all element names into an array to be used as a parameter for the second method named "Define\_Monitors", which associates three monitors with each array item. The first monitor collects power metrics using mode 1, the second collects voltage and current measurements using mode 0, and the third collects power loss for the associated equipment using mode 9.

As implementation considerations, the monitor mode values are predefined in OpenDSS, the measurements are **stored and** accessed in memory using the OpenDSS DLL **and once the HC condition is identified, the data is then transferred to the database.** This logic is triggered for each daily power flow calculation to always have an empty monitor before starting the execution, as described in Subsection 3.3.4. **While this approach may seem excessive, it is appropriate for investigative purposes.** For a specific application, the amount of data can be significantly reduced by only measuring the essential metrics and equipment.

---

**Algorithm 7** Implementation of OpenDSS Monitor elements.

---

```

...
def Add_Monitors(Rede2):
    for element in GetAllElementNames(Rede2):
        if element.split('.')[0] != 'Monitor':
            DF_List_Monitors.loc[len(DF_List_Monitors),
                                "Element_w_monitor"] = element
            Define_Monitor(Rede2, DF_List_Monitors["Elemento_com_monitor"].values)

def Define_Monitors(Rede2, List_Monitores):
    for element in List_Monitores:
        Command = []
        Command.append("New monitor." + str(element.replace('.', '_')) + \
                        "_power element=" + str(element) + \
                        " terminal=1 mode=1 ppolar=no enabled=Yes")
        Command.append("New monitor." + str(element.replace('.', '_')) + \
                        "_voltage element=" + str(element) + \
                        " terminal=1 mode=0 enabled=Yes")
        Command.append("New monitor." + str(element.replace('.', '_')) + \
                        "_loss element=" + str(element) + \
                        " terminal=1 mode=9 enabled=Yes")

    [Rede2.text(Cmd) for Cmd in Command]
...

```

---

### 3.3.4 Daily Power flow Implementation

The power flow calculation, implemented in Algorithm 8, is divided into two methods. The first compiles the original grid definition to restore default configurations and establishes a starting point for all power flow analyses using the "Compile\_DSS2" method. The PV and inverter units are defined in the grid based on power and location references, and all monitors are also associated with the respective elements.

To perform the power flow calculation, the "solve" method from the OpenDSS interface is used and represents the second step of the calculation. This method assesses the generation units and load definitions, considering the daily load flow for each component. The power flow is computed for every simulation sample, with the outcomes being saved in the corresponding monitor throughout the process. It's important to note that this architecture assesses the figure of merits once the daily execution concludes, Subsection 3.3.5 explains this decision in detail, but in summary, this architecture is more efficient than validating the metrics on each step of the day.

---

**Algorithm 8** Implementation of the daily power flow calculation logic.

---

```
...
def Solve_Daily(Rede2, Case, Pot_GD):
    # Preparation
    Compila_DSS2(Rede2)
    Add_PVs(Rede2, Pot_GD, Case)
    Add_Monitors(Rede2)

    #Power Flow Calculation
    Rede2.solution_solve()
    ...
```

---

### 3.3.5 Evaluation of the figure of merits

A figure of merit validation logic overview is shown in Algorithm 9 detailing its implementation. The first step is to assess the "Check\_Voltages" and "Check\_Current" methods, which populate the "DF\_Violations\_Data" data frame with all the violation occurrences based on the storage information of daily simulations from each monitor element. Explaining the details of these methods would be extensive, but it is important to clarify that they validate the measurements based on the limits defined in Section 2.2.

The "DF\_Violations\_Data" data frame, which contains all the violations registered by the monitors, is the end result of these check methods. Additionally, four keys are defined to identify voltage rise, voltage drop, voltage imbalance, or current rise violations within this data. If any, the respective key value is set to one, the result validation returns False, and the HC identification implementation, described in Subsection 3.3.6, stops.

**Algorithm 9** Implementation of the figure of merits validation logic.

---

```

...
def Check(Rede2, Case):
    Check_Voltages(Rede2, Case)
    Check_Current(Rede2, Case)

    overvoltage = 1 if
        DF_Violations_Data["ViolationType"][DF_Violations_Data["ViolationType"]
            == ViolationType.overvoltage.value].count() > 0
    else 0
    undervoltage = 1 if
        DF_Violations_Data["ViolationType"][DF_Violations_Data["ViolationType"]
            == ViolationType.undervoltage.value].count() > 0 \
    else 0
    imbalance = 1 if
        DF_Violations_Data["ViolationType"][DF_Violations_Data["ViolationType"]
            == ViolationType.imbalance.value].count() > 0 \
    else 0
    overcurrent = 1 if
        DF_Violations_Data["ViolationType"][DF_Violations_Data["ViolationType"]
            == ViolationType.overcurrent.value].count() > 0 \
    else 0

    Ress = True if
        overvoltage == 0 and undervoltage == 0
        and overcurrent == 0 and imbalance == 0
    else False
...

```

---

### 3.3.6 HC Identification Implementation

The Algorithm 10 summarizes the HC identification and is designed to improve understanding by emphasizing the main logic implemented. Although not detailed, secondary infrastructure procedures methods are required for properly implementing the logic, such as data clean-up, control case coordination, and logging. Moreover, an identification process is carried out with a "for" loop that covers all possible cases for each simulation. The property "Num\_Simulations" is set to five to cover the control configurations described in Section 3.1. The first scenario doesn't require the internal "while" loop as it evaluates the case without control and PV units. However, this loop is necessary for the other cases as the logic increases the PV power reference, triggering violations in the figure of merits. The increase ratio is based on the PCC transformer, and the "Incremento\_Pot\_gd" is set to 1% of its kVA power value.

Additionally, the "Solve\_Daily" method in subsection 3.3.4 calculates the daily power flow for each case. It always starts from a reference power equal to 0 and increases until the HC condition. Moreover, the "Check" method described in Subsection 3.3.5 is invoked for violation verification.

This process repeats until a violation is registered. At that point, the logic performs a step back, decreases the PV power reference by the same "Incremento\_Pot\_gd" value, and recalculates the daily power flow. The end result data is saved in the database and associated with a specific case for a defined simulation PV disposition. This process is required because the HC condition is defined as the configuration before a violation occurs.

---

**Algorithm 10** Implementation of the HC identification calculation process.

---

```

...
def HC(Rede2):
    for Case in range(1, Num_Simulations + 1):
        Pot_GD = 0
        while Nummero_Simulacoes == 0 or Verify is True:
            Pot_GD += Incremento_Pot_gd
            Solve_Daily(Rede2, Case, Pot_GD)
            Nummero_Simulacoes += 1
            Verify = Check2(Rede2, Case)
            if Simulation == 1:
                Sem_GD = 1
                break
        Pot_GD -= Reduction
        Solve_Daily(Rede2, Case, Pot_GD)
        Save_General_Data(Case)
        Save_Data(DF_Monitors_Data_2)
...

```

---

### 3.3.7 Simulation Control Implementation

The implementation section provides an overview of the simulation process using the simulation by simulation implementation, as presented in Algorithm 11. During each simulation configuration, the LV current limits of the transformer and lines are determined, and the location buses for the PV are selected as explained in Subsection 3.3.2. The "Simulation\_By\_Simulation" method is the foundation of the HC identification process and can be repeated as many times as the user wishes by defining the "Num\_Simulations" property, 150 simulations in the case of this study.

---

**Algorithm 11** Implementation of the logic responsible for executing multiple simulations with different PV allocations.

---

```

...
def Simulation_By_Simulation(Rede2):
    for Caso in range(Num_Simulations):
        Identify_Overcurrent_Limits(Rede2)
        FindBusGD(Rede2, Num_GDs)
        HC(Rede2)
...

```

---

## 3.4 Chapter Conclusion

This chapter outlines the concepts adopted in the development of this thesis. It starts with the proposed approach for identifying the HC condition at a distribution network. The logic and architecture aim to detail the system's operation step by step and is particularly useful for study applications as it generates a large amount of data to be analyzed. However, incorporating such a high level of detail demands more computational power and may not be ideal for large-scale analysis with a significant number of grids. Section 6.2 addresses some feature enhancements that could be implemented to handle this need.

The OpenDSS software proved to be efficient in performing power flow calculations within a short amount of time. In fact, each daily simulation only took milliseconds for this case study. Moreover, the development experience significantly increases when using the `py_dss_interface` library instead of the COM interface for code implementation. The library is updated according to the pattern of the latest technologies and easily integrates with the IDE platform, unlike the COM interface, which lacks these characteristics. Additionally, the BESS sizing logic is also explained, focusing on how it is performed. The four different steps may seem like overkill, but they help in retrieving specific information when needed. For instance, the second table stores the curtailed power for each time stamp in every case and simulation, eliminating the need to calculate it all over again when this value is needed in another analysis.

The Python programming language and SQL server are widely used technologies and relatively easy to learn, with abundant learning resources available. Although other options exist, these tools were selected based on their qualities and previous experience working with them. Specifically related to the database structure, it performed a crucial role in data processing because a large amount of data must be generated, stored, and processed during each simulation. Performing all these tasks at the development level increases the complexity and may result in inconsistencies that make it hard to identify the root cause. In this regard, the database structure stores and saves all measurements to be processed later. This creates an additional step in the execution process where it is possible to visualize the results in tables rather than lists, arrays, and data frames stored in run-time memory. Appendix A has more details regarding the database structure and definitions, it explains the relationship between tables. Moreover, the data processing stage is performed by views and store procedures, which are generic logic establishing rules and procedures for handling the data and extracting important information. Section 3.2 exemplifies the use of these procedures to describe the BESS sizing process.

~~These are fundamental concepts related to the developed tool that must be explained to comprehend the HC identification approach used in this thesis.~~

## Chapter 4

### Case Study

The purpose of this chapter is to provide a detailed description of the case study used in this [research](#). It begins with a general overall description of the LV grid, including the real location used, operation characteristics, and a unifilar diagram to depict the power circuit. Additionally, this chapter explains the meanings of each element of OpenDSS, detailing the configurations used and defining every variable. The values for these parameters can be found in Appendix [B](#). These definitions are the basis of the case study being analyzed, but the software developed for this research accepts all types of grid configurations defined as .dss files. However, the grid definition must follow an implementation model that considers a main .dss file to coordinate the definition of all other elements.



## 4.1 Low-Voltage Grid

This section discusses the case study of this project, which applies the proposed methodology to a real LV grid in Américo Brasiliense, São Paulo. This particular power system was chosen because it had already been evaluated and validated in terms of HC limits by (Torquato et al. [2018]). This allows the validation of the results when considering the baseline case, which operates with PV units without voltage control, and Subsection 5.1.1 presents this comparison. Additionally, this distribution system already contains the daily load profile for each customer and represents a typical residential neighborhood with a radial layout, which is in line with the focus of the current study.

To better understand the case study and how the power is distributed in the neighborhood, Figure 10 illustrates all the bus locations in a topographical map and the PCC transformer in the red square with a bus named as 001/SEC. These buses are defined in OpenDSS, and Figure 11 shows the same configuration but as a single-line diagram, highlighting the load and wire disposition. It's noticed that the main branches are usually a 3-phase connection, while the branches leading to the loads are mostly 1-phase connections. There are also some 2-phase and 3-phase loads, but they are less common.

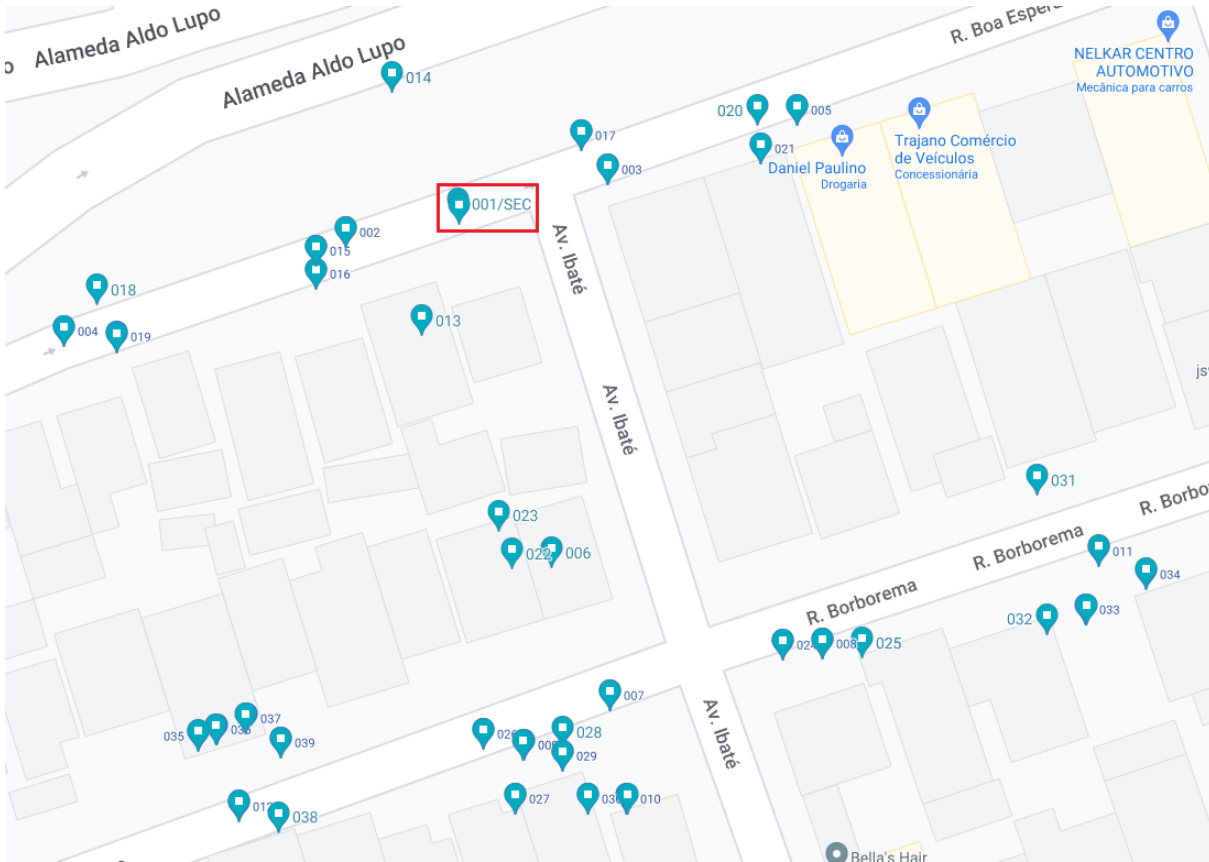


Figure 10 – LV grid street view.

Source: Author



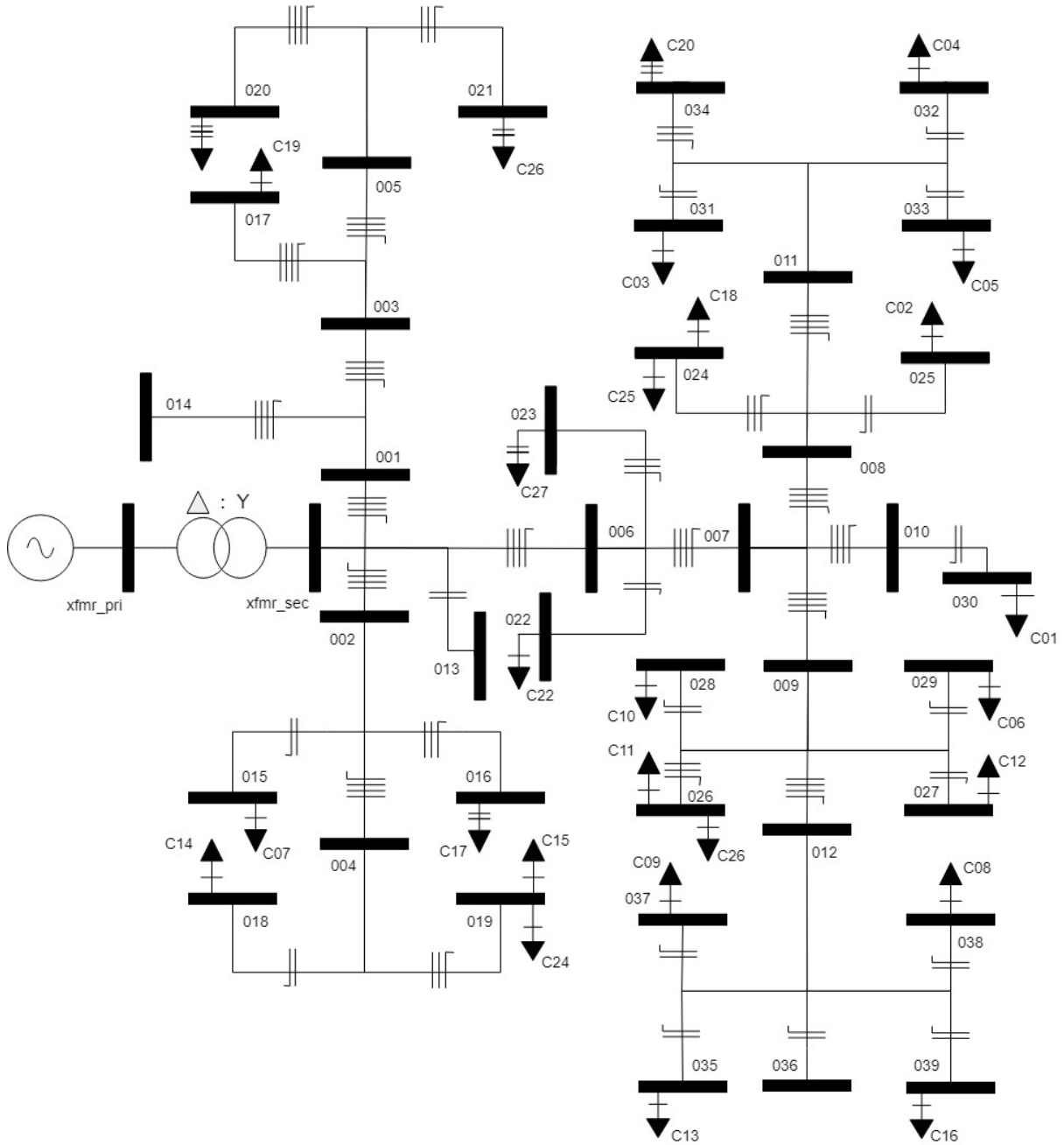


Figure 11 – LV grid single-line diagram.

Source: Author

This grid consists of 27 loads that operate on a voltage range of 127-220V under different daily profiles. These components are spread out across 41 buses and are connected by 484.75 meters of cables. The case study also contains a 45kVA transformer in the MV/LV coupling point. This transformer supplies a maximum power of 14.408 kW and 4.777 kVAr, as well as a daily energy demand of 160.876 kWh and 111.138 kVArh to support the load operations. More information on the values used can be found in the element definition section, referencing the respective tables in Appendix B.

### 4.1.1 Line Geometry and Wire Elements

This section presents a brief overview of the Line Geometry and Wire elements, focusing on how it is defined, configured, and used in this study. The base knowledge regarding this element comes from ([Electric Power Research Institute \(EPRI\) \[2021\]](#)), the OpenDSS reference guide.

The algorithms 12 and 13 present the wire and line geometry elements structure definition in OpenDSS, followed by the respective description of the respective variables. Tables 24 and 25 in the Appendix B contain the values associated with each defined element.

---

**Algorithm 12** OpenDSS specification of Wire element.

---

```
New WireData.<WireName> Rdc=<Rdc> Runits=<Runits> GMRac=<GMRac>
~ GMRunits=<GMRunits> Radunits=<Radunits> NormAmps=<NormAmps> Diam=<Diam>
```

---

Where **WireName** is the name of the wire object. **Rdc** is the dc Resistance, ohms per unit length. **Runits** is the length unit for resistance. **GMRac** is the effective radius of the conductor at 60Hz. **GMRunits** is the unit used in geometric mean radius. **Radunits** is the unit for the outside radius. **NormAmps** is the normal amperes operation limit. And **Diam** is the diameter of the wire.

---

**Algorithm 13** OpenDSS specification of Line Geometry element.

---

```
New LineGeometry.<LineGeometryName> Nconds=<Nconds> Nphases=<Nphases>
~ Cond=<Cond> Wire=<WyreName> H=<Height> Units=<XHUnits>
```

---

Where **LineGeometryName** is the object name. **Ncond** is the number of conductors. **Nphases** is the number of phases. **Cond** is the conductor number. **WyreName** is the conductor wire type. **XCoord** is the coordinate of the line, **H** is the height of the conductor. The number of conductors will specify how many times a conductor needs to be defined, each one with its own **Cond**, **WyreName**, **H**, and **XHUnits**.

### 4.1.2 Line Element

This section presents a quick overview of the line element, focusing on how it is defined, configured, and used in this study. The base knowledge regarding this element comes from ([Electric Power Research Institute \(EPRI\) \[2021\]](#)), the OpenDSS reference guide.

The algorithm 14 presents the line element structure definition in OpenDSS, followed by the description of the respective variables. Table 26 in the Appendix B contains the values associated with each defined element.

---

**Algorithm 14** OpenDSS specification of Line element.

---

```
New Line.<LineName> Bus1=<BusName1> Bus2=<BusName2> Length=<LineLength>
~ Geometry=<Geometry> Units=<Units>
```

---

Where **LineName** is the object name. **BusName1** is the bus name at the beginning of the line. **BusName2** is the bus name at the end of the line. **LineLength** represents the length of the object. **Units** is the length metric for use, km in this case. And **Geometry** represents the geometry of the line, defined in Subsection 4.1.1.

### 4.1.3 PCC Transformer

This section presents a quick overview of the transformer element, focusing on how it is defined, configured, and used in this study. The base knowledge regarding this element comes from ([Electric Power Research Institute \(EPRI\) \[2021\]](#)), the OpenDSS reference guide.

The algorithm 15 presents the transformer elements definition in OpenDSS followed by the description of the respective variables. The respective values are already in place for this element since only one in the LV grid represents the PCC connection with the MV network.

---

**Algorithm 15** OpenDSS specification of Transformer element.

---

```
New Transformer.t1 Windings=2 XHL=3.091723719
~ Wdg=1 Bus=bus_xfmr_pri_33998182.1.2.3 Conn=delta kV=11.9 kVA=45.0
~ Tap=1.0 %R=c
~ Wdg=2 Bus=bus_xfmr_sec_33998182.1.2.3.4 Conn=wye kV=0.22 kVA=45.0
~ Tap=1.0 %R=0.776666667
```

---

Where **t1** is the transformer object name. **Windings** is the number of terminals. **XHL** is the percent reactance high-to-low (winding 1 to winding 2), on the kVA base of winding 1. **Wdg** is the number of winding that the following parameters are associated with **Bus** is the winding connection location, **Conn** is the type of connection, **kV** is the phase-to-phase voltage base, **kVA** is the base power rating of the winding, **Tap** is the per unit tap that this winding is on and **%R** is the percent resistance this winding. The resulting specifications are resented in Table 23, in Appendix B, which summarizes the operation voltage and power conditions to each terminal configuration.

### 4.1.4 Load Element

This section presents a quick overview of the load element, focusing on how it is defined, configured, and used in this study. It also shows the resulting power measurements

for each load in a daily simulation. The base knowledge regarding this element comes from (Electric Power Research Institute (EPRI) [2021]), the OpenDSS reference guide.

The Algorithm 16 shows how to define a load shape curve, an object used as input value in the load, and a PVSystem definition to simulate daily variations. Furthermore, Algorithm 17 presents the load element structure definition in OpenDSS, followed by the description of the respective variables. Tables 27 and 28 in the Appendix B contain the values associated with each defined element.

---

**Algorithm 16** OpenDSS specification of LoadShape element.

---

```
New LoadShape.<LoadShapeName> Npts=<Npts>
~ Mult=(0.131409, 0.133167, ... , 0.124863, 0.124277)
~ Hour=(0.0, 0.25, ... , 23.5, 23.75)
```

---

Where **LoadShapeName** is the object name, the **Npts** is the number of samples to expect in the simulation. **Mult** is the load power multiplier in pu unit, and **Hour** is the sample time that covers a one-day simulation in this case. These last two parameters were presented with values just as an example, and each load has its own load shape with different values.

---

**Algorithm 17** OpenDSS specification of Load element.

---

```
New Load.<LoadName> Bus1=<LoadBus> model=<LoadModel> Phases=<Phases>
~ kV=<kV> kW=<Kw> PF=<pf> Vmaxpu=<Vmaxpu> Vminpu=<Vminpu> Daily=<Daily>
```

---

Where **LoadName** is the object name. **LoadBus** is the bus location where the load is connected. **LoadModel** is an integer code representing the load model and how it associates with the grid. The loads in the case study use model 6, meaning that it operates under a constant active and reactive power. **Phases** is the number of phases for this load. **kV** is the nominal related voltage. **Kw** is the total base power reference. **pf** is the load power factor, set to 0.85 inductive for all loads. **Daily** is the load shape object to use for daily simulations. **Vmaxpu** and **Vminpu** represent the maximum and minimum per unit voltages for which the model is assumed to be applicable. The load model switches to a constant impedance mode when the voltage exceeds this range.

The load operation is the same in all simulations, but some properties vary from element to element. Table 27, in Appendix B, summarizes these configurations presenting the locations, voltage, and power definitions for each load. Regarding distribution along phases, the case study has a prevailing 1-phase load element but concentrated in only two phases as indicated in Table 2. Furthermore, the load power profile array is the multiplication of the load power reference, column Active Power in Table 27, with each factor defined in the daily property. Figure 12 presents the resulting power profile for all loads during a daily operation, the active values are in Figure 12a, and reactive ones are in

Table 2 – Total number of loads connected per phase.

	Phase A	Phase B	Phase C
Number of Loads	11	8	13

Figure 12b. This plot illustrates the different load profiles used based on customers, and the average result is highlighted in black in both plots.

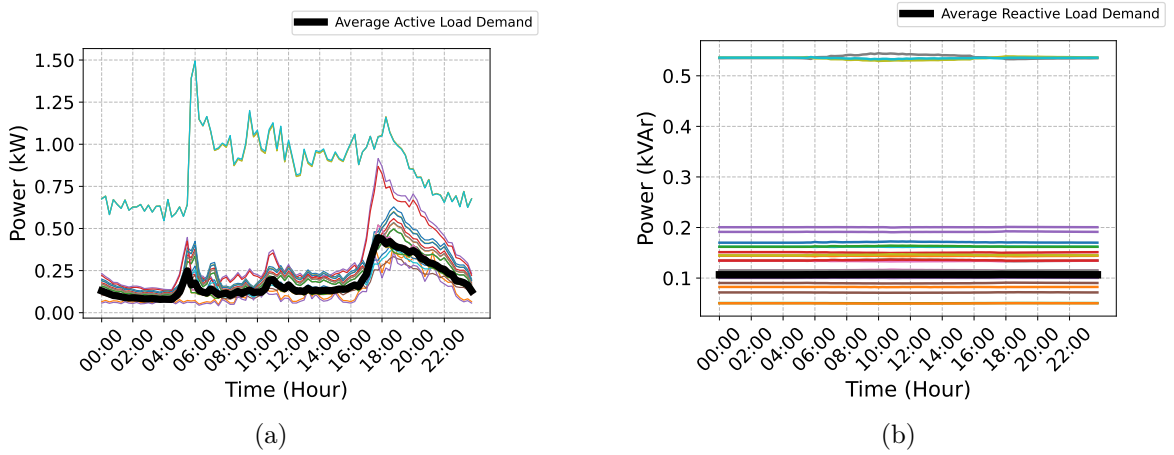


Figure 12 – Load Power Profile: (a) Active Power; (b) Reactive Power.

Source: Author

#### 4.1.5 PVSystem Element

This section presents a quick overview of the PVSystem and focuses on how it is defined, configured, and used in this study. The base knowledge regarding this element comes from (Paulo Radatz and Peppanen [2020]), a technical report that presents all properties and definitions associated with this DER unit. In addition, (EPRI [2013]) is another document focusing on the PVSystem modeling processing for high penetration in distribution networks. These references were created by the company responsible for the OpenDSS development, classifying them as one of the most reliable sources of information regarding this subject.

Figure 13 shows the PVSystem diagram covering the generation process, starting with the operation condition inputs that, inside the element model, are converted to DC power references by the PV element and converted to alternate power by the inverter and delivered into the grid by a norton equivalent circuit. The max power point calculation is delegated to the PV model since it already provides a reliable result that includes this step, a significant simplification since it is not the focus of this study.

The Algorithm 18 shows the necessary XYCurve used as input variables in the PV definition. Moreover, Algorithm 19 presents the PVSystem structure implementation using

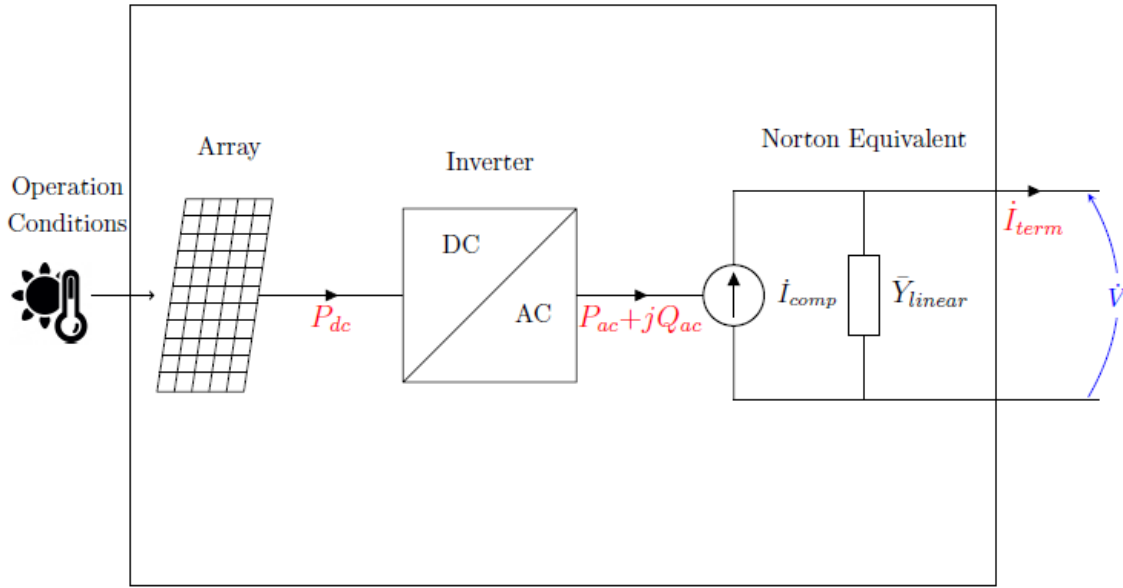


Figure 13 – Block diagram of the PVSystem element model.

Source: (Paulo Radatz and Peppanen [2020])

those curves for each new element. The used variables are explained after each definition, but for a more detailed properties review, please refer to (Paulo Radatz and Peppanen [2020]).

---

**Algorithm 18** OpenDSS specification of PV System Curves elements.

---

```

New XYCurve.FatorPvsT npts=4 xarray=[0 25 75 100] yarray=[1.2 1.0 .8 .6]

New XYCurve.Eff npts=4 xarray=[.1 .2 .4 1.0] yarray=[.86 .9 .93 .97]

New TShape.Temp npts=96 mininterval=15 "
~ "temp=(File=C:\\Users\\hugo1\\Desktop\\Rede_03\\LoadShapeGeradores\\Temp.txt)

New LoadShape.irrad npts=96 mininterval=15 "
~ "mult=(file=C:\\Users\\hugo1\\Desktop\\Rede_03\\LoadShapeGeradores\\Irrad.txt)

```

---

Where **FatorPvsT** is an array containing adjusts for the maximum PV power to the expected depending on temperature variations. The unit will generate the nominal 1 pu power at 25°C but only 0.8 pu at 75°C. The **Eff** XYCurve is used by the inverter and represents the operation variation based on the pu power reference from the PV unit, also adjusting the final power values at the PPC connection in the grid. Finally, the **Temp** and **irrad** curves replicate the operational conditions where the PV element is installed. They are defined using the **mult** property, which reads a text file containing the data. Each of these curves consists of 96 records.

Where **PVSystemName** is the object name. The number of phases, **NumOf-**

---

**Algorithm 19** OpenDSS specification of PV System element.

---

```

New PVSystem.<PVSystemName> phases=<NumOfPhases> bus1=<PVLoc>
~ Pmpp=<Pmpp> kv=<kv> kVA=<kVA> con=<con> EffCurve=<EffCurve>
~ %Cutin=<Cutin> %cutout=<Cutout> P-TCurve=<P-TCurve> pf=<pf>
~ VarFollowInverter=<VarFollowInverter> irradiance=<irradiance>
~ temperature=<temperature> daily=<daily> Tdaily=<Tdaily>
~ wattpriority=<wattpriority>

```

---

**Phases**, and the PV bus location, **PVLoc**, varies depending on random installation choices, but the logic identifies and adjusts these variables accordingly before each simulation. **Pmpp** is the PV max power for  $1.0kW/m^2$  corrected by irradiance and temperature curves. **kV** is the nominal related element voltage for 2 and 3-phase elements, it uses a line-to-line metric. But for 1-phase with a wye connection, it considers a line-to-ground metric, which requires conversion when analyzing the data. **kVA** is the power rating of the inverter. **Conn** is the type of connection, defined as wye for all elements. **EffCurve** represents the inverter efficiency curve. **Cutin** is a percentage of the rated power at which the PV system will start generating power, and **Cutout** is the percentage at which it will stop generating power. **P-TCurve** represents the power correction based on temperature and irradiance. **pf** is the power factor for the output power. **VarFollowInverter** is set to true in order to cease reactive power depending on the inverter status, defined based on the %cutout and %curtin properties. **irradiance** is the present irradiance value in  $kW/m^2$ , **temperature** is the temperature, and this value varies based on **daily** XYCurve during a defined period of time, a day in this case. **Tdaily** is the temperature shape to use for daily simulations and, finally, the **wattpriority** is a boolean value that sets the inverter to operate in a watt priority configuration instead of the default var priority.

#### 4.1.6 InvControl Element

This section presents a quick overview of InvControl and focuses on how it is defined, configured, and used in this study. The base knowledge regarding this element uses the same references as Subsection 4.1.5, (Paulo Radatz and Peppanen [2020]) and (EPRI [2013]). In addition, (Radatz et al. [2020]) is a recent publication highlighting enhancements to smart inverter modeling and internal processing methodology. Moreover, Figure 14 presents a simplified diagram of the PVSystem associated with smart inverted control. The PVSystems operates as described in Subsection 4.1.5, but the diagram includes one additional step, a voltage verification. Before delivering the active and reactive power to the grid, the power references are only provided to the network when the control requirements are satisfied.

The Algorithm 20 shows the necessary VV and VW control curves used as input variables in the InvControl definition. The corresponding properties are explained below.

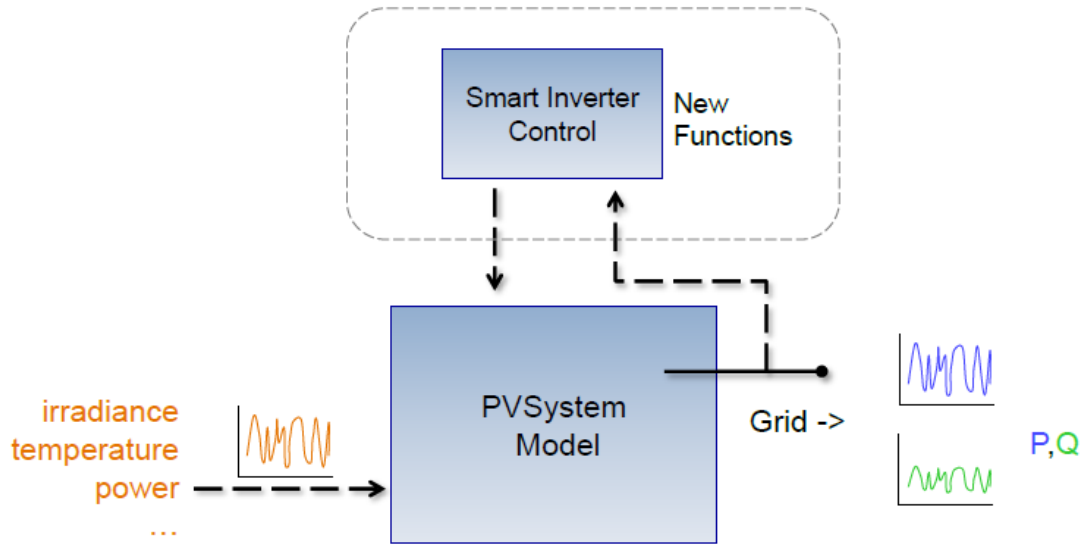


Figure 14 – Simplified block diagram of the PVSystem operation with InvControl element.

Source: (EPRI [2013])

---

**Algorithm 20** OpenDSS specification of VV and VW XYCurves elements

---

```
New XYcurve.vv_curve npts=4 Xarray=(0.92, 0.99, 1.01, 1.05)
~ Yarray=(1.0, 0, 0, -1.0)
```

```
New XYcurve.vw_curve npts=4 Xarray=(0.8 1.03 1.05 2)
~ Yarray=(1 1 0.50 0.50)
```

---

Where, using the illustrative voltage control activation from Figure 4, **vv\_curve** represents the VV reference array definition. Equation 4.1 presents the Xarray in terms of  $V_n$  and Yarray as  $Q_n$  references. The same occurs for the VW curve **vw\_curve** with equation 4.2 but with Yarray representing  $P_n$  values and 15% curtailment as an example. Those values follow the Modulo 8 recommendations (Brazilian Elec. Reg. Agency [Set.2020]).

$$\begin{cases} (Q_1, Q_2, Q_3, Q_4) = (1.0, 0, 0, -1.0) \\ (V_1, V_2, V_3, V_4) = (0.92, 0.99, 1.01, 1.05) \end{cases} \quad (4.1)$$

$$\begin{cases} (P_1, P_2) = (1.0, 0.85) \\ (V_1, V_2, V_3, V_4) = (0.92, 0.99, 1.01, 1.05) \end{cases} \quad (4.2)$$

Moreover, Algorithm 21 presents the InvControl structure implementation using those curves for each new element depending on the control strategy in use. The associated variables are explained after each definition, but for a more detailed properties review, please refer to (Paulo Radatz and Peppanen [2020]).



---

**Algorithm 21** OpenDSS specification of InvControl element.

---

```

New InvControl.<InvPVCtrlName> DERList=PVSystem.<PVSystemName>
~ mode=<Mode> voltage_curvex_ref=<voltage_curvex_ref>
~ vvc_curve1=<vvc_curve1> RefReactivePower=<RefReactivePower>
~ voltwatt_curve=<voltwatt_curve> VoltwattYAxis=<VoltwattYAxis>
~ varchangetolerance=<varchangetolerance>
~ voltagechangetolerance=<voltagechangetolerance>
~ monVoltageCalc=<monVoltageCalc>

```

---

Where **InvPVCtrlName** is the object name. **PVSystemName** is the name of the associated PVSystem element to be controlled. **Mode** is the function that the element will follow in the control set as VOLTVAR or VOLTWATT accordingly, if using both VV and VW controls, change the mode property to combine mode and set the value to VV\_VW. **voltage\_curvex\_ref** voltage that is used as the base value to convert the monitored voltage to pu, the rated value is used. **vvc\_curve1** is the name of the XYCurve object containing the VV curve if activated. **RefReactivePower** defines that the base value for the delivered reactive power is the available reactive power of the unit. **voltwatt\_curve** is the name of the XYCurve object containing the VW curve if activated. **VoltwattYAxis** sets the y-axis to the value in pu of the available active power of the PVSystem when set to PAVAILABLEPU. **varchangetolerance** is the tolerance in pu of the control loop convergence associated with the monitored voltage. And finally, **monVoltageCalc** represents how to monitor the voltage measurements, set as the average voltage result between phases.



## 4.2 Chapter Conclusion

This chapter outlines the concepts related to the case study used in this thesis. Firstly, it explains the case study grid which includes the bus locations, the single-line diagram, and the electrical characteristics. The low-voltage grid has a typical residential demand profile with a balanced load distribution across phases, although phase C has slightly more loads than phases A and B.

The OpenDSS offers numerous features to characterize each element and integrate them to form a distribution system. However, the definition process is time-consuming and requires careful consideration of all details, as any errors may impact the final outcome. The most efficient way to perform this task is by using the reference guide and the examples provided in the installation folder. Moreover, the OpenDSS download center's online search feature is an effective tool that includes a forum for users to centralize their doubts. Related to the several studies using OpenDSS, they have not provided specific implementation details but delve into the concepts of where the software can be applied and how it is used.

## Chapter 5

# Simulation Results

The following section discusses the enhancement of HC in a LV grid with a high penetration of rooftop PV inverters using small distributed BESS units. The case study has a known HC value when operating with PV units, perfect for validating the proposed architecture under similar conditions. Moreover, voltage control strategies, VV and VW, can play an essential role in increasing the grid HC. This study also evaluates these configurations and the actual gains they provide to the overall operation. Although active power curtailment may compromise revenues when operating with VW control, the presented BESS structure covers this untapped potential for batteries to operate along with PV units and store the power that would otherwise be lost.

The simulation environment consolidates the methodology discussed in [3](#) to evaluate the grid operation results in all HC case scenarios in detail. All grid elements have an associated monitor element to store electrical metrics like voltage, current, and power values for each time interval. This data provides reliable information to evaluate multiple limits of curtailment, such as 15%, 30%, and 50% reductions in VW control under different case scenarios, such as baseline, only VV control, only VW control, and the combined VV and VW controls activated.

## 5.1 Hosting capacity analysis

This section is dedicated to assessing HC, following the methodology outlined in Section 3.1. The discussion begins by comparing the baseline HC values with the results from (Torquato et al. [2018]), a reference that has already analyzed the ~~case study~~ and identified the HC values ~~in their findings~~. The same baseline is then used as a reference to compare with the curtailment scenarios, which are described in their own subsection using a table showcasing the HC results for each control strategy. The table includes a column indicating the case under test, the average HC, and its standard deviation, followed by the restricted HC value and the enhancement provided by the respective technique. Detailing the last two columns, the restricted HC refers to a conservative consideration that uses the average result minus the respective standard deviation to define the grid HC, and the HC enhancement refers to a calculation that compares the restricted HC control result to the baseline, representing the HC gain in the worst condition.

Additionally, the discussion carries on with a box plot for every curtailment configuration. This provides a robust side-by-side contrast of the HC outcomes for each scenario. It assesses the median sample, average result, sample distribution, and variability for all situations in a single plot. For a better understanding of interpreting this plot, please refer to section 2.5, which includes detailed definitions and discussions on this type of plot.



### 5.1.1 Baseline Comparison

This subsection focuses on validating the methodology for assessing HC. The study conducted by (Torquato et al. [2018]) is used as a reference in terms of HC values for the case study presented in this thesis. The paper’s authors assessed the average HC results from a 50,000 LV grid distributed throughout the southeast region of Brazil. A simplified Monte Carlo method performed the simulations considering only PV units without any enhancement technique.

This thesis analyzes one of the LV grids from the paper as a case study. A simulation case is conducted without enhancement techniques while evaluating the average results to ensure a fair comparison. This case serves as the baseline for comparison, allowing the results from the paper to be compared and the effectiveness of the enhancement methods presented in this section to be quantified.

Table 3 compares key characteristics between two works based on reference parameters. Although the results are not identical, they are based on the same LV grid type. The middle column values were obtained from multiple LV grids, including the one in the right column, the case study presented in this thesis. Generally, the average circuit total length is higher in the reference results, with a total difference of 283.17 m in length between the two. The X/R ratio is the second metric being evaluated, the value is slightly below the average reference value, but it is still comparable considering the associated standard deviation of 0.32. The case study has 70.47% less two-phase loads than the reference results, but the number of single-phase and three-phase clients is almost equal. Lastly, the transformer-rated power from the reference results ranges from 30 kVA to 75 kVA, which is expected considering the number of LV grids evaluated and the 45 kVA rated power from the case study in this thesis is included in that range.

Table 3 – Grid metrics comparison between reference results and the proposed case study.

Metric	Results from (Torquato et al. [2018])	Case Study
Circuit Total Length (m)	767.92	484.75
Average X/R ratio	1.01	0.72
Average conductor ampacity	82.26	73.51
Average Number of single-phase costumers	20.41	21
Average Number of two-phase costumes	13.55	4
Average Number of three-phase costumers	2.77	2
Transformer Rated Power (kVA)	30 to 75	45

In both studies, a 20% PV penetration is considered, which means that 20% of the customers have PV installed. For this division, (Torquato et al. [2018]) presented a table with average HC values from different PV penetrations, using many LV grids as the data source for that analysis. Table 3 displays the final results from both studies. The slight variation can be explained by the different simulation methods, Monte Carlo and OpenDSS. Additionally, the variance in the number of iterations conducted to attain the average outcomes contributes to the differences. Primarily, it's important to note that the reference results encompass 20,529 LV grids which align with the equivalent transformer-rated power.

Table 4 – A HC comparison between reference results and the proposed case study.

Study	Average HC	Standard Deviation
Results from (Torquato et al. [2018])	37,40%	17,40%
Case Study from this thesis	37,11%	11,81%

Considering the very close results, it is safe to say that the proposed methodology correctly assesses the HC values from a LV grid. The baseline results can be used as a reference point for further enhancements analysis.



### 5.1.2 Curtailment condition at 15%

The first scenario being analyzed is the 15% curtailment condition, and the results for HC are presented in Table 5. The restricted HC values are as follows: 25.30% for the baseline case, 34.68% for VV control, 25.65% for VW control, and 35.62% for combined operation. The VV strategy shows a significant improvement compared to the baseline condition, with a 37.07% improvement compared to a 1.38% improvement for the VW strategy. However, the most significant one came from combining operations showing a 40.79% increase.

The boxplot in Figure 15 displays the data from Table 5. Compared to the baseline, the voltage control cases increase their median and mean HC values, indicating that the grid can now support more power from distributed sources. Additionally, the increase in IQR is particularly noticeable in VV and combined operations cases, which indicates an ampler range of possible HC conditions for the grid operations. Section 5.1.5 discusses this variability analysis and the slight VW enhancement in detail, evaluating all three curtailment scenarios.

Table 5 – Average HC values for the proposed case scenarios with 15% curtailment.

Cases	Average HC	Standard Deviation	Restricted HC	HC Enchancement
Baseline	37.11%	11.81%	25.30%	-
VV	49.46%	14.78%	34.68%	37.07%
VW	39.16%	13.51%	25.65%	1.38%
VV&VW	50.88%	15.26%	35.62%	40.79%

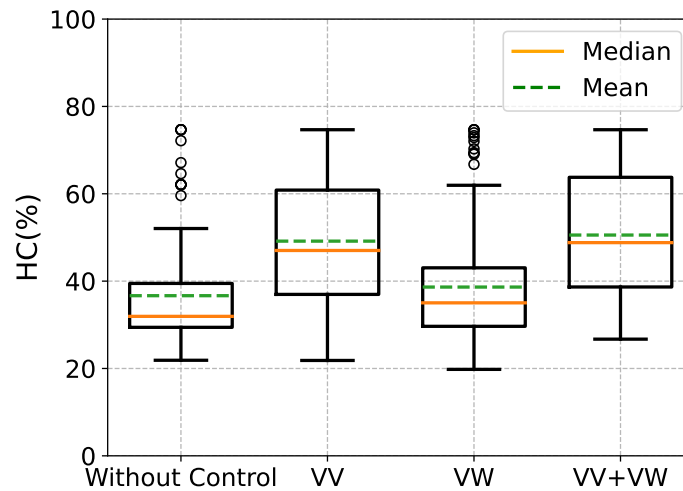


Figure 15 – HC box plots divided by case studies: 15% active power curtailment.

Source: Author

### 5.1.3 Curtailment condition at 30%

The second scenario being analyzed is the 30% curtailment condition, and the results for HC are presented in Table 6. The restricted HC values are as follows: 27.19% for the baseline case, 37.16% for VV control, 29.38% for VW control, and 38.73% for combined operation. The VV control resulted in a significant increase of 36.67% in HC, compared to VW control which only saw an 8.05% increase. Nonetheless, the VW control enhancement is higher than the previous 15% curtailment scenario. The table ends with the combined operation, which showed the most significant improvement with a 42.44% increase.

The boxplot in Figure 16 displays the data from Table 6. The voltage control cases also showed an increase in their median and mean HC values compared to the baseline results. The VW case generated a better response for the 30% curtailment, registering higher HC and IQR outcomes than the 15% scenario. Additionally, greater variability is also evident in all controls due to the IQR expansion, the analysis of this observation is available in Section 5.1.5.

Table 6 – Average HC values for the proposed case scenarios with 30% curtailment.

Cases	Average HC	Standard Deviation	Restricted HC	HC Enhancement
Baseline	36,94%	9,79%	27,19%	-
VV	51,76%	14,60%	37,16%	36,67%
VW	42,45%	13,07%	29,38%	8,05%
VV&VW	53,50%	14,77%	38,73%	42,44%

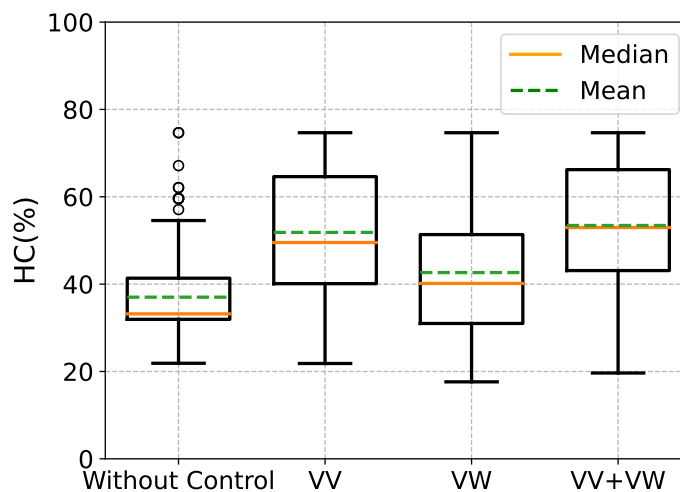


Figure 16 – HC box plots divided by case studies: 30% active power curtailment.

Source: Author



### 5.1.4 Curtailment condition at 50%

The second scenario being analyzed is the 50% curtailment condition, and the results for HC are presented in Table 7. The restricted HC values are as follows: 26.00% for the baseline case, 34.86% for VV control, 32.04% for VW control, and 36.03% for combined operation. As observed in the previous two scenarios, the VV control also resulted in a significant improvement of 34.07%. On the other hand, the VW control generated a 23.23% increase in this scenario, way higher than the previous results. However, the combined operation remained consistent with the previous results at 38.57% enhancement.

The boxplot in Figure 17 displays the data from Table 7. The median and mean HC enhancement can also be observed in these results but with an even higher response in the VW one. The restricted HC value is very similar between all controls, although they control different metrics, active and reactive power. Additionally, it was noticed that the combined control operation resulted in a skewed-to-the-left distribution, meaning that the occurrence of high HC values is more probable because 25% of the samples are concentrated in a small quartile range.

Table 7 – Average HC values for the proposed case scenarios with 50% curtailment.

Cases	Average HC	Standard Deviation	Restricted HC	HC Enhancement
Baseline	37.30%	11.30%	26.00%	-
VV	50.99%	16.13%	34.86%	34.07%
VW	47.01%	14.97%	32.04%	23.23%
VV&VW	52.53%	16.50%	36.03%	38.57%

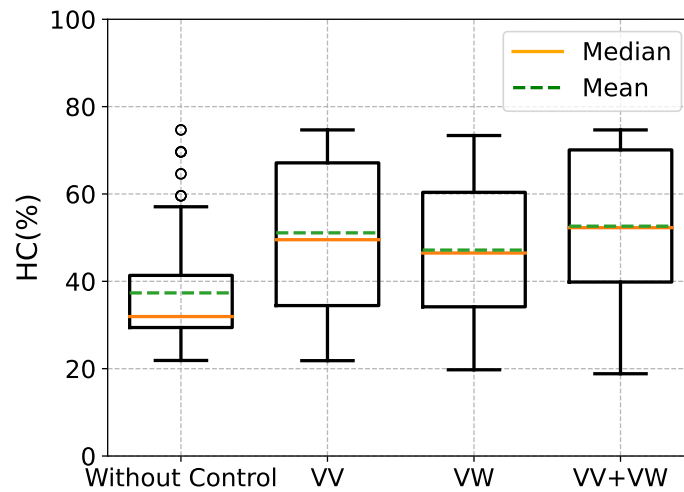


Figure 17 – HC box plots divided by case studies: 50% active power curtailment.

Source: Author

### 5.1.5 Curtailment Condition Comparison

This section compared the baseline scenario, which operates without voltage control, to the results presented in a paper that evaluated the same case study to assess HC conditions. The methodology was validated through the similarities between the results and the other projects, presented in section 5.1.1.

Each control case in three different curtailment scenarios: 15%, 30%, and 50% was evaluated, presenting the average HC and the enhancement values for 150 different simulations for each scenario. The location of the PV affects the HC result, as shown by the baseline case in the boxplot graphic, which summarized the data with a high standard deviation. Besides, the control operation added more variables and increased the variability of the possible configurations the grid could operate with. Some configurations reached higher HC values by associating the voltage control strategies with the PV inverters. Moreover, a side-by-side comparison expressed each case distribution, and Table 8 displayed the enhancement results by case and compared them with each curtailment limit. There was little difference between the Baseline and VV values, and the random PV location along the grid could explain their slight differences.

The VW case registered the most significant enhancement compared to the combined control operation, increasing up to 16.69% when comparing the 15% with 50% curtailment and 9.68% for the 30% to 50% comparison. Both strategies enhanced HC, with the VW control gaining more relevance when operating under a higher active power reduction limit. However, a higher curtailment range results in more energy curtailed, causing a disadvantage to the unit's owner by reducing their profits. This situation can be alleviated by exploiting soft curtailment operation, with results discussed in section 5.2, along with BESS units to store the amount of energy that would be lost during VW activation, presented in section 5.3.

Table 8 – Comparison of HC enhancements based on curtailment scenarios and voltage control techniques.

Case	15->30	15->50	30->50
Baseline	-0.44%	+0.50%	+0.94%
VV	+4.44%	+2.99%	-1.51%
VW	+7.75%	+16.69%	+9.68%
VV&VW	+4.91%	+3.15%	-1.84%

## 5.2 Control strategies

~~This section is dedicated to assessing voltage control operation within proposed curtailment limits of 15%, 30%, and 50%, following the methodology outlined in Section 2.3.~~ The purpose of the analysis is to provide a detailed understanding of the control activation, highlighting the power loss caused by the control, the relationship associated with the number of control activations, and the location sensitivity on the grid under test in this thesis.

### 5.2.1 Detailed Control Activation

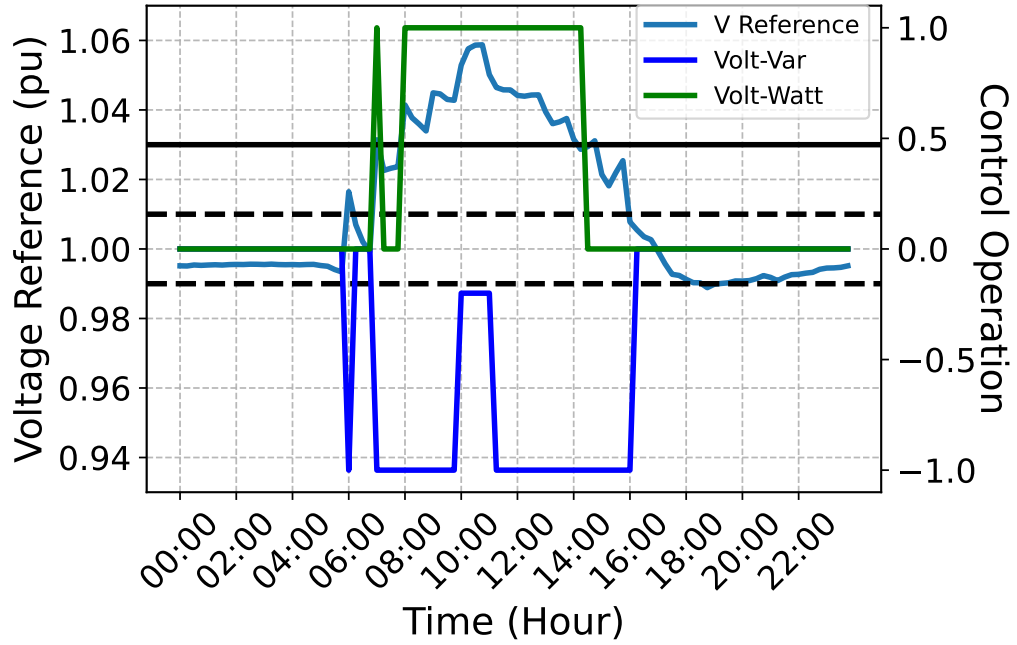
This subsection details the voltage control strategies applied to the case study. Figure 18 details a single PV control operation in a daily operation. It uses the average voltage measure between phases to determine whether or not the control will be triggered. Figure 18a shows the reference voltage comparison with the respective control limits. The right Y-axis represents different control activations, with 0 as not active, 1/−1 as active, and 0.2/−0.2 as partially active. The left one represents voltage values in (pu) and is used to quantify the reference voltage value during the day. **The limits define whether the control will activate and** are represented by dashed lines for the VV limits, 0.99 pu and 1.01 pu, and a solid one for the VW limit, 1.03 pu.

Figure 18 provides an example of various scenarios during daily operations. The first possibility involves using both VV and VW controls, but VW may not always be activated despite being configured. This is because VV control is the first to be triggered by the reference voltage comparison and may be sufficient to stabilize the bus voltage. For instance, the combined control operation starts at 10:00 a.m. with both controls activated due to the reference voltage exceeding the VW and VV upper limits. During that time, and for this example, the inverter requires more reactive power than the unit can process to stabilize the bus voltage. The situation is stabilized an hour later, with both controls operating at total capacity. In such a case, the PV watt priority configuration prevails, and the unit prioritizes the active power supply over the reactive one to avoid operating in an overcapacity state. It activates partial VV control since the unit is operating with less reactive power than the reference determined by the control.

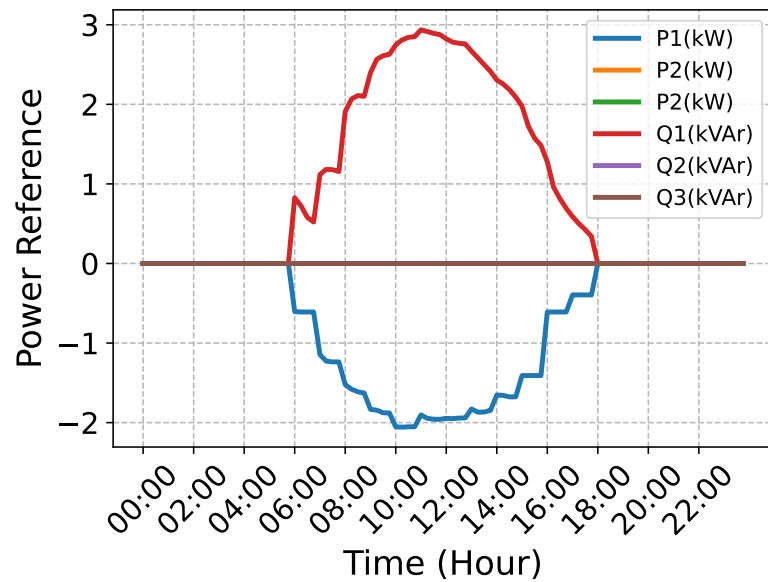
The other possibilities are related to the individual activation of each control and the combined operation without triggering the watt priority rule. These controls will only function when the reference measurement exceeds its voltage limit, alternating between activation and deactivation throughout the day. For instance, the VV control is triggered at 6:00 AM, with the voltage reference level going beyond the VV upper limit, causing the inverter to ask for reactive power even when the generation rate is low due to the time. Half an hour later, the voltage returns to regular operation, and the VV control is turned down. Moving to the VW control, it occurs at 7:00 a.m. with the voltage exceeding both VW and VV upper limit, but in this case, the inverter was able to satisfy both active and reactive power requirements. As the day ends and PV power generation decreases, the voltage levels drop. This results in a sudden undervoltage occurring at 6:45 pm, the same time as the peak load demand as noticed in Figure 22. This figure displays the power flow through the PCC transformer with and without voltage control strategies, further explanations about this plot will be discussed in section 5.2.4. However, the VV control remains inactive as there is no further power generation from the PV components.

Therefore, Figure 18b presents the resulting power operation during all scenarios

described. Specifically to the combined operation with watt priority, the system injects reactive power until the unit reaches its limit. The partial VV operation stabilizes the reactive power output to continue supplying the maximum active power possible. The active power curve follows the regular PV generation minus VW curtailment, caused by the VW control activation, and induces energy loss depending on the scenario. Further discussion on power loss is in section 5.2.2.



(a)



(b)

Figure 18 – Voltage control strategies response: (a) Control response; (b) Power response.

Source: Author

### 5.2.2 Power Loss

A comparison is presented to evaluate the expected active power delivered versus the inverter output power, using a single VW control and a combined VV and VW operation. The power difference is a significant concern for DG owners, as less active power injected into the grid results in smaller revenues. The comparisons use the exact same PV location, load stress, time range, and power reference for the DGs to ensure reliability and highlight the power difference in a zoom area. The maximum curtailment value allowed for each VW curtailment limit is also presented.

Starting with the results, Figure 19 displays the active power reduction of 15%. The single VW control operation is shown for a single PV unit in Figure 19a, where the active power reduction reached its limit at 11:00 am, with a 14.55% curtailment. Additionally, Figure 19b shows the same configuration but with both controls operation, resulting in a 6.86% active power curtailment, which represents 47.14% of what would be lost when operating with the VW control only.

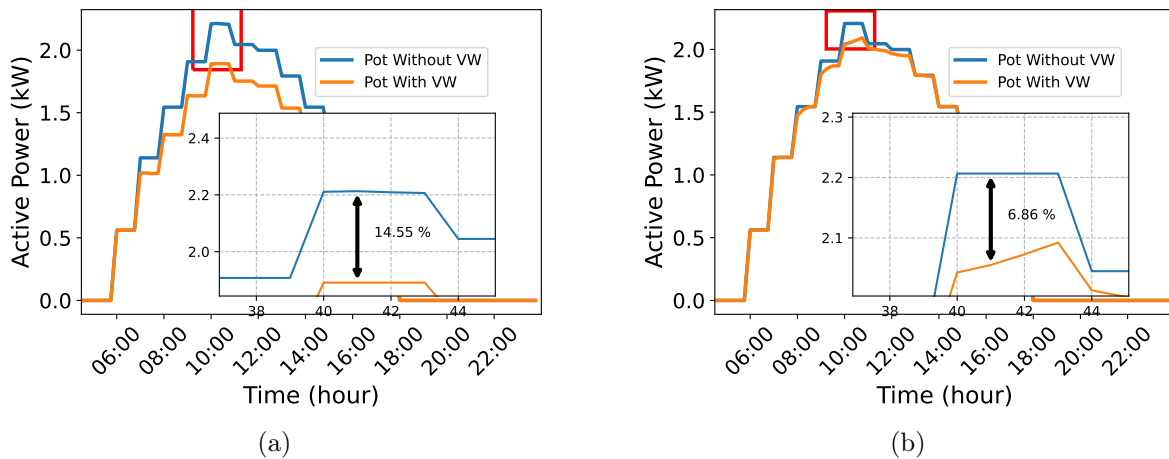


Figure 19 – Active power curtailment reduction at 15%: (a) Single VW control operation; (b) Combined control operation, VV and VW.

Source: Author

Furthermore, Figure 20 displays the active power reduction of 30%. The single VW control operation is shown for a single PV unit in Figure 20a, where the active power reduction reached its limit at 10:00 am, with 29.16% curtailment. Additionally, Figure 20b shows the same configuration but with both controls in operation, resulting in a 12.41% active power curtailment. Another significant reduction in the active power loss improved the amount of power delivered to the grid. The combined control limited only 42.55% of what the single VW control would have curtailed.

As the last active power loss result, Figure 21 displays the active power reduction of 50%. The single VW control operation is shown for a single PV unit in Figure 21a, where the active power reduction reached its limit at 10:00 am, with 49.16% curtailment.

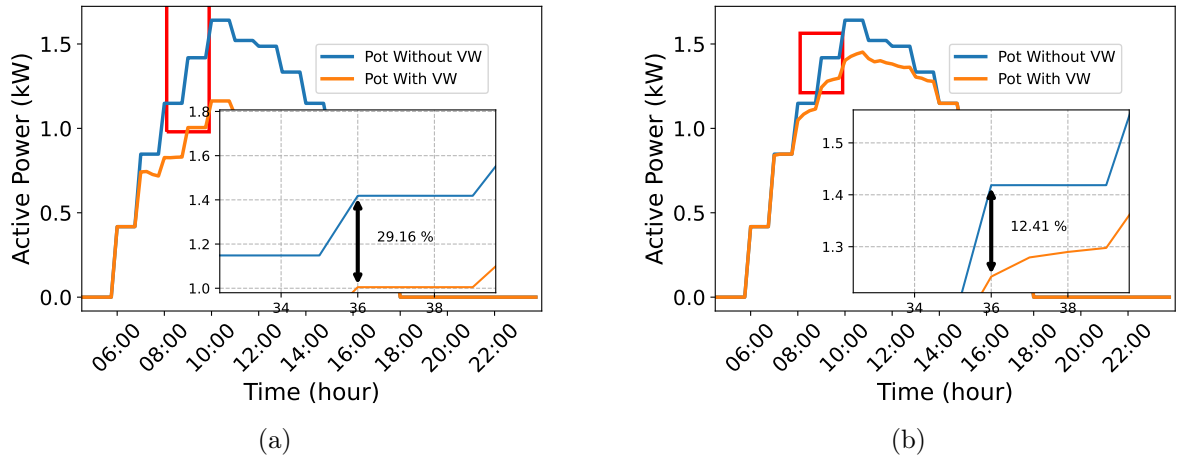


Figure 20 – Active power curtailment reduction at 30%: (a) Single VW control operation; (b) Combined control operation, VV and VW.

Source: Author

Additionally, Figure 21b shows the same configuration but with both controls in operation, resulting in a 13.75% of active power curtailment. The reduction is a little smaller this time, 27.96%.

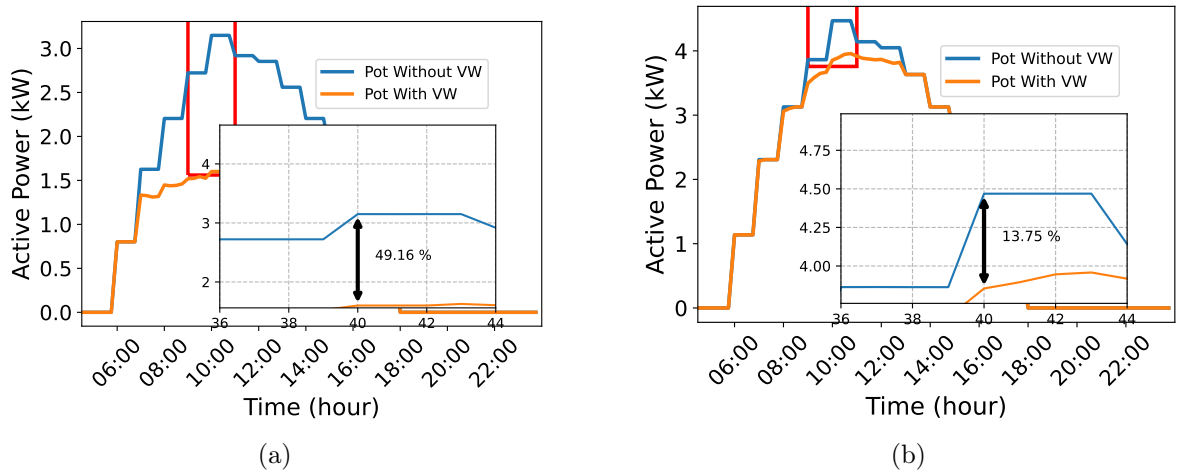


Figure 21 – Active power curtailment reduction at 50%: (a) Single VW control operation; (b) Combined control operation, VV and VW.

Source: Author

To summarize, operating the PV unit with VV and VW voltage controls resulted in a noticeable reduction in the curtailed active power. Although the 15% and 30% limits showed similar reductions, the 50% is not far behind and presented improvements. This was demonstrated through a single PV element in a single bus, illustrating the occurrence and evaluation of active power loss. More information about the complete operation will be provided in section 5.3.

### 5.2.3 Activation counts

This subsection focuses on the overall activation frequency of voltage controls, divided by curtailment scenario and control case. The results so far detailed how one element operates independently under each control strategy and combined operation. However, this can occur for all PV units at the same time, it only depends on the bus voltage reference where the unit is installed. The following three tables summarize the count of control activation, each for a different curtailment limit. Each row from these tables shows a control strategy, and the columns represent the number of units that operate with that specific control in an HC condition. There is a special case in those tables when no PV unit has a voltage control strategy operating in the HC condition, but a violation still occurs, which implies that the violation is not occurring at a bus without PV units and is indicated in the "0" column. The "Total" column shows the number of simulations for each control case.

Table 9 shows the number of activations with a 15% curtailment limit. The results show that in the VV case, most configurations required reactive control with 5 to 6 PV units. On the other hand, VW control and combined operation commonly needed 2 to 3 units, with a higher concentration of 2 units in the latter case.

Table 9 – Number of elements operating in a HC condition with a voltage control strategy and 15% curtailment.

Num. of Units / Controls	0	1	2	3	4	5	6	Total
VV	4.6%	0.0%	0.6%	2.6%	12.6%	31.3%	48.0%	150
VW	6.0%	9.3%	26.0%	32.6%	18.0%	7.3%	0.6%	150
VV&VW	9.3%	10.6%	34.0%	28.0%	14.0%	4.0%	0.0%	150

Furthermore, Table 10 shows the number of activations with a 30% curtailment limit. The results show that the VV case continues to show a concentration within 5 and 6 PV units, reassuring the previous results. Additionally, 2 and 3 units are the most common configurations required with VW control and the combined operation, repeating the concentration of 2 units in the last case.

Table 10 – Number of elements operating in a HC condition with a voltage control strategy and 30% curtailment.

Num. of Units / Controls	0	1	2	3	4	5	6	Total
VV	0.0%	0.0%	0.0%	3.3%	14.0%	28.6%	54.0%	150
VW	1.3%	10.6%	33.3%	32.0%	18.6%	4.0%	0.0%	150
VV&VW	3.3%	16.0%	38.0%	34.60%	6.0%	2.0%	0.0%	150



For the last curtailment limit, 50%, the results are shown in Table 11. VV control still follows the same arrangement, concentration within 5 and 6 units. However, the VW and combined control operation are still concentrated with 2 and 3 units but not very different from the 30% curtailment limit.

Table 11 – Number of elements operating in a HC condition with a voltage control strategy and 50% curtailment.

Num. of Units / Controls	0	1	2	3	4	5	6	Total
VV	0.0%	0.0%	0.0%	2.6%	10%	37.3%	50.0%	150
VW	0.0%	5.3%	26.0%	29.3%	31.3%	8.0%	0.0%	150
VV&VW	3.3%	18.0%	32.0%	32.60%	11.3%	2.6%	0.0%	150

The VV control usage in almost all units benefits the operator controller and DG owner by enhancing the HC value without any additional investment besides the inverter for this control. However, VW cases have a different scenario with curtailment issues, causing a reduction in the active power delivered to the grid. If a BESS unit is installed to store this extra energy that would be lost, it can reduce power loss. But, there are costs involved in installing storage elements in all units. Finding a balance between the curtailment limit and battery size can optimize financial returns and adjust the physical space available with smaller BESS units.



### 5.2.4 Activation locations frequency

This subsection aims ~~to determine~~ which buses on the grid are sensitive and require extra attention during operation. This discussion utilizes the combined voltage control strategy to demonstrate the increases in HC duo active and reactive power management. It also identifies and describes the sensitive PV locations, phase distribution, and distance from the feeder. A frequency diagram is also presented for each curtailment scenario to enhance visualization and comprehension.

Table 12 shows the most common buses for all curtailment scenarios and their associated phases. The distribution of phases is similar considering all curtailment configurations, with 6 occurrences for phase C, 4 for phase B, and 5 for phase A. Although phase C is associated with more buses, the grid remains balanced with regard to loads and PV penetration in sensitive buses, with a more significant differentiation in demand during peak load consumption from 6:00 pm to 8:00 pm. Figure 22 reassures this statement by comparing the PCC power flow in the baseline condition, case 1, with the 50% curtailment scenario, case 5. Figure 22a represents the regular operation without PV units and with high demand at the end of the day, while Figure 22b shows the HC condition when PV units and both controls are activated. The last one displays a duck curve with reverse power flow, represented by a negative value, which indicates excessive generation in the middle portion of the day, surpassing the load demand on the grid.

The 150 different simulation outcomes are analyzed for each curtailment level and randomly varied the location of six PVs across the grid. Figures 23 to 25 provide a frequency plot with the number of voltage control activations by the respective PV bus location in (a) and the actual position of the bus on the grid in (b). The number of occurrences is represented by a color map ranging from red to blue, with higher values shown in red and smaller ones in blue. As an example, in 30 out of 150 simulations for Figure 23a, 30 out of 150 simulations for Figure 24a, and 25 out of 150 simulations for Figure 25a, bus 031 utilized a voltage control strategy. This is a significant occurrence given that the location was randomly selected for each group of simulations, characterizing it as a sensitive bus in this case study. Additionally, it is worth noting that bus 031 is an end-line bus, as per the single-line diagram associated with the frequency chart in each figure..

This analysis identifies the top ten most sensitive buses and shows that some repeat in multiple curtailment scenarios despite being randomly selected. One of the main constraints observed is the distance between the bus and the feeder. Inverters that were further away from the PCC had more control activations compared to those that were closer, Figures 23, 24, and 25 illustrates this behavior and Table 12 quantifies the distances for those buses. The lengths are in meters, and the total length of the grid in this case study is 484.75 meters, which is a reference when analyzing the values.

Table 12 – List of buses frequently operating with voltage control activated.

Bus	Phase	Length (m)	Bus	Phase	Length (m)	Bus	Phase	Length (m)
018	A	73.92	019	B	74.02	022	B	35.69
024	C	82.68	025	B	82.69	027	C	69.41
028	A	67.75	029	C	67.75	030	A	63.16
031	C	126.14	032	C	125.15	033	A	121.88
035	A	109.48	037	C	110.20	038	B	104.44

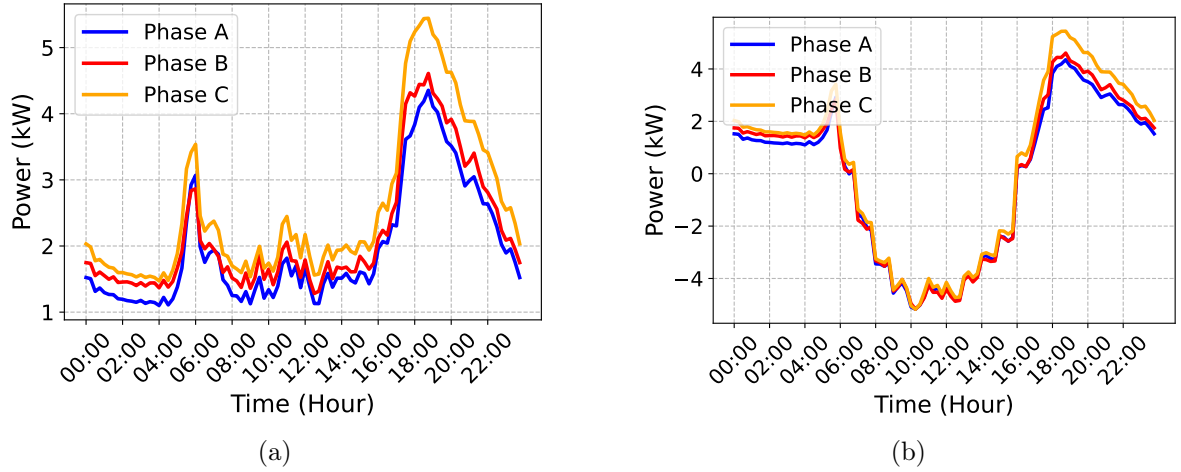


Figure 22 – Average power measurement in the transformer: (a) Case 1 - Operation without PV elements; (b) Case 5 - Operation with PV elements and both VV and VW controls.

Source: Author

In summary, PV units operating with some voltage control tend to be situated at the grid's edges, making these buses more sensitive than other areas. However, this is not limited to higher or lower curtailment limits, as there are samples of this occurring in all three results. For instance, bus 031 is one of the first or second buses in all frequency plots, which experience more numbers of activation regardless of the curtailment level.

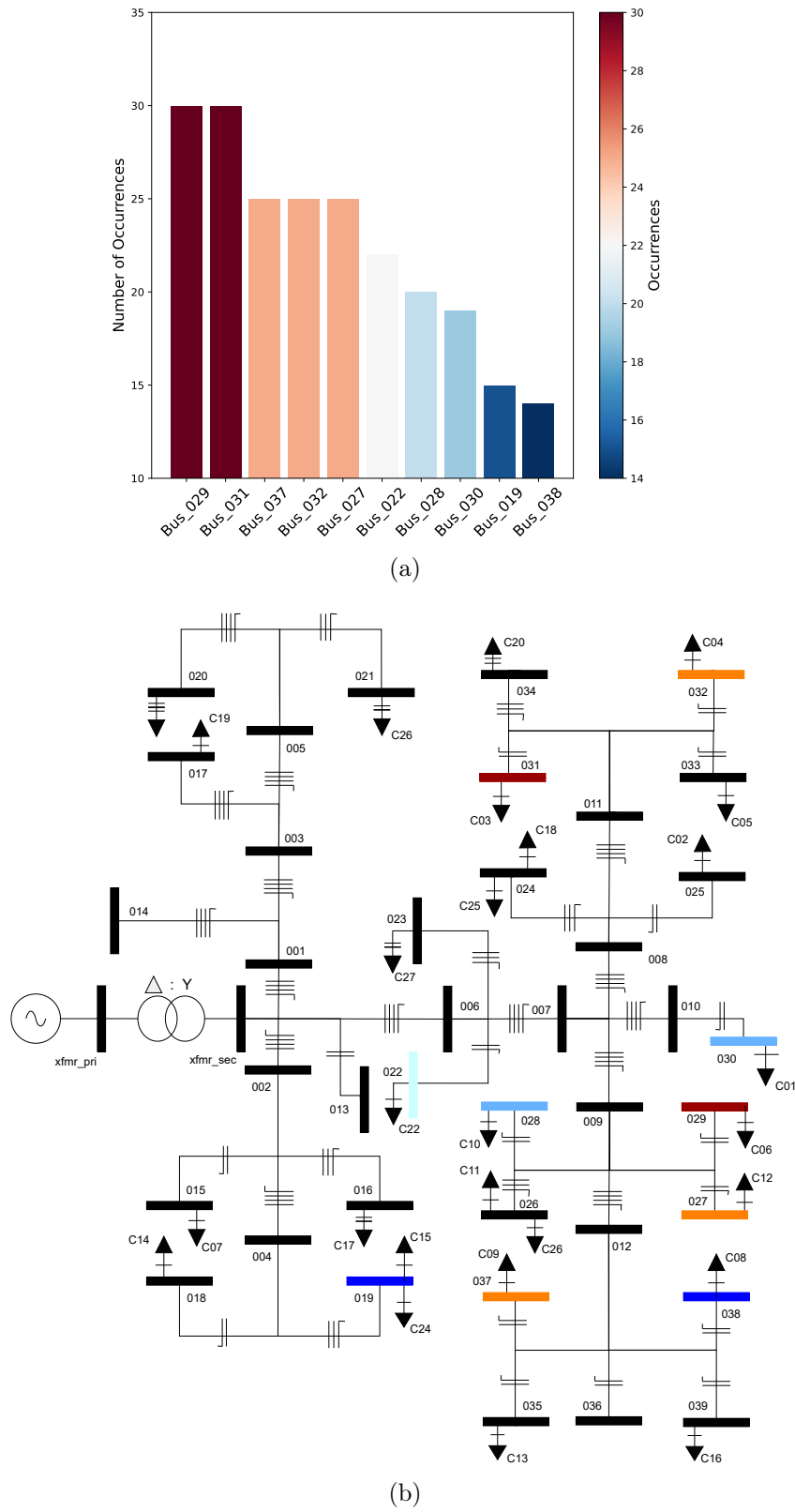
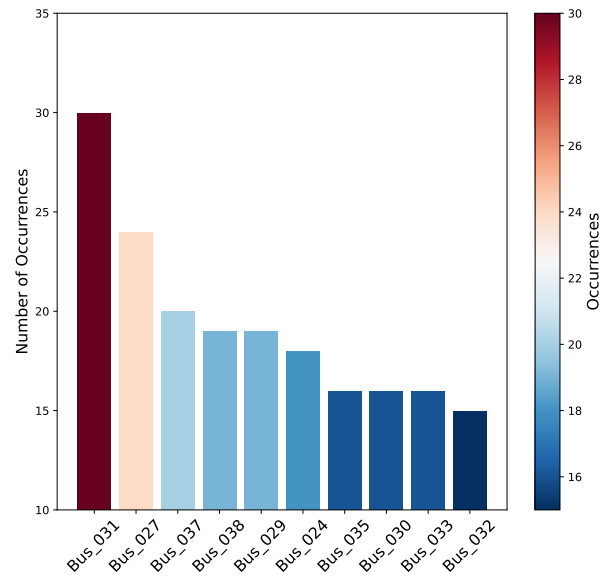
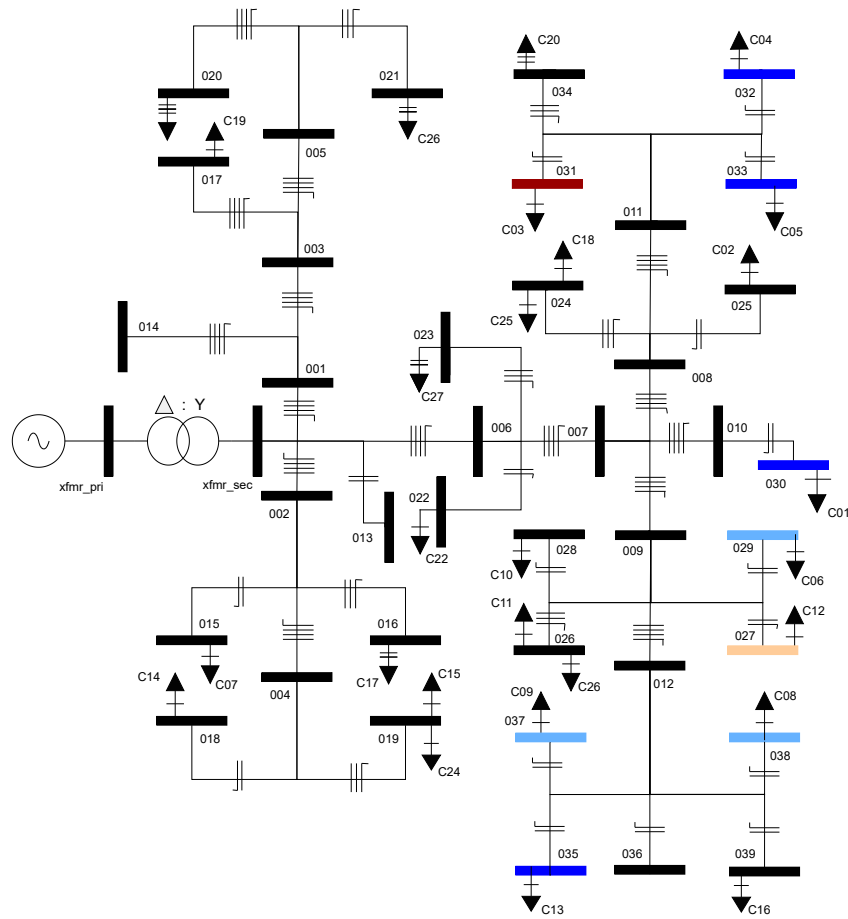


Figure 23 – Activation locations frequency for a 15% curtailment limit: (a) Number of occurrences by bus; (b) Occurrence representation into the grid.

Source: Author



(a)



(b)

Figure 24 – Activation locations frequency for a 30% curtailment limit: (a) Number of occurrences by bus; (b) Occurrence representation into the grid.

Source: Author

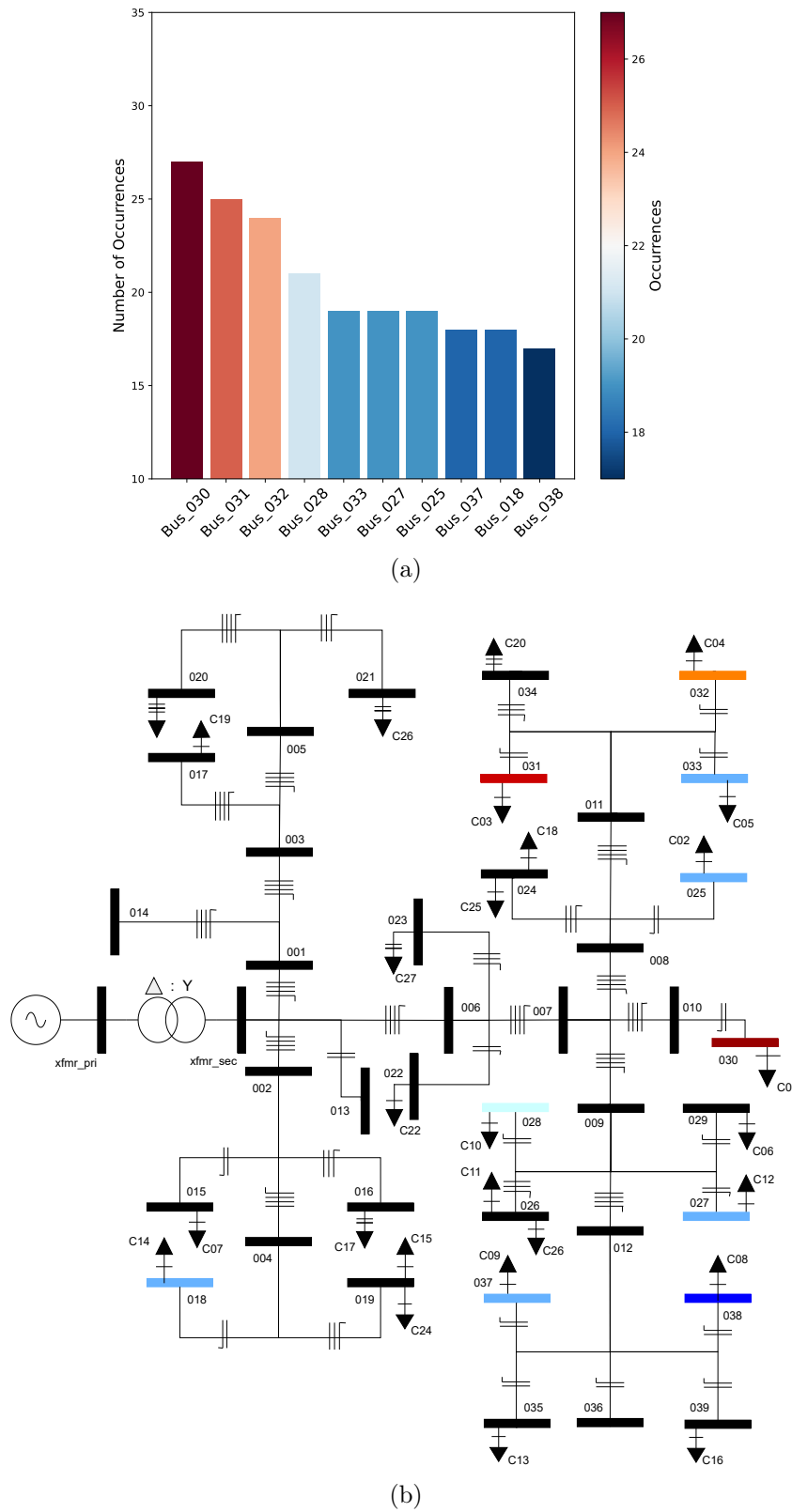


Figure 25 – Activation locations frequency for a 50% curtailment limit: (a) Number of occurrences by bus; (b) Occurrence representation into the grid.

Source: Author

## 5.3 BESS Sizing analysis

The following section discusses the sizing results and performance indicators of BESS units designed to absorb the power lost due to the active power curtailment. The analysis begins by evaluating the average maximum power and battery capacity under single and combined voltage control, metrics commonly used in the sizing process. While this thesis uses power reference, the values can be easily converted to ampere reference using the voltage measurement at the installed location.

### 5.3.1 Average BESS Sizing results

This subsection aims to display the end outcomes of the sizing process through the use of two tables and three box plots, which help in comprehending the results more effectively. The tables provide information on the average BESS maximum power and energy requirements to be associated with each PV unit, with different curtailment scenarios and separate analyses for the VW and combined control. On the other hand, the box plot highlights the distribution of these metrics, presenting a comparison between the outcomes of both strategies.

Based on the BESS sizing process described in Section 2.4, Table 13 presents the results for the VW control case. To mitigate the energy loss during the curtailment scenario, the active and energy values required are as follows: For 15% reduction curtailment limit, 149.53 W is the average maximum operation power with 70.97 W standard deviation and 45.79 Wh is the average energy capacity with 21.73 Wh standard deviation. For 30% reduction, the value changes to 338.96 W with 165.04 W standard deviation and 103.81 Wh with 50.54 Wh standard deviation. An even more considerable reduction is observed for the 50% curtailment, requiring 729.24 W average maximum active power with 373.67 W standard deviation and 223.33 Wh average energy capacity with 114.43 Wh standard deviation.

Table 13 – BEES average results by curtailment configuration operating with VW control.

Curtailment	Average Maximum Power (W)	Standard Deviation	Battery Capacity (Wh)	Standard Deviation
15%	149.53	70.97	45.79	21.73
30%	338.96	165.04	103.81	50.54
50%	729.24	373.67	223.33	114.43



Furthermore, Table 14 shows a similar result but for the combined control case. In order to mitigate the energy loss during the curtailment scenario, the active and energy values required are as follows: For the 15% curtailment limit, 78.95 W is the average maximum operation power with 43.69 W standard deviation and 24.18 Wh is the average

energy capacity with 21.73 Wh standard deviation. For 30% reduction, the value changes to 126.39 W average maximum active power with 6.3 W standard deviation, and 38.70 Wh is the average energy capacity with 20.93 Wh standard deviation. An even more considerable reduction is observed for the 50% curtailment, requiring 183.32 W average maximum active power with 108.11 W standard deviation and 56.14 Wh average energy capacity with 33.11 Wh standard deviation.

Table 14 – BEES average results by curtailment configuration operating with VV and VW controls.

Curtailment	Average Maximum Power (W)	Standard Deviation	Battery Capacity (Wh)	Standard Deviation
15%	78.95	43.69	24.18	13.38
30%	126.39	68.36	38.70	20.93
50%	183.32	108.11	56.14	33.11



In summary, it can be observed from Tables 13 and 14 that the BESS maximum power and energy exhibit an increase with the rise in allowable curtailment limit. This outcome was expected as higher active power reduction leads to more power loss. However, by implementing a combined VV and VW control operation, the size of the BESS can be significantly reduced in terms of both power and energy measurement. It can be observed that the VW increases by 4.87 times as it shifts from 15% to 50% curtailment. On the other hand, the VV and VW control scenarios only increase by 2.32 times under the same curtailment comparison. Additionally, there is a reduction in average BESS sizing comparison, which is about 47.21% for 15% curtailment, 62.71% for 30% curtailment, and 74.86% for 50% curtailment. These results consider all energy that would be lost in all PV units together for a defined simulation. It is worth noting that Figures 19 to 21 already emphasized this behavior but for a single PV element operating with both control cases. However, these were just examples at the time, and now we have the average results from 150 different simulations.

In order to examine the data, three separate box plots have been created for each curtailment limit. These plots offer insights into the battery power and energy, and although they share a similar box shape, the Y-axis values differ between them. In this case, relying solely on average values to analyze outcomes may not be the most accurate approach. This is because there is a significant standard deviation. A more effective method would be to utilize a box plot, which displays the entire range of data, containing outliers and whisker ranges. Key metrics indicate the distribution's highest and lowest points, which can be used as a benchmark for choosing the optimal battery size.

From the scenario where the curtailment limit is set at 15%, the finding reveals a noteworthy decrease in the average and median battery power as displayed in Figure 26a



when comparing the VW and VV cases with the VW alone. Additionally, the whiskers range is narrower, indicating that the consistent reduction in the dataset is concentrated towards smaller battery power. A similar outcome is observed in Figure 26b, but this time for battery energy.

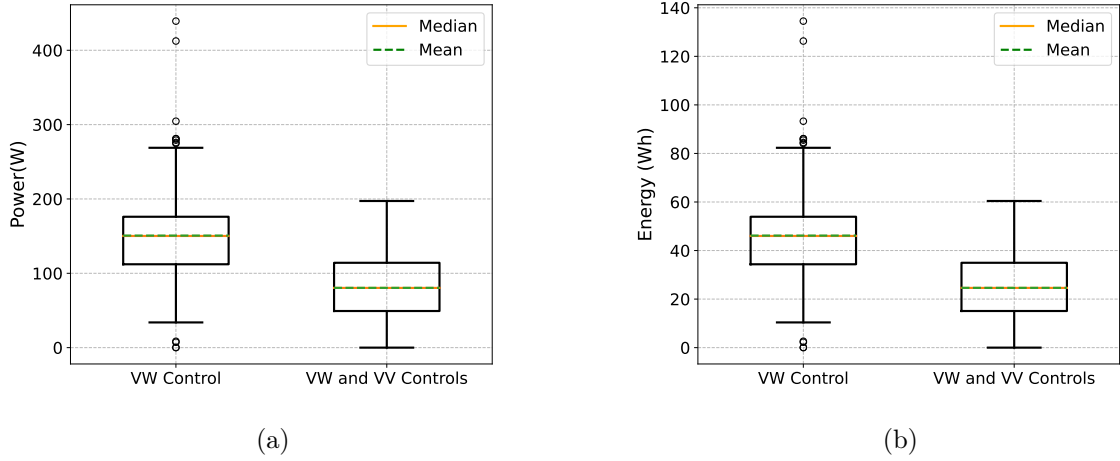


Figure 26 – BESS sizing results box plots considering 15% active curtailment: (a) Maximum Battery Power; (b) Battery Adjusted Energy.

In addition, the scenario where the curtailment limit is set at 30% also reveals a substantial decrease in the average and median battery power as displayed in Figure 27a when comparing the VW and VV cases with the VW case alone. Additionally, the whiskers range is narrower, indicating that the consistent reduction in the dataset is concentrated towards smaller battery power. A similar outcome is observed in Figure 27b, but this time for battery energy.

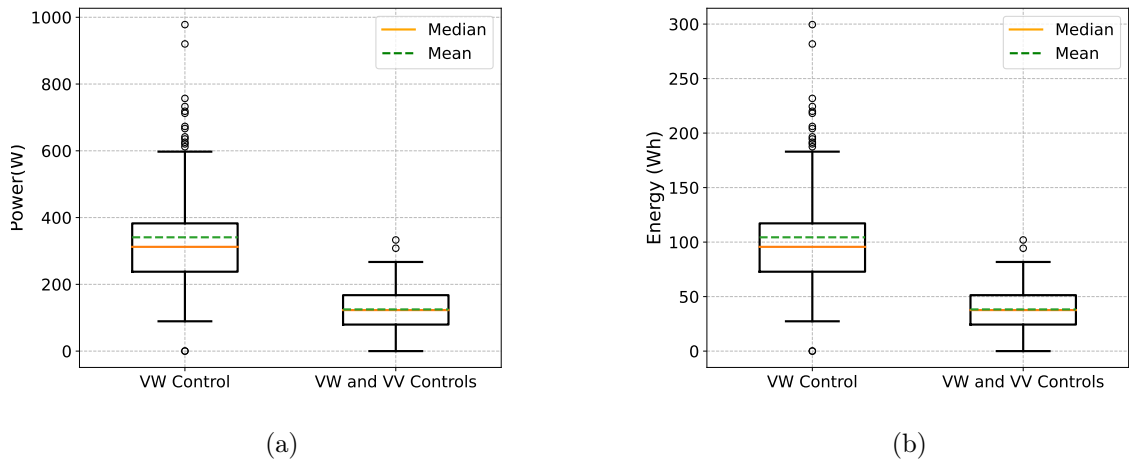


Figure 27 – BESS sizing results box plots considering 30% active curtailment: (a) Maximum Battery Power; (b) Battery Adjusted Energy.

Finally, the scenario where the curtailment limit is set at 50% also reveals a substantial decrease in the average and median battery power as displayed in Figure 28a when comparing the VW and VV cases with the VW case alone. Additionally, the whiskers range is narrower, indicating that the consistent reduction in the dataset is concentrated towards smaller battery power. A similar outcome is observed in Figure 28b, but this time for the battery energy.

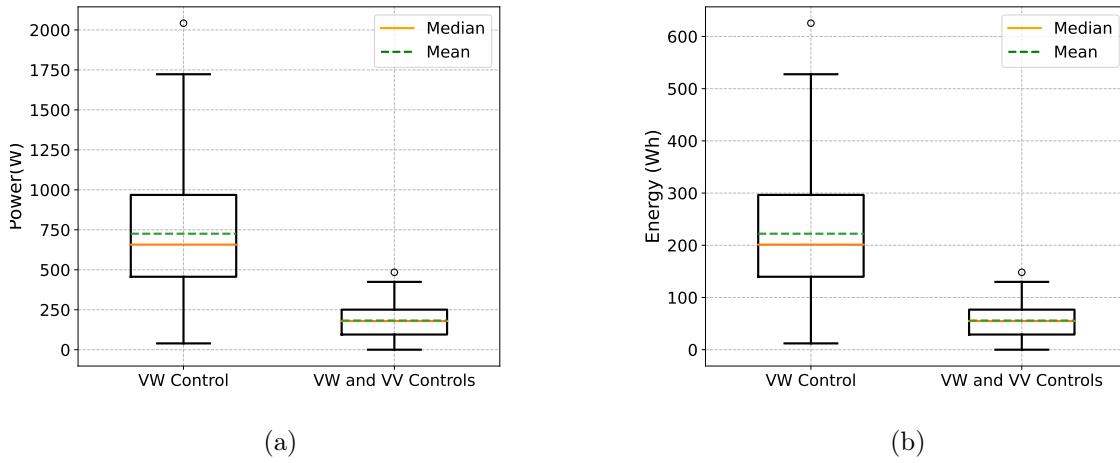


Figure 28 – BESS sizing results box plots considering 50% active curtailment: (a) Maximum Battery Power; (b) Battery Adjusted Energy.

After analyzing the results in this section, it was observed that implementing combined voltage control leads to a significant decrease in the size of the BESS. This reduction is evident when considering average and outlier values, as shown in the box plots. It is reflected in the financial investment required for BESS installation because smaller BESS units are less expensive and require less physical space to be allocated. This finding is particularly relevant for small LV grids but can also be applied to larger distribution systems. Using small battery energy units will be able to reduce the power that would be lost during the HC enhancement using VW control with the PV generation.

### 5.3.2 Average BESS KPI results

This subsection discusses the average results for the two KPIs presented in section 2.4. These KPIs help to understand the BESS sizing process by comparing the adjusted BESS energy with its maximum power operation and the maximum power with the PV size. Tables 15 and 16 show each curtailment limit's average and standard deviation values. The first table is for the single VW control operation, while the second is for the combined voltage control case, VV and VW.

The results were consistent across all curtailment limits when measuring the average energy of the BESS divided by its maximum power operation. This is due to the energy calculation method, which uses a fixed 15-minute sampling interval and the same adjustment metrics to determine capacity based on power measurements. However, the average maximum power of the BESS divided by the PV size varied depending on the curtailment limit. Table 15 shows that in the single VW control case, the KPI increased 229.01% and 422.85% when comparing the 15% curtailment with 30% and 50%, respectively. Table 16 also showed an increase in the combined control, with a 149.06% and 212.1% increase from 15% to 30% and 50%, respectively. As a result, as the curtailment limit increases, the BESS power becomes closer to the PV unit size.

The E-Rate results classify the battery in a E/3 rating, which means it will fully charge or discharge in 3 hours. It is a slow to medium velocity and adsorbs only the power that the VW control would lose. This condition benefits the BESS element by prolonging its lifetime since no rapid charge or discharge is required. It also results in units with smaller sizes, occupying less physical space for the installation. Related to the control strategies, there are no significant differences because battery capacity and maximum power are reduced at the same proportion, which implies the same ratio result between them.

A different scenario when comparing the BESS with the PV unit. As the curtailment increases, the battery gains prominence and reaches almost half the PV power value. It reflects the increase in the BESS size presented in subsection 5.3.1. However, the results for the combined operation are significantly smaller than the single VW control, which is another indicator that the BESS size decreases when operating with bot controls simultaneously.

Table 15 – Average E-ratio and PV power ratio results by curtailment with VW control.

Curtailment	Average BESS Energy by BESS Power.	Standard Deviation	Average BESS Power by PV Size	Standard Deviation
15%	30.62%	0.01%	13.65%	4.88%
30%	30.62%	0.01%	31.26%	12.62%
50%	30.62%	0.01%	57.72%	35.97%



Table 16 – Average E-ratio and PV power ratio results by curtailment with VV and VW control.

Curtailment	Average BESS Energy by BESS Power.	Standard Deviation	Average BESS Power by PV Size	Standard Deviation
15%	30.62%	0.01%	4.79%	2.56%
30%	30.62%	0.01%	7.14%	4.68%
50%	30.62%	0.01%	10.16%	7.13%

Table 17 shows the overall results for analyzing the PVLoadRatio indicator described in Equation 2.10. Each line represents a different curtailment scenario, and each column displays the corresponding result for the case under test. The values presented represent the percentage of energy generated by all PV elements divided by the load demand in a daily perspective. The ratio growth considering the VV control is significant, 46% higher than the baseline case. The enhancement with VW control tends to rise as the curtailment level increases, starting with a slight 1.08% enhancement for the 15% scenario and reaching 29.03% in the 50% one.

Table 17 – Average PV by Load ratio energy results by curtailment configuration.

Curtailment	Baseline	VV	VW	VV&VW
15%	62%	90%	67%	94%
30%	62%	93%	74%	98%
50%	62%	91%	80%	96%

In order to analyze the HCC indicator, the overall results are shown in Table 18. It includes HC values to make comparing and understanding HCC results easier. The data is presented as average values followed by the standard deviation for each active control strategy and curtailment configuration. As mentioned in Section 2.4, HC tends to increase as curtailment levels increase, and HCC follows this pattern, with 4.39% for the 15% configuration and 5.83% for the 50% one. However, unlike HC results, this coefficient does not increase with the combined VV and VW operation. In fact, it significantly reduces to 0.36% for the 15% configuration and 1.45% for the 50% one. These smaller HCC results benefit both the DG owner and the system operator. This is because less curtailed energy produced HC enhancements, reducing power loss and assisting with grid operation.

To better understand the results of the HCC analysis, some related metrics are included in Table 19. An example represents each curtailment strategy, and the table shows the results for all three scenarios for the single and combined VW control. The initial three columns of the table specify the example by displaying the curtailment scenario, the bus name where every PV component is installed, and the associated control strategy. The table also shows the HC value for the particular simulation, which is expected to differ from the average result in Table 18 because it is one example out of 150 results. The following

Table 18 – Average HCC results by curtailment configuration.

Curtailment	VW Control			VV and VW Control		
	HC (%)	Average HCC (%)	Standard Deviation (%)	HC (%)	Average HCC (%)	Standard Deviation (%)
15%	39.16	4.39	15.24	50.88	0.36	1.87
30%	42.45	5.06	14.27	53.50	0.58	2.55
50%	47.01	5.83	17.81	52.53	1.45	2.56

columns, Curtailed Energy and Capacity above initial HC, display the values utilized in Equation 2.9 to generate the HCC result, which is presented in the last column. When operating with VV and VW controls, all three examples show a significant reduction as the numerator decreases and active power control strategies lose less energy. Additionally, the capacity above the initial HC has increased for all the scenarios, which means that a higher amount of DG generation can be allowed into the grid without compromising the figure of merit metrics.

Table 19 – HCC examples for each curtailment scenario.

Curtailment	Location	Control Strategy	HC (%)	Curtailed Energy (Wh)	Capacity Above Initial HC (Wh)	HCC (%)
15%	016, 037, 010, 032,	VW	29.26	51.56	3.08	16.74
	023, and 025	VV & VW	31.10	17.36	7.49	2.31
30%	029, 017, 023,016,	VW	50.80	65.96	1.24	53.12
	020, and 015	VV & VW	67.70	51.15	65.58	0.7757
50%	023, 033, 031, 027,	VW	30.04	177.8	2.66	66.85
	016, and 020	VV & VW	39.11	53.01	4.45	11.91

In summary, four KPIs related to battery size were presented in order to quantify the required BESS size when operating in a HC condition right before a violation of the figures of merits established for this case study. The presented results are average values from all simulations performed and indicate that a BESS unit designed to absorb the energy that would be lost with the VW curtailment is relatively small when comparing the charge/discharge rates and reduces even more when operating with both voltage controls, VV and VW, activated.

### 5.3.3 HC Results Considering BESS Units

When operating rooftop PV systems with BESS, the results for the HC may vary due to the additional power that is stored in the storage unit. It's important to note that this extra power is still generated by the PV element, as required by the HC definition, but is delivered to the system at a more favorable time. This is a way to interpret this condition, and this subsection assesses the associated enhancements.

The changes made to the calculation method are related to how the power generated by the PV system is calculated. The results presented in Section 5.1 only consider the power delivered by the PV system to the grid. The current subsection, however, considers both PV and BESS powers, summing them up based on the simulation time interval. The HC identification logic remains the same, with only the highest measurement being considered in the HC results. The following results were evaluated by considering 150 different PV distributions for each curtailment scenario, referring to the HC values as an average metric with a standard deviation associated.

Table 20 presents the results for the PV unit operating with VW control, referred to as case 4. Based on the results, it was found that there were no significant differences in standard deviation. However, the average HC increased in all curtailment scenarios, with an increase of only 4.9% in the first curtailment, 10.27% in the second, and a significant increase of 19.65% in the 50% scenario. Analyzing the last scenario, an increase in HC from 47.01% to 56.25% is noticed and is consistent with the higher BESS power requirement shown in Table 13, which also indicates that the 50% curtailment scenario had the most elevated BESS power requirement.

Table 20 – Average HC values comparison when considering PV with VW control and BESS units for different curtailment scenarios.

Curtailment	With PV		With PV and BESS	
	Average HC (%)	Standard Deviation	Average HC (%)	Standard Deviation
15%	39.16	13.65	41.08	13.66
30%	42.45	13.20	46.81	13.17
50%	47.01	15.11	56.25	15.82

Table 21 presents the results for the PV unit operating with both VV and VW control, referred to as case 5. The standard deviation results are still very similar, and the HC enhancement is significantly smaller than the ones presented in Table 20. The HC enhancement remains within 4% for all curtailment scenarios, indicating that the active power reduction is small for this case. This is consistent with the BESS size values presented in Table 14 when both controls are operating together and the required storage is also small.

Table 21 – Average HC values comparison when considering PV with VV and VW control and BESS units for different curtailment scenarios..

Curtailment	With PV		With PV and BESS	
	Average HC (%)	Standard Devition	Average HC (%)	Standard Deviation
15%	50.88	15.42	51.57	15.26
30%	53.50	14.92	54.71	14.75
50%	52.53	16.67	54.44	16.26

The results resented in Tables 20 and 21 are illustrated in Figures 29 to 31 also considering the average daily power curves from all simulations. The (a) plot shows the results for VW control, while the (b) plot presents the combined control operation of VV and VW. After comparing (a) with (b), it is evident that there is a comparable decrease in the limited power. While Figure 29 displays a minor distinction, Figure 30a, which illustrates a 30% curtailment for the PV operating solely with VW control, shows a more pronounced red area that is not present in Figure 30b. The red area on the graph shows the amount of power that is absorbed by the BESS units. This is called the curtailed difference because this power was produced by the PV but not delivered directly to the grid. Additionally, the biggest difference in HC enhancement is noticed when PV operates only with VW control in the 50% curtailment scenario, presented in Figure 31a. Compared to Figure 31a, the curtailed energy significantly reduces, the red line follows the blue one, meaning that the BESS is not storing energy.

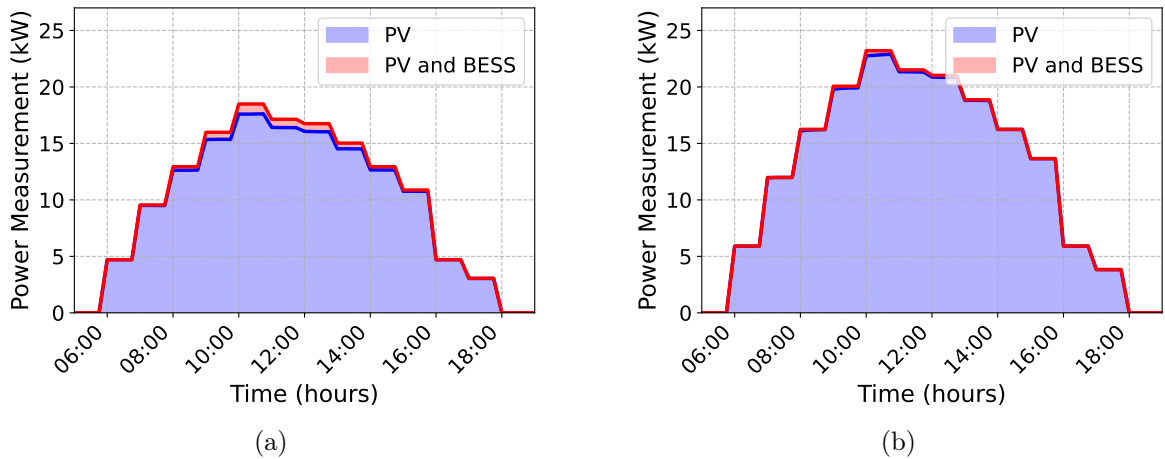


Figure 29 – Average power comparison when PV operating at 15% curtailment with and without BESS: (a) PV with VW control; (b) PV with VV and VW control.

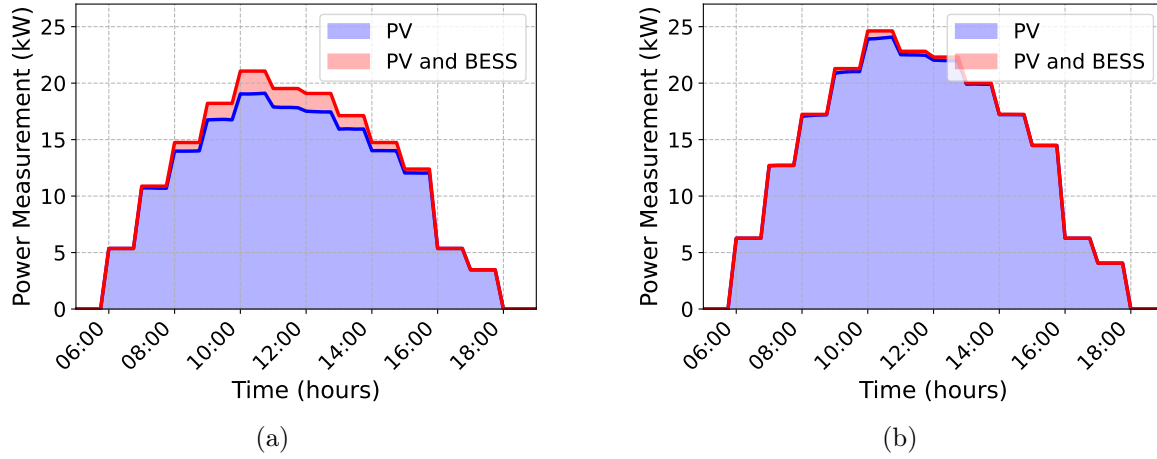


Figure 30 – Average power comparison when PV operating at 30% curtailment with and without BESS: (a) PV with VW control; (b) PV with VV and VW control.

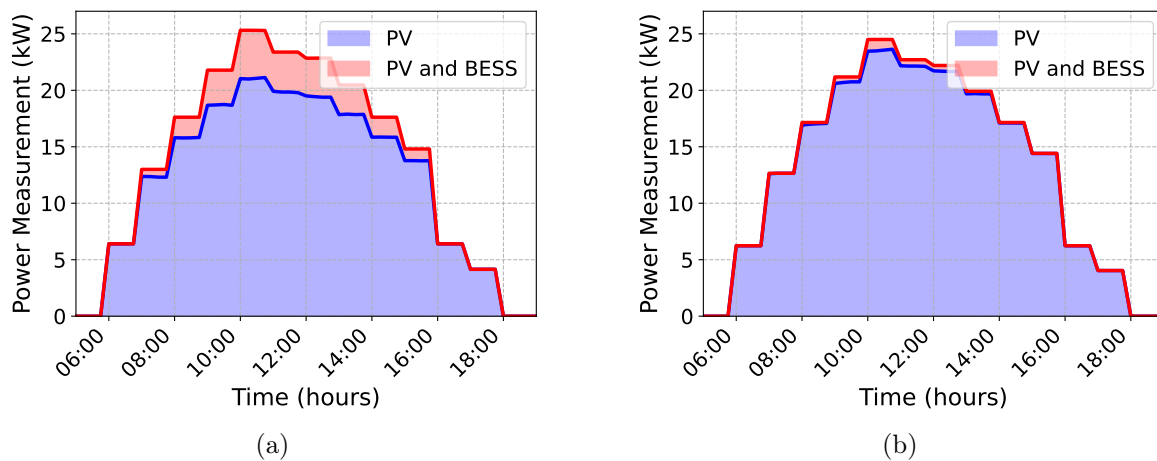


Figure 31 – Average power comparison when PV operating at 50% curtailment with and without BESS: (a) PV with VW control; (b) PV with VV and VW control.



## Chapter 6

# Final considerations and feature works

### 6.1 Conclusion

This thesis proposes and quantifies the use of distributed BESS to mitigate the active power loss caused by VW control in rooftop PV inverters. The active and reactive power controls were applied to PV inverters to enhance the grid HC. To efficiently quantify the enhancement in a LV grid, a simulation tool was developed using multiple software platforms, including OpenDSS, Python, and SQL. Ultimately, the small distributed BESS units were sized.

The case study assessed 150 different PV allocations in a LV grid with 20% PV penetrations based on the number of consumers. The HC analysis compares the baseline case with the control results under three different scenarios, each with a specific limit for curtailment. The first involves limiting the active power reduction to 15%, which results in a HC enhancement of 37.07% for single VV control operation, 1.38% for single VW control operation, and 40.79% for combined control. The second scenario involves a 30% reduction limit, which results in a HC enhancement of 36.67% for single VV control operation, 8.05% for single VW control operation, and 42.44% for combined control. Finally, the third scenario limits curtailment to 50%, resulting in a HC enhancement of 34.07% for single VV control operation, 23.23% for single VW control operation, and 38.57% for combined control. These results demonstrate the effectiveness of voltage control strategies and quantify the enhancement of HC when PV operates with them in distribution systems. The relation between the energy generated by the PV units and the load demand also follows the enhancement. Since the VW control is more effective for the 50% curtailment, it gradually increases the ration up to 80% and the VV case remains at a constant 90%. The combined operation reached an average 96% ratio. However, there is a mismatch between generation and consumption, and the reverse power flow is intensified in the middle of the day as the PV penetration increases.

The activation of voltage control depends on the location of the PV unit. To help

system operators plan where and how each PV unit should operate based on its location and impact on the grid, a single-line diagram is presented for each curtailment scenario. The diagram highlights the more frequent buses where control is activated, with those further from the PCC connection being more likely to activate regulation strategy. In general, VV control is used by most of the inverters, while the VW one is concentrated within 20% to 50% of the units at a time, this pattern repeats for all curtailment scenarios.

The number of PV units using the VW control affects the number of BESS units required to address the curtailed energy problem. The curtailment scenarios were analyzed under both single and combined voltage control. The optimal size of the storage unit varies depending on the curtailment level and ranges from 13% to 57% for the VW and 4.79% to 10% for both power controls, in comparison to the size of the associated PV unit. These results are directly tied to the curtailed power, and quantifying the effectiveness of this reduction in terms of HC improvement is the aim of the HCC indicator. As a result, the VW control had to reduce more power to increase the HC values, reaching 4.39%, 5.06%, and 5.83% HCC, compared to the VV and the VW control, which reached 0.36 0.58%, and 1.45% HCC values for the 15%, 30%, and 50% curtailment scenarios.

Considering the power that is absorbed by the BESS unit in the HC calculation and comparing with the previous results, the bigger storage size from the VW control resulted in a greater enhancement: 4.9% for the 15% scenario, 10.27% for the 30% scenario, and 19.65% for the 50% scenario. On the other hand, the combined control operation requires smaller storage and, consequently, resulted in a smaller HC increase: 1.35% for the 15% scenario, 10.27% for the 30% scenario, and 3.63% for the 50% scenario.

In conclusion, the proposed software can perform HC identification considering voltage control techniques. Additionally, it can size a BESS unit to store the energy that would be lost with the active power curtailment. The voltage control techniques have proven to be effective in improving the supported HC value in the case study despite the fact that they increase the current values and the power loss. In such cases, BESS can provide a possible solution when working with the PV unit to absorb what would be lost in the active power control. Furthermore, the combined VV and VW control operation requires less storage capacity than the VW control alone, thus reducing the space required.

## 6.2 Future works

This thesis focuses on enhancing HC through voltage control strategies and proposes using a BESS unit to reduce power loss. However, more research is required to quantify specific aspects of the conclusions presented here.

- Incorporate the BESS unit into the simulation and determine the optimal method for delivering the BESS energy back to the grid.
- ~~Conduct an analysis of the transmission system to assess viable options from the perspective of the system controller rather than that of the end user.~~
- To enhance the methodology, it would be beneficial to adjust the simulation time for the most sensitive part of the day, reduce the time required to convert to the HC condition by adjusting the PV increase step and run this process using a multi-thread application to generate data in parallel.
- Generate databases with reliable data from different LV grids. It allows the researchers to split the analysis into two areas, one responsible for generating the data and another for processing it.

## 6.3 Published Articles

The articles below were published while working on the presented thesis:

- TORQUATO, Hugo; ANTUNES, Hélio; BRAGA, Thiago; BRANDÃO, Danilo. **Estratégia para estimação de hosting capacity em redes de baixa tensão usando opendss:inversores fotovoltaicos com serviços ancilares.** In: CONGRESSO BRASILEIRO DE AUTOMÁTICA – CBA 2022, n<sup>o</sup> 24, 2022. Fortaleza-CE.
- BRAGA, Thiag; ANTUNES, Hélio; TORQUATO, Hugo; BRANDÃO, Danilo. **Modelagem e capacidade de hospedagem da rede de distribuição de baixa tensão.** In: CONGRESSO BRASILEIRO DE AUTOMÁTICA – CBA 2022, n<sup>o</sup> 24, 2022. Fortaleza-CE.

~~The article mentioned below is currently in its final writing stages and is related to the discussion presented in this document:~~

- ~~TORQUATO, Hugo; ANTUNES, Hélio; ARAUJO, Lucas; BRANDÃO, Danilo. Increased rooftop PV hosting capacity using distributed battery energy storage systems.~~



# References

- A. M. Amuna, R. Karandeh, and V. Cecchi. Voltage regulation in distribution systems using distributed energy resources. In *SoutheastCon 2021*, pages 1–7, 2021. doi: 10.1109/SoutheastCon45413.2021.9401910.
- A. D. Bank. *Handbook on Battery Energy Storage System*. Asian Development Bank, 2018. ISBN 978-92-9261-471-3.
- M. Bayer et al. *SQLAlchemy: The Python SQL Toolkit and Object-Relational Mapper*, 2023. URL <https://www.sqlalchemy.org/>.
- H. Bhoje and G. Sharma. An analysis of one mw photovoltaic solarpower plant design. *International Journal of Advanced Research in Electrical, Electronics and Instrumentation Energy*, 3:6969–6973, 2014. URL <https://api.semanticscholar.org/CorpusID:55374300>.
- B. Bletterie, S. Kadam, and J. Le Baut. Increased hosting capacity by means of active power curtailment. In *CIREN Workshop 2016*, pages 1–4, 2016a. doi: 10.1049/cp.2016.0794.
- B. Bletterie, S. Kadam, and J. Le Baut. Increased hosting capacity by means of active power curtailment. In *CIREN Workshop 2016*, pages 1–4. IET, 2016b.
- M. Bollen and F. Hassan. *Integration of Distributed Generation in the Power System*. Springer, 2011. ISBN 978-3-319-19823-1.
- Brazilian Elec. Reg. Agency. Electrical energy distribution procedures in the national electrical system, module 8: Power quality, Set.2020. URL <http://www.aneel.gov.br/>.
- P. Bruce and A. Bruce. *Practical Statistics for Data Scientists: 50 Essential Concepts*. O’Reilly Media, 2020.
- CEMIG. Mapa de disponibilidade de geração distribuída. <https://geo.cemig.com.br/mca/Secure/Authorize?ReturnUrl=2023>.
- W. S. Cleveland. *Visualizing Data*. Hobart Press, 1993. ISBN 978-0963488404.
- T. B. R. David Linden. *Handbook of Batteries*. Asian Development Bank, 2002. ISBN 0-07-135978-8.

- Electric Power Research Institute (EPRI). OpenDSS Reference Guide. OpenDSS Version 34.1.0, 2021. Available at <https://sourceforge.net/projects/electricdss/>.
- EPRI. Modeling high-penetration pv for distribution interconnection studies: Smart inverter function modeling in opendss, rev. 2. Technical Report 3002002271, Electric Power Research Institute (EPRI), Palo Alto, CA, 2013.
- EPRI. Common functions for smart inverters, version 3. Technical report, Electric Power Research Institute (EPRI), Palo Alto, CA, 2013.
- N. Etherden and M. H. Bollen. Overload and overvoltage in low-voltage and medium-voltage networks due to renewable energy – some illustrative case studies. *Electric Power Systems Research*, 114:39–48, 2014. ISSN 0378-7796. doi: <https://doi.org/10.1016/j.epsr.2014.03.028>. URL <https://www.sciencedirect.com/science/article/pii/S0378779614001230>.
- N. Etherden, M. Bollen, S. Ackeby, and O. Lennerhag. The transparent hosting-capacity approach—overview, applications and developments. In *International Conference and Exhibition on Electricity Distribution: 15/06/2015-18/06/2015*, 2015.
- O. Gandhi, D. S. Kumar, C. D. Rodríguez-Gallegos, and D. Srinivasan. Review of power system impacts at high pv penetration part i: Factors limiting pv penetration. *Solar Energy*, 210:181–201, 2020. ISSN 0038-092X. doi: <https://doi.org/10.1016/j.solener.2020.06.097>. URL <https://www.sciencedirect.com/science/article/pii/S0038092X20307118>. Special Issue on Grid Integration.
- IEEE-1547. Ieee standard for interconnection and interoperability of distributed energy resources with associated electric power systems interfaces. *IEEE Std 1547-2018*, 2018. doi: 10.1109/IEEESTD.2018.8347739.
- S. M. Ismael, S. H. Abdel Aleem, A. Y. Abdelaziz, and A. F. Zobaa. State-of-the-art of hosting capacity in modern power systems with distributed generation. *Renewable Energy*, 130:1002–1020, 2019. ISSN 0960-1481. doi: <https://doi.org/10.1016/j.renene.2018.07.008>. URL <https://www.sciencedirect.com/science/article/pii/S0960148118307936>.
- M. Karimi, H. Mokhlis, K. Naidu, S. Uddin, and A. Bakar. Photovoltaic penetration issues and impacts in distribution network – a review. *Renewable and Sustainable Energy Reviews*, 53:594–605, 2016. ISSN 1364-0321. doi: <https://doi.org/10.1016/j.rser.2015.08.042>. URL <https://www.sciencedirect.com/science/article/pii/S136403211500903X>.
- J. Lee, J.-P. Bérard, G. Razeghi, and S. Samuelsen. Maximizing pv hosting capacity of distribution feeder microgrid. *Applied Energy*, 261:114400, 2020. ISSN 0306-2619. doi:

- <https://doi.org/10.1016/j.apenergy.2019.114400>. URL <https://www.sciencedirect.com/science/article/pii/S0306261919320872>.
- M. Z. Liu, A. T. Procopiou, K. Petrou, L. F. Ochoa, T. Langstaff, J. Harding, and J. Theunissen. On the fairness of pv curtailment schemes in residential distribution networks. *IEEE Transactions on Smart Grid*, 11(5):4502–4512, 2020. doi: 10.1109/TSG.2020.2983771.
- K. Luo and W. Shi. Comparison of voltage control by inverters for improving the pv penetration in low voltage networks. *IEEE Access*, 8:161488–161497, 2020a. doi: 10.1109/ACCESS.2020.3021079.
- K. Luo and W. Shi. Comparison of voltage control by inverters for improving the pv penetration in low voltage networks. *IEEE Access*, 8:161488–161497, 2020b. doi: 10.1109/ACCESS.2020.3025337.
- T. Ma, H. Yang, and L. Lu. A feasibility study of a stand-alone hybrid solar–wind–battery system for a remote island. *Applied Energy*, 121:149–158, 2014a. ISSN 0306-2619. doi: <https://doi.org/10.1016/j.apenergy.2014.01.090>. URL <https://www.sciencedirect.com/science/article/pii/S0306261914001202>.
- T. Ma, H. Yang, and L. Lu. Feasibility study and economic analysis of pumped hydro storage and battery storage for a renewable energy powered island. *Energy Conversion and Management*, 79:387–397, 2014b. ISSN 0196-8904. doi: <https://doi.org/10.1016/j.enconman.2013.12.047>. URL <https://www.sciencedirect.com/science/article/pii/S0196890413008236>.
- W. McKinney. *Python for Data Analysis*. O’Reilly Media, 2017. ISBN 978-1491957660.
- W. McKinney et al. *pandas: powerful data analysis tools for Python*, 2023. URL <https://pandas.pydata.org/>.
- Microsoft. Microsoft sql server documentation. Website, 7 2023.
- P. Mohammadi and S. Mehraeen. Challenges of pv integration in low-voltage secondary networks. *IEEE Transactions on Power Delivery*, 32(1):525–535, 2017. doi: 10.1109/TPWRD.2016.2556692.
- E. Mulenga, M. H. Bollen, and N. Etherden. Limits set by component loadability on solar power integration in distribution networks. *Electric Power Systems Research*, 209: 107951, 2022. ISSN 0378-7796. doi: <https://doi.org/10.1016/j.epsr.2022.107951>. URL <https://www.sciencedirect.com/science/article/pii/S037877962200181X>.
- B. Palmintier, R. Broderick, B. Mather, M. Coddington, K. Baker, F. Ding, M. Reno, M. Lave, and A. Bharatkumar. On the path to sunshot. emerging issues and challenges

- in integrating solar with the distribution system. 5 2016. doi: 10.2172/1253980. URL <https://www.osti.gov/biblio/1253980>.
- S. Papathanassiou, N. Hatziaargyriou, P. Anagnostopoulos, L. Aleixo, B. Buchholz, C. Carter-Brown, N. Drossos, B. Enayati, M. Fan, V. Gabrion, B.-N. Ha, L. Karstenti, J. Malý, W. Namgung, J. Pecas-Lopes, J. Pillai, T. Solvang, and S. Verma. *Capacity of Distribution Feeders for Hosting Distributed Energy Resources*. CIGRE (International Council on Large Electric Systems), June 2014. ISBN 978-2-85873-28 2-1.
- W. S. M. R. Paulo Radatz, Celso Rocha and J. Peppanen. Opendss pvsystem and invcontrol element models. Technical report, Electric Power Research Institute (EPRI), Palo Alto, CA, 2020.
- P. Radatz. *Py-dss-interface is a Python package that provides a Python interface to the OFFICIAL version of OpenDSS software.*, 2023. URL <https://py-dss-interface.readthedocs.io/en/latest/>.
- P. Radatz, C. H. Rocha, J. Peppanen, and M. Rylander. Advances in opendss smart inverter modelling for quasi-static time-series simulations. In *CIREN 2020 Berlin Workshop (CIREN 2020)*, volume 2020, pages 243–246, 2020. doi: 10.1049/oap-cired.2021.0319.
- A. Rajabi and S. Elphick. Voltage control and pv hosting capacity of distribution networks. Report type, Australian Power Quality Research Centre - AQRC, Australia, January 2022. URL <https://documents.uow.edu.au/content/groups/public/@web/@eis/@secte/documents/doc/uow272598.pdf>.
- R. Torquato, D. Salles, C. Oriente Pereira, P. C. M. Meira, and W. Freitas. A comprehensive assessment of pv hosting capacity on low-voltage distribution systems. *IEEE Transactions on Power Delivery*, 33(2):1002–1012, 2018. doi: 10.1109/TPWRD.2018.2798707.
- T. S. Ustun and Y. Aoto. Analysis of smart inverter’s impact on the distribution network operation. *IEEE Access*, 7:9790–9804, 2019a. doi: 10.1109/ACCESS.2019.2891241.
- T. S. Ustun and Y. Aoto. Analysis of smart inverter’s impact on the distribution network operation. *IEEE Access*, 7:9790–9804, 2019b. doi: 10.1109/ACCESS.2019.2891241.
- D. Wu, D. Aliprantis, and K. Gkritza. Electric energy and power consumption by light-duty plug-in electric vehicles. *Power Systems, IEEE Transactions on*, 26:738 – 746, 06 2011. doi: 10.1109/TPWRS.2010.2052375.
- M. Zeraati, M. E. Hamedani Golshan, and J. M. Guerrero. A consensus-based cooperative control of pev battery and pv active power curtailment for voltage regulation in distribution networks. *IEEE Transactions on Smart Grid*, 10(1):670–680, 2019. doi: 10.1109/TSG.2017.2749623.



- G. Zubi, R. Dufo-López, M. Carvalho, and G. Pasaoglu. The lithium-ion battery: State of the art and future perspectives. *Renewable and Sustainable Energy Reviews*, 89: 292–308, 2018. ISSN 1364-0321. doi: <https://doi.org/10.1016/j.rser.2018.03.002>. URL <https://www.sciencedirect.com/science/article/pii/S1364032118300728>.



# Appendix A

## Database Structure

This appendix presents the database architecture developed for this study. It starts with an overall definition of the tool, presenting its usage and how it is beneficial to this project. Furthermore, it summarizes the design and organization of the database highlighting the relationships between tables with a small example regarding the control activation. To conclude, it presents an overview of how this tool was utilized to generate the findings presented in Chapter 5.

By definition, SQL Server is a relational database management system (RDBMS) developed by Microsoft and designed to be used as an efficient, robust, and scalable data management tool, suitable for a wide range of data applications. [Microsoft \[2023\]](#) presents a SQL Server technical documentation that contains all usages, available tools, and examples on how to work with SQL databases, it is one of the main references associated with SQL databases. Applying these benefits to this study, efficiency is important to manage the 1.5 million records created on each simulation, remembering that the results are generated by analyzing 3 curtailment scenarios with 150 simulations each. It requires a robust platform to handle the data transferring, from Python to the database, in order to not lose any data or sort the information, for this point SQL enhances the reliability of the study. And the data processing needs to be scalable to efficiently perform calculations and retrieve specific data from the group of data. These are some examples that justify the use of a relational database structure to store the information, and SQL Server choice comes based on previous professional knowledge working with this technology.

As a starting point, the data collection covers all electrical devices in the grid by associating monitors with each one of them. The data collection is divided into three groups: operational metrics, power measurements, and InvControl operation. The first is responsible for general metrics like voltage and current measurements, converging the grid operation indicators. The power monitor is associated with loads and PVSystems elements, focusing on the power flow parameters. The third, and last monitor type, is associated with InvControl elements, they are responsible for collecting the overall control indicators

like reference voltage, activation triggering, and power data. They collect data every 15 minutes over a daily operation and, by the end of the simulation, all measurements are transferred to a table in the database, Table 22. Where each column represents:

- **Id:** Expresses a unique number responsible for identifying the record.
- **Simulation:** Represents the simulation number associated with this record.
- **Case:** Represents the case number associated with this record.
- **TimeStamp:** Represents measurement time during the day.
- **Monitor:** Presents the monitor element responsible for this measurement.
- **Element:** Represents the element associated with this measurement.
- **Measurement:** Represents the kind of measurement (i.e. Voltage, Current, Power).
- **Value:** Represents the measurement information.

Table 22 – Data structure of the monitor table in the database.

Id	Simulation	Case	TimeStamp	Monitor	Element	Measurement	Value
----	------------	------	-----------	---------	---------	-------------	-------

All monitor information is stored in one central large table called tblMonitorData. It was a trade-off circumstance with two options, process the data in Python, associating each sample to the respective table, or provide a large table with all the data, delegating the data processing to SQL Server. Both options require computer power allocation, but the second one promotes more flexibility once the data is generated in Python, but analysis can be performed afterward in SQL Server. It allows the user to perform new analyses without simulating everything again, and the metrics are already saved in the database.

For instance, the voltage control strategies tables are presented in Figure 32, which is a straightforward example from the data processing stage. It filters some activation metrics from the tblMonitorData table and includes them in two new tables exclusively for the voltage control analysis. They are called spSummary\_InvControl and spSummary\_InvControlData, Summary, and Data tables to simplify the following explanation. Both of them were created with a key relationship in order to associate one Summary record with many Data values, the Summary table has a primary key called ID, and the Data table has a foreign key called ID\_Summary. Consequently, the results retrieval exhibits remarkably enhanced efficiency compared to querying the large tblMonitorData table. Moreover, regarding the proposed example, Algorithm 22 shows a simple query responsible for retrieving all measurements data from the pvsystem\_pv\_3\_voltage monitor in the first simulation for PV units operating with VV control, case 3.

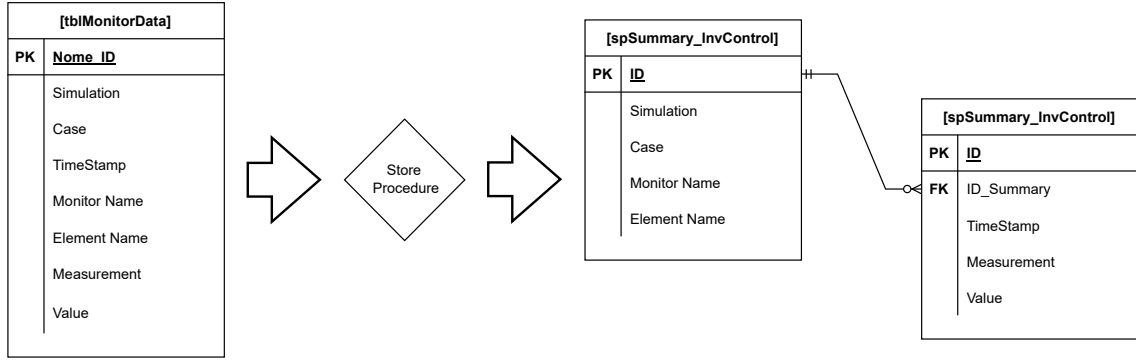


Figure 32 – Hosting capacity boxplots divided by case studies

**Algorithm 22** SQL query implementation responsible for retrieving voltage data from a monitor element.

```

SELECT
    *
FROM spSummary_InvControlData
WHERE
    id_Summary = (
        SELECT
            id
        FROM spSummary_InvControl
        WHERE
            [Simulation] = 1 AND [Case] = 3
            AND [Monitor] = 'pvsystem_pv_3_voltage'
    )

```

Looking at the stored procedure process from Figure 32, Algorithm 23 defines it. The process starts verifying whether both tables exist and removing data from previous executions. Afterward, a query returns a monitor list associating a unique ID for each of them, the primary key. Furthermore, the Data table stores all measurements associated with that element, like the reference voltage, VV activation, VW activation, and power values. In the end, a specific entity is created containing specific information about the control activation results, making it possible to use this entity as the main resource to generate the analysis presented in Section 5.2, along with more relationships between entities to generate specific data as in Section 5.2.4 that evaluates the activation location within the grid. In this case, the control entity relates with the PV system entity to retrieve the location where each PV unit operates with some control strategy activated.

Overall, the SQL Server significantly improved data manipulation within this study and promoted efficient processing of all the information, leading to all the analyses explained in Chapter 5. It calculates the HC values for all proposed configurations, generates the control strategies analysis, and, ultimately, four store procedures sizes BESS units based on the active power that would be lost due to VW operation.

---

**Algorithm 23** SQL query implementation responsible for defining a store procedure that retrieves inverter controls measurements.

---

```

CREATE OR ALTER    PROCEDURE [dbo].[spGenerateInvControlTables]
AS
BEGIN
    ----- CREATE OR DELETE DATA -----
    IF (EXISTS (SELECT * FROM INFORMATION_SCHEMA.TABLES
        WHERE TABLE_NAME IN ('spSummary_InvControl',
                                'spSummary_InvControlData'))
        ) )
    BEGIN
        DELETE FROM spSummary_InvControlData
        DBCC CHECKIDENT('spSummary_InvControlData', RESEED, 0)
        DELETE FROM spSummary_InvControl
        DBCC CHECKIDENT('spSummary_InvControl', RESEED, 0)
    END

    ----- POPULATE DATA -----
    -- DESCRIPTION: This query will populate the Summary table
    -----
    INSERT INTO spSummary_InvControl
    ([Case], Simulation, Monitor, Elemento)
    SELECT DISTINCT
    [Case],
    Simulation,
    Monitor,
    Elemento
    -- Adicionar aqui
    FROM tblMonitoresData MD2 WITH (NOLOCK)
    WHERE Elemento like 'pvsystem%'
    ORDER BY Simulation, [Case]

    -----
    -- DESCRIPTION: This query will populate the Data table
    -----
    INSERT INTO spSummary_InvControlData
    (id_Summary, TimeStep, Measurement, [Value])
    SELECT
    SI.id AS id_Summary,
    MD2.TimeStep AS TimeStep,
    MD2.Measurement AS Measurement,
    MD2.[Value] AS [Value]
    FROM spSummary_InvControl AS SI WITH (NOLOCK)
    JOIN tblMonitoresData AS MD2 WITH (NOLOCK)
    ON SI.[Case] = MD2.[Case]
        and SI.Simulation = MD2.Simulation
        and SI.Elemento = MD2.Elemento
        and SI.Monitor = MD2.Monitor
    WHERE Measurement in ('Vreg', 'volt-var', 'volt-watt',
        'vars', 'watts', 'P1(kW)', 'P2(kW)', 'P3(kW)',
        'Q1(kvar)', 'Q2(kvar)', 'Q3(kvar)')
    ORDER BY Measurement, id_Summary, TimeStep
END

```

---

## Appendix B

### Case Study Overview Data

This appendix describes each group of elements as it is defined in OpenDSS. It starts with the service transformer specifications in Table 23, detailing each terminal definition. Additionally, Table 24 displays information about each wire data which is used to define the line geometry in Table 25. Table 26 provides a detailed list of every line element utilized to connect all grid components, with references to wire and geometry types. Additionally, Table 28 outlines all load shape profiles for the loads. The respective type is then linked to the load in Table 27, which presents further information about the consumers.

Table 23 – Service Transformer Data Overview.

Terminal	Bus	Connection	Voltage	Rated Power	%R	X/R	CC
1	xfmr_pri	Delta	11.9kV	45kVA	0.7766		
2	xfmr_sec	Star	0.22kV	45kVA	0.7766		

Table 24 – Wire Data Overview.

Wire Type	Name	Rdc	GMRac	NomAmps	Diam
1	CA-16mm2-XLPE-1kV	1.91	0.1927	59	0.47
2	CA-2AWG-1kV	0.8595	0.3038	95	0.74
3	CA-70mm2-XLPE-1kV	0.443	0.3997	157	0.97
4	CA-4/0AWG-1kV	0.2684	0.54366	210	1.32

Table 25 – Geometry Data Overview.

Geometry Type	Number of Cond.	Cond.	Wire Type	H	Geometry Type	Number of Cond.	Cond.	Wire Type	H
1	4	1	2	880	4	4	1	1	900
		2	2	860			2	1	900
		3	2	840			3	1	899
		4	4	820			4	1	900
2	2	1	3	901	5	2	1	1	901
		2	3	990			2	1	990
3	3	1	1	900	6	4	1	2	880
		2	1	900			2	2	860
		3	1	900			3	2	840
							4	2	820

Table 28 – Load Shape Data Overview

TimeStep	Load Shape Type					
	0	1	2	3	4	5
1	0,547668	0,821856	0,807639	0,74436	0,344506	0,248221
2	0,492937	0,726285	0,718316	0,782212	0,316961	0,254942
3	0,550114	0,694656	0,660743	0,800896	0,327436	0,241577
4	0,481973	0,636393	0,616273	0,67398	0,3518	0,238178
5	0,531448	0,604764	0,55478	0,776985	0,318125	0,231456
6	0,51994	0,569414	0,551432	0,74407	0,304236	0,244899
7	0,464938	0,580969	0,506771	0,717157	0,313857	0,234856
8	0,565609	0,518299	0,490226	0,774468	0,310055	0,234856
9	0,492575	0,532987	0,469473	0,704281	0,305788	0,228134
10	0,471371	0,508997	0,485635	0,725579	0,310055	0,231456
11	0,52583	0,480599	0,487261	0,726741	0,311607	0,224735
12	0,453249	0,472668	0,473107	0,743586	0,312383	0,231456
13	0,470284	0,496756	0,441069	0,697408	0,317737	0,234856
14	0,509429	0,48197	0,449581	0,738842	0,321229	0,234856
15	0,455333	0,4853	0,455893	0,691309	0,331703	0,234856
16	0,547034	0,464834	0,451111	0,730904	0,3054	0,234856
17	0,602489	0,445054	0,439826	0,73255	0,302684	0,231456
18	0,58636	0,488139	0,427298	0,631966	0,311219	0,254942
19	0,534982	0,492742	0,422612	0,777759	0,325496	0,261663
20	0,567512	0,477857	0,42242	0,65791	0,335971	0,278427
21	0,455333	0,537296	0,548085	0,6825	0,376629	0,285149
22	0,586179	0,616515	0,710091	0,727128	0,455539	0,268384
23	0,470193	0,894024	1,0627	0,66246	0,50512	0,214692
24	0,546218	1,40429	1,37619	0,743683	0,467954	0,134192
25	0,523383	1,33673	0,730844	1,6107	0,469118	0,127471
26	0,536976	1,54403	0,730461	1,72881	0,459807	0,254942
27	0,382751	0,904012	0,666386	1,32918	0,490378	0,345562

*Continue in next page*



Table 28 – *Continue in previous page*

28	0,444097	0,708365	0,668012	1,28358	0,561219	0,345562
29	0,489041	0,782002	0,593894	1,34632	0,720669	0,362327
30	0,460588	1,06118	0,661413	1,24631	1,01986	0,432783
31	0,591162	1,08859	0,52781	1,11639	1,34691	0,556855
32	0,354027	0,755367	0,526185	1,1285	1,42124	0,734696
33	0,679692	0,570883	0,643625	1,16083	1,47463	1,51636
34	0,569234	0,577248	0,677671	1,14021	1,44211	1,80151
35	0,430595	0,550417	0,577732	1,21059	1,48665	2,03297
36	0,43422	0,616123	0,64219	1,01281	1,55284	2,09338
37	0,842162	0,636686	0,729314	1,05734	1,58915	2,18732
38	0,701348	0,626307	0,632913	1,04631	1,54973	2,03637
39	0,639731	0,737252	0,683409	1,1556	1,46919	2,10682
40	1,17317	0,627384	0,797788	1,38	1,48782	2,14368
41	0,649336	0,562364	0,711908	1,21272	1,59575	2,1504
42	1,29414	0,653627	0,690008	1,2436	1,4986	2,11687
43	0,802473	0,72981	0,647641	1,11988	1,47889	2,12691
44	1,10884	0,833117	0,765751	1,10042	1,5284	2,17056
45	0,951351	1,00203	1,08785	1,24989	1,47967	2,16044
46	0,946277	0,984504	1,14083	1,29656	1,56789	1,94575
47	0,984062	0,914196	0,953291	1,11678	1,52646	1,22782
48	0,574943	1,02044	0,792433	1,27284	1,55664	1,13727
49	0,754992	0,878944	0,756092	1,0405	1,56013	1,06682
50	0,734785	1,01574	0,873627	1,17719	1,55548	0,95271
51	0,499733	0,915763	0,734287	1,06044	1,49239	0,942667
52	0,499643	0,779456	0,677384	0,939816	1,54314	1,01645
53	0,586088	0,745183	0,716212	0,947174	1,55664	1,64051
54	0,653233	0,822542	0,637121	1,11669	1,56246	1,96259
55	1,21277	0,928787	0,741077	1,02965	1,60079	2,0196
56	0,721827	0,84663	0,657587	1,00787	1,55129	2,06318
57	0,938212	0,853681	0,697276	1,10691	1,54624	1,99944
58	0,708507	0,8245	0,670211	1,09907	1,56013	1,94575
59	0,594877	0,895395	0,667151	1,1194	1,53228	2,05645
60	0,625867	0,848099	0,686852	1,04911	1,46764	2,18393
61	0,727626	0,797278	0,693259	1,03992	1,56323	2,10682
62	1,01659	0,773777	0,739929	1,10042	1,54702	2,13363
63	0,725452	0,838209	0,757717	1,05647	1,44716	2,00956
64	0,541234	0,726676	0,796928	1,04021	1,49783	2,07994
65	0,53018	0,820583	0,766611	1,10584	1,49395	2,06657
66	0,492756	0,891185	0,846467	1,16577	1,51257	2,22085
67	0,575214	0,923009	0,913316	1,22579	1,42008	2,19405

*Continue in next page*

Table 28 – *Continue in previous page*

68	0,940568	1,02896	0,789659	1,01697	1,44522	2,13031
69	1,0976	1,14284	1,05533	1,10497	1,51567	2,21081
70	1,07975	0,99459	1,38939	1,13566	1,42504	2,29803
71	2,20599	1,25859	1,94694	1,21156	1,49317	2,24774
72	3,01589	1,75015	2,30978	1,12327	1,51567	1,83504
73	2,47375	1,74105	2,80594	1,20817	1,60583	1,19429
74	1,78599	1,92171	2,66612	1,21659	1,52995	0,858845
75	2,30068	2,02365	2,38944	1,34389	1,47307	0,748139
76	2,17944	2,20128	2,42167	1,23954	1,53538	0,681004
77	3,16214	2,28608	2,20334	1,18048	1,37205	0,560254
78	2,54705	2,1956	2,14691	1,14902	1,35195	0,499841
79	2,43614	2,1579	2,13085	1,1254	1,33837	0,469634
80	2,5679	1,95902	2,13286	1,08242	1,33993	0,449548
81	2,28174	1,8989	2,0311	0,98977	1,37205	0,419341
82	2,43904	1,79843	2,16547	0,986575	1,3016	0,422663
83	2,39075	1,78531	2,05616	0,928974	1,06168	0,399177
84	2,14419	1,64655	1,86546	0,930716	0,647501	0,399177
85	1,61247	1,57252	1,8296	0,858497	0,519397	0,362327
86	1,96477	1,57174	1,68605	0,914162	0,452436	0,345562
87	2,703	1,60014	1,6368	0,808738	0,426132	0,342163
88	2,02077	1,53149	1,57425	0,817935	0,442814	0,335442
89	1,61047	1,42809	1,48349	0,80777	0,388966	0,325399
90	1,48062	1,49996	1,40421	0,758204	0,369258	0,301913
91	1,35204	1,35083	1,28543	0,826357	0,346756	0,301913
92	1,37162	1,21883	1,27816	0,763238	0,352188	0,305312
93	0,855573	1,05902	1,05878	0,802639	0,354903	0,278427
94	0,667912	1,03033	1,03774	0,72829	0,371197	0,271784
95	0,559357	1,0319	0,977583	0,832843	0,335195	0,265062
96	0,620612	0,93378	0,904517	0,724224	0,349084	0,25162

Table 26 – Lines Data Overview.

Names	Bus1	Bus2	Phases	Norm. Amps (A)	Length (m)	Geo. Type	X/R
abcn_l01-sec	xfmr_sec	001	1.2.3.4	95	15	1	1.03
cn_l02-ramal	xfmr_sec	013	3.4	157	05	2	1.85
abcn_l03-sec	xfmr_sec	006	1.2.3.4	95	30	1	1.03
abcn_l04-sec	001	014	1.2.3.4	95	17	1	1.03
abcn_l05-sec	001	002	1.2.3.4	95	14	1	1.03
abcn_l06-sec	001	003	1.2.3.4	95	19	1	1.03
an_l07-ramal	002	015	1.4	59	04	5	0.50
bcn_l08-ramal	002	016	2.3.4	59	06	3	0.50
abcn_l09-sec	002	004	1.2.3.4	95	37	1	1.03
abcn_l10-sec	003	005	1.2.3.4	95	24	1	1.03
abcn_l11-ramal	003	017	1.2.3.4	59	05	4	0.50
an_l12-ramal	004	018	1.4	59	06	5	0.50
bcn_l13-ramal	004	019	2.3.4	59	06	3	0.50
abcn_l14-ramal	005	020	1.2.3.4	59	04	4	0.50
acn_l15-ramal	005	021	1.3.4	59	06	3	0.50
bn_l16-ramal	006	022	2.4	59	05	5	0.50
abcn_l17-sec	006	007	1.2.3.4	95	19	1	1.03
bcn_l18-ramal	006	023	2.3.4	59	08	3	0.50
abcn_l19-sec	007	008	1.2.3.4	95	27	6	1.03
abcn_l20-sec	007	009	1.2.3.4	95	12	6	1.03
abcn_l21-sec	007	010	1.2.3.4	95	13	1	1.03
bcn_l22-ramal	008	024	2.3.4	59	04	3	0.50
abcn_l23-sec	008	011	1.2.3.4	95	36	6	1.03
bn_l24-ramal	008	025	2.4	59	05	5	0.50
abn_l25-ramal	009	026	1.2.4	59	05	3	0.50
cn_l26-ramal	009	027	3.4	59	06	5	0.50
abcn_l27-sec	009	012	1.2.3.4	95	36	6	1.03
an_l28-ramal	009	028	1.4	59	05	5	0.50
cn_l29-ramal	009	029	3.4	59	05	5	0.50
an_l30-ramal	010	030	1.4	59	05	5	0.50
cn_l31-ramal	011	031	3.4	59	11	5	0.50
cn_l32-ramal	011	032	3.4	59	10	5	0.50
an_l33-ramal	011	033	1.4	59	07	5	0.50
acn_l34-ramal	011	034	1.3.4	59	06	3	0.50
an_l35-ramal	012	035	1.4	59	10	5	0.50
bn_l36-ramal	012	036	2.4	59	10	5	0.50
cn_l37-ramal	012	037	3.4	59	10	5	0.50
bn_l38-ramal	012	038	2.4	59	05	5	0.50
an_l39-ramal	012	039	1.4	59	09	5	0.50

Table 27 – Load Data Overview.

Nome	V	Active Power	kvar	Bus	Phases	Loadflow Type
c01	127.017	0.217	0.134	030.1.4	1	2
c02	127.017	0.244	0.151	025.2.4	1	2
c03	127.017	0.261	0.161	031.3.4	1	2
c04	127.017	0.323	0.200	032.3.4	1	3
c05	127.017	0.179	0.111	033.1.4	1	2
c06	127.017	0.133	0.082	029.3.4	1	1
c07	127.017	0.165	0.102	015.1.4	1	2
c08	127.017	0.115	0.071	038.2.4	1	1
c09	127.017	0.232	0.144	037.3.4	1	2
c10	127.017	0.261	0.161	028.1.4	1	2
c11	127.017	0.081	0.050	026.2.4	1	1
c12	127.017	0.055	0.034	027.3.4	1	1
c13	127.017	0.233	0.144	035.1.4	1	2
c14	127.017	0.217	0.134	018.1.4	1	2
c15	127.017	0.145	0.090	019.2.4	1	2
c16	127.017	0.274	0.169	039.1.4	1	2
c17	220.000	0.130	0.081	016.2.3.4	2	1
c18	127.017	0.308	0.191	024.3.4	1	3
c19	220.000	2.592	1.606	017.1.2.3.4	3	0
c20	220.000	0.323	0.200	034.1.3.4	2	3
c21	220.000	0.166	0.103	020.1.2.3.4	3	0
c22	127.017	0.080	0.050	022.2.4	1	1
c23	127.017	0.021	0.013	026.1.4	1	0
c24	127.017	0.001	0.000	019.3.4	1	1
c25	127.017	0.217	0.134	024.2.4	1	2
c26	220.000	0.370	0.229	021.1.3.4	2	3
c27	220.000	0.001	0.000	023.2.3.4	2	1